INFORMATION TO USERS

This material was produced from a microfilm copy of the original document. While the most advanced technological means to photograph and reproduce this document have been used, the quality is heavily dependent upon the quality of the original submitted.

The following explanation of techniques is provided to help you understand markings or patterns which may appear on this reproduction.

1. The sign or "target" for pages apparently lacking from the document photographed is "Missing Page(s)". If it was possible to obtain the missing page(s) or section, they are spliced into the film along with adjacent pages. This may have necessitated cutting thru an image and duplicating adjacent pages to insure you complete continuity.

2. When an image on the film is obliterated with a large round black mark, it is an indication that the photographer suspected that the copy may have moved during exposure and thus cause a blurred image. You will find a good image of the page in the adjacent frame.

3. When a map, drawing or chart, etc., was part of the material being photographed the photographer followed a definite method in "sectioning" the material. It is customary to begin photoing at the upper left hand corner of a large sheet and to continue photoing from left to right in equal sections with a small overlap. If necessary, sectioning is continued again — beginning below the first row and continuing on until complete.

4. The majority of users indicate that the textual content is of greatest value, however, a somewhat higher quality reproduction could be made from "photographs" if essential to the understanding of the dissertation. Silver prints of "photographs" may be ordered at additional charge by writing the Order Department, giving the catalog number, title, author and specific pages you wish reproduced.

5. PLEASE NOTE: Some pages may have indistinct print. Filmed as received.

Xerox University Microfilms
300 North Zeeb Road
Ann Arbor, Michigan 48106

PROPAGATION AND OBSERVATIONS OF VLF EMISSIONS IN THE AURORAL ZONE

A

DISSERTATION

Presented to the Faculty of the

University of Alaska in Partial Fulfillment

of the Requirements

for the Degree of

DOCTOR OF PHILOSOPHY

by

R. N. Srivastava, B.Sc.(Hons), M.Sc., M.S.

College, Alaska

May 1974

PROPAGATION OF VLF EMISSIONS IN THE MAGNETOSPHERE

AND THE IONOSPHERE

RECOMMENDED:

Daniel L. Swift

R. M. Stanley

Albert E. Belon

R Parthasarathy

APPROVED:

Charles R. Wilson

Coordinator for Graduate Studies in Geophysics

Aug 14 1975

Date

Vice President for Research

18 August 1975

Date

ABSTRACT

VLF data from the two auroral zone ground stations at College (dp. lat. 64.62°N) and Bar I (dp. lat. 70.20°N) situated on the same geomagnetic meridian have been collected for almost a year and a half and have been analysed. The data contained many naturally occurring very-low-frequency emissions called hiss and chorus in the range of a few hundred Hz to a few kHz which were identified at the ground level both from the chart records and by aural monitoring of the magnetic tape data. Examples of events, indicating relationships of ELF/VLF emissions with the manifestations of auroral substorm phenomena, were studied using all-sky camera data, magnetic and 30 MHz riometer records.

The diurnal variation of the narrow band chorus emissions below approximately 4 kHz is found to peak around local noon and shows a strong correlation with the large and anisotropic ($\geq$ 40 kev) electron flux at $\sim$ 2000 km. Chorus emissions also display a latitudinal variation with more events on the equatorward rather than the poleward side of the auroral oval. Although the diurnal variations of chorus seem to reflect more on the variation in the conditions responsible for the generation of chorus emissions, the seasonal dependence of chorus observations on the ground is controlled primarily by ionospheric propagation conditions. Comparison of chorus events observed on the ground with the magnetic activity index Kp reveals that the relationship is not as consistent as expected. The non-simultaneous appearance of VLF emissions on both College and Bar I records seem to suggest that the emissions may be localized in latitude and that the propagation of VLF signals in the earth-ionosphere waveguide is not an important factor in determining whether

they should be observed on the ground.

Ground observations of wideband VLF hiss typically in the range of 4-10 kHz reveals that it is primarily a late evening phenomena and is closely related to the visual aurora. The examples of correlation between occurrences of VLF hiss and auroral activation presented in this dissertation are sufficiently convincing to believe that there does exist a causal connection between the two which may be due to the same precipitating particles responsible for both hiss and the auroral light. The contradictory examples, however, point out that the controlling factor, as to whether or not hiss is observed on the ground, is the propagation condition in the ionosphere. There is no consistent relationship found between VLF hiss emission and the riometer absorption but in the cases corresponding hiss and auroral substorm activity, the peak hiss emission occurs at the time of brightening of the auroral forms during breakup after which the absorption usually tends to increase due to intense ionization and the hiss intensities practically drop to zero.

Comparison of the low altitude polar orbiting Injun 5 satellite data with the ground VLF data has clearly revealed that there is a definite scarcity of VLF events on the ground. Reasons for this have been investigated by performing ray tracing computations for the propagation of VLF signals in an inhomogeneous and anisotropic medium, such as the magnetosphere and the ionosphere. It is found that the actual region which determines whether or not signals can be observed on the ground, occurs in the 60-125 km altitude region. Wave normal computations in the lower ionosphere using snell's law have been conducted to determine the cone of zenith angles of phase normal at 125 km beyond which the VLF

signals are reflected from the lower boundary of the ionosphere and do not reach the ground. In addition to collisional absorption, the spatial attenuation of the VLF signals resulting from the divergence of the ray paths from the vertical has been determined. In conclusion, many of the near auroral zone VLF events are frequently either reflected by, or heavily attenuated in, the lower ionosphere and these losses in the lower ionosphere are the principal causes for the rarity of hiss and chorus emissions at the ground level. A separate computation for VLF signals which are observed by the high altitude OGO satellites and are generated in the equatorial plane of the magnetosphere indicates that these signals are more or less trapped in the magnetosphere at altitudes $\geq 1\ R_E$ and cannot reach the ground.

ACKNOWLEDGEMENTS

The research in this dissertation was supported in part by the U.S. Army contract DAHC 04-69-C-0054 and in part by the National Science Foundation Grant GA-29158X.

My sincerest gratitude is reserved for Professor Daniel W. Swift for suggesting the problem and for helpful comments throughout the preparation of this paper. Thanks are also due to Professors R. Parthasarathy and Al Belon with whom I have had many stimulating discussions on this subject.

TABLE OF CONTENTS

LIST OF FIGURES

LIST OF TABLES

CHAPTER I

INTRODUCTION

Propagation, observations and analysis of the naturally occurring very-low-frequency (VLF) electromagnetic radio signals are the subjects of this study. The frequency range for this electromagnetic energy varies from a few hundred Hz to a few tens of kHz and is within the audio range so that the various types of emissions can be identified by listening to the undetected signal fed into a loudspeaker. These sounds are the source of nomenclature for various emissions called VLF hiss, chorus and ELF hiss. VLF hiss is usually a broadband white noise, typically 4-10 kHz and can be identified aurally by a hissing sound. Chorus is characterized by a sequence of closely spaced discrete events of a narrow bandwidth, often overlapping in time and sounds like the chirping of a flock of birds. ELF hiss is another continuous broadband emission, often heard in conjunction with chorus. Typical frequencies of ELF hiss are of the order of 400 Hz and it sounds like wind blowing through pine trees when heard over a loudspeaker.

VLF hiss, chorus and ELF hiss are all near-auroral zone phenomena and are intimately related to the auroral and magnetospheric substorms and to the precipitation of energetic electrons into the atmosphere (Harang and Larsen, 1965; Morozumi and Helliwell, 1966; Morozumi, 1967; Brice, 1967; Oliven and Gurnett, 1968 and Gurnett and Frank, 1972). VLF hiss emission is observed primarily in the late evening or around local midnight and is closely associated with the visual aurora. The VLF hiss event is often of short duration, typically lasting only for a few minutes during the passage of bright auroral forms and shows marked variations in amplitude

over periods of the order of a second. Chorus and ELF hiss events are primarily daytime phenomena extending from morning to late afternoon hours with a few notable exceptions in the very early morning periods. Chorus events are of longer duration, often lasting for several hours, and consist of superposition of different sets of periodic emissions mainly of a multitude of rising tones.

Chorus emissions are usually observed in association with the precipitation of energetic (∿ 40 kev) electrons into the atmosphere (Oliven and Gurnett, 1968) whereas auroral hiss is correlated with intense fluxes 10^4 to 10^7 electrons $(cm^2 \text{ sec ster ev})^{-1}$, of electrons with energies on the order of 100 ev to several kev (Gurnett and Frank, 1972). This leads to the following considerations: The outer zone Van Allen belt, extending to about six earth radii on the earth's night side, is populated with energetic (∿ 40 kev) electrons whereas much softer electrons (a few hundred ev to a few kev) are found in the auroral zone corresponding to equatorial plane distances greater than six earth radii from the center of the earth. The agent responsible for the precipitation of electrons into the auroral zone atmosphere may also be responsible for the generation of VLF emissions. A possible mechanism is pitch angle scattering of electrons by electro-magnetic waves at VLF frequencies (Kennel and Petschek, 1966). However, we do not observe any chorus in the midnight sector. Swift (1968) has discussed the morphology of chorus emissions and has suggested that the energy source of chorus emissions and of consequent electron microbursts is the free energy associated with a loss-cone distribution in the ring current. Some of the other mechanisms for the generation of VLF emissions are mentioned in the next section.

I.1 Generation Mechanisms of VLF Emissions

A number of theories have been proposed in the past to explain the mechanisms of the origin of VLF emissions. In some of the theories put forward, the electromagnetic energy of the emission is derived primarily from the kinetic energy of streams of charged particles trapped on the lines of force of the earth's magnetic field. If this energy conversion is due to the longitudinal motion of the charged particles, the resulting radiation is of the Cerenkov type (Ellis, 1957; Jørgensen, 1968; Lim and Laaspere, 1972). The transverse motion of charged particles in the earth's magnetic field is very nearly circular and the associated radiation is the Doppler shifted proton and electron cyclotron radiation (MacArthur, 1959, Dowden, 1963). A basic difficulty with mechanisms of generation such as Cerenkov and cyclotron radiation is that the calculated flux densities are too low to account directly for the observed intensities (Maeda and Kimura, 1962, 1963). However, Lim and Laaspere (1972) have pointed out that by considering an electron flux spectrum of the approximate form $\frac{dJ}{dE} \alpha E^{-2}$, electrons in the range 100 ev - 1 kev contribute about two orders of magnitude more to the intensity of incoherent Cerenkov hiss than those in the range of 1 kev - 10 kev.

Theory of plasma instability provoked by energetic electrons of the outer Van Allen belt in the equatorial plane of the magnetosphere (Thorne and Kennel, 1967; Kennel and Petschek, 1968) has also received considerable attention. Kindel and Kennel (1971) have proposed that electrostatic ion cyclotron waves can be unstable to field-aligned currents comparable to those expected in the auroral zone. However, two other theories that successfully attempt to explain some observed features of

VLF hiss and chorus are suggested by Swift (1965 and 1968). It is pointed out that hiss events may be caused by a two-stream instability associated with sufficiently strong currents flowing parallel to the magnetic field (Swift, 1965) and that auroral zone chorus is generated by an electrostatic loss-cone instability associated wtih ring current protons (Swift, 1968).

1.2 A Brief Review of Ground and Satellite Observations

Ground measurements of VLF emissions have been carried out at a number of stations (Helliwell, 1965 and the references therein) principally in the auroral zone in both the hemispheres. However, with strong magnetic storms, VLF emissions may even appear at mid-latitude stations because the plasmasphere shrinks and moves inward to the earth. Ground measurements indicate that the intensities of VLF emissions are two to three orders of magnitude lower than the satellite observations made in the same geographical region at altitudes of a few hundred to a few thousand kilometers. The differences between ground and satellite flux values are attributed to attenuation losses encountered by VLF waves in crossing the lower boundary of the ionosphere. Attenuation factors include collisional absorption in the ionosphere and absorption resulting from divergence of the signals towards the horizontal from the top of the lower ionosphere to ground receiver (see Chapter VIII).

A considerable amount of information of VLF emissions has been made available from direct observations in the magnetosphere since the inception of artificial satellites. Satellite records have shown examples of subprotonospheric whistlers (SP), magnetospheric reflected whistlers (MR), ion whistlers and lower hybrid resonance noise (LHR bands) where the lower frequency

cut-off of the noise is identified with a plasma resonance known as the lower hybrid resonance (Brice and Smith, 1965). Simultaneous occurrences of VLF emissions with auroral particle precipitations have also been repeatedly observed. However, comparison of simultaneous records from ground and satellite receivers has shown that a satellite frequently observes intense ELF and VLF noise bands not seen by ground station located near the same field line (Barrington et al., 1963; Gurnett, 1966). Reflection of VLF signals in the magnetosphere has been considered by Thorne and Kennel (1967), Kennel and Thorne (1967), Russel et al. (1969), Dunckel and Helliwell (1969) and Lyons and Thorne (1969). Reflection loss could also occur in the lower ionosphere before the VLF signal emerges from the lower boundary of the ionosphere. Although, there have been several studies of VLF emissions with respect to absorption (Harang and Larsen, 1964; Morozumi and Helliwell, 1966), the relationship has not been clearly understood because the occurrence or non-occurrence of VLF emissions on the ground does not appear to be well related to the absorption of 30 MHz radio noise as observed by riometers.

1.3 Outline of Research

The primary purpose of our study has been to determine the detailed relationships between VLF and ELF emissions and the auroral substorm, and to the extent possible, provide an understanding of these relationships. An effort has been made to explain theoretically why many VLF events (hiss and chorus) are unable to penetrate to the ground. Attenuation of VLF signals due to defocussing of their propagation paths in the 125 to 60 km altitude range is given particular attention. In order to understand reflection and absorption processes in the magnetosphere and ionosphere,

we have made VLF ray path computations using the ray tracing technique developed by Haselgrove (1954).

In Chapter II, we shall describe the method of observation, data collection and processing along with system sensitivity computations. Data used in this study has been collected from the VLF receivers located near Fairbanks, Alaska, and the Bar I DEW-line located on the arctic coast of the Yukon Territory, Canada. Chapter III presents a statistical analysis of the occurrence of VLF chorus as a function of magnetic activity, time of day and month of the year. A detailed study of the relation of VLF records to magnetometer and auroral all-sky camera data will be presented in the fourth chapter. Chapter V deals with the results of a comparative study between VLF hiss events observed on the ground and by Injun 5 satellite in order to determine whether or not propagation conditions above the earth's atmosphere exert any controlling influence on the observability of VLF signals on the ground. Chapter VI presents VLF ray tracing computations in a model ionosphere which is carried out to determine the ionospheric characteristics necessary to permit VLF signals generated in the magnetosphere to be observed on the ground. The behavior of these ray paths for two different sets of initial conditions will be interpreted in Chapter VII. VLF ray path computations in the lower ionosphere and their implications to signal accessibility are included in Chapter VIII. Finally, Chapter IX will be confined to a general discussion and concluding remarks, where observational and theoretical studies are coordinated to give a self-consistent picture of VLF/ELF emissions and certain recommendations are proposed to improve the measurements and calculations.

CHAPTER II

METHOD OF OBSERVATION

The VLF program at the Geophysical Institute consisted of operating two VLF sites, near College and at Bar I, on the same geomagnetic meridian. The VLF receiver used at the Poker Flat Rocket Facility at Chatanika near College (dp. lat. 64.62°N) since August 1969 was on loan from the Lockheed Corporation. However, it was replaced late in August 1970 by another receiver, Model No. 102, which was built at the Geophysical Institute. The Bar I DEW line station (dp. lat. 70.20°N) program which started around April 1970 also used the Institute-built receiver Model No. 101. Both of these Institute-built receivers were solid state devices. The Poker Flat VLF site was closed down due to increased interference from power line noise at the end of December 1970 whereas the Bar I observations continued until August 1971. Data were obtained both on chart paper and on magnetic tapes. A summary of the data availability is given in Table 2.1.

2.1 Description of Equipment

The VLF receivers, Model Nos. 101 and 102, were designed and built so as to detect the VLF emissions at five preset frequencies: 400 Hz, 800 Hz, 1500 Hz, 4000 Hz, 8000 Hz, and the broadband signal in the frequency range of 200 Hz to 10 kHz. In addition, a separate undetected output of the whole 200-10,000 Hz band was also provided for tape recording. The six detected and filtered outputs, five at the above preset frequencies plus an overall broadband receiver spectrum, were fed to a multichannel chart recorder. The receivers were built using plug-in printed circuits and boards with linear integrated circuits for all active

TABLE 2.1

Month & the Year of VLF observation	College (Poker Flat)		Bar I (DEW-line station)	
	Days	Reason & Period of Gap	Days	Reason & Period of Gap
	1st to 31st		1st to 31st	
Sept, '69				
Oct		Oct 8-16, '69 Instru. Malfunction		
Nov				
Dec				
Jan, '70				
Feb		Feb 28-Mar 9, '70 Instru. malfunction		
Mar		Mar 14-19, '70 Instru. malfunction		
April				Bar I station oper. from Apr 17, '70
May				
June		June 27-Sept 3, '70 Installation of new receiver		
July				July 20-Aug 19, '70 moving to Elvey building
Aug				
Sept				
Oct				
Nov				
Dec		Terminated on Dec 31, '70 due to high noise		
Jan, '71				
Feb				
March				
April				
May				
June				
July				
Aug				VLF observations terminated on Aug 18, '71

Data Available

elements. All input and output connections to the main receiver were made on the rear panel. Signal level and receiver performance were monitored by means of a meter, a speaker and oscilloscope output on the front panel. The detected signal level on each of the channels could be displayed on the meter on the front panel by connecting the output of the filter card to the meter through the selector switch, also on the front panel. In addition, the power supply voltages at various points in the receiver could be displayed on the meter to aid in isolating a possible receiver malfunction. The receiver was also equipped with a speaker to permit aural monitoring of the undetected broadband signal. An oscilloscope output was also provided to make it possible to monitor the undetected VLF signal at various stages of amplification and filtering throughout the receiver. The test points within the system could be selected by means of another switch on the front panel. All controls to adjust the receiver performance such as the amplifier gains were located inside the cabinet.

A separate high gain preamplifier thermally locked to the ground to help avoid wide temperature changes was mounted at the antenna some distance away from the receiver. The preamplifier was designed to work with a low impedance, single turn loop antenna. The antenna, in the shape of a delta with an elevation of about thirty feet, was oriented such that the normal to the plane of the antenna pointed geomagnetically east-west; thus the system had greater sensitivity to signals propagating in the magnetic meridian plane than to signals propagating in an east-west direction.

The antenna consisting of a single turn of No. 10 stranded wire was

connected directly to the input terminals of the preamplifier. The DC resistance of the antenna was 0.1 ohm. Two RG 58/AU coax cables with BNC connectors and one four wire line with Cannon connectors were then run from the preamplifier to the receiver. These carried the preamplifier output signal, input calibration signal, calibration control and power. A 1 kHz square wave calibration oscillator was built into the receiver for providing a calibration signal. In order to check the constancy of the gain of the entire system, the calibration signals were fed into the input of the preamplifier across a voltage divider. Also, on the Model 102 receiver used at Poker Flat, the input to the preamplifier was short-circuited for 10 seconds as part of the calibration sequence. This gave an indication of the system noise level.

2.2 Circuit Description

2.2.1 Preamplifier

The VLF preamplifier circuit diagram shown in Figure 2.1a consisted of four major sections which were: input matching transformer, input amplifier, 60 Hz notch filter and output amplifier. The amplifier used Fairchild metal cased linear operational amplifiers 709 and 709C for operation over a wide temperature range (-55°C to +125°C). The 60 Hz notch filter was provided to cut down interference picked up from power lines. It was adjustable to the exact line frequency by means of a trimpot on the printed circuit board.

The antenna signal in the low microvolt range was fed through the matching transformer to the input amplifier. This provided a 40 db voltage gain. Next the notch filter gave over 30 db of filtering at 60 Hz. The output amplifier gave 35 db of gain and had a low impedance to the RG 58/AU

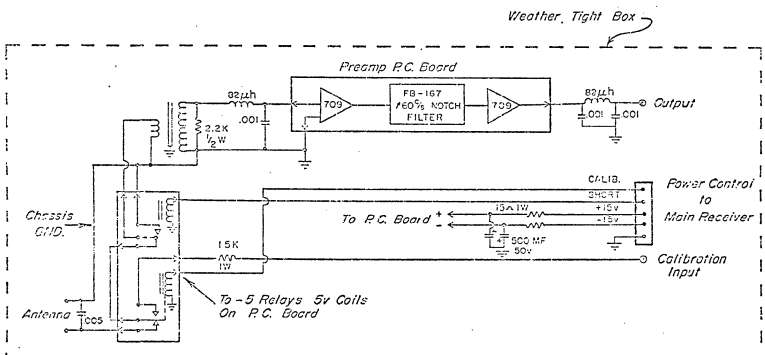

Figure 2.1a VLF Preamplifier

coaxial cable to the receiver.

2.2.2 Receiver

The main receiver card (J9) contained in the VLF receiver circuit diagram (Figure 2.1 b) performed four major functions. First the output of the preamplifier was restricted to the range of 200-10,000 Hz. Second, a 1/f response was provided to correct for the response of the loop antenna. Third, an audio amplifier was added to drive the speaker, and fourth a variable gain amplifier with low impedance output was added to feed the tape recorder.

The receiver input signals were sent to this receiver card through two Kinetic Technology FS-20 hybrid universal active filter units. The first filter was a low pass filter with a cutoff at 10 kHz to eliminate interference from VLF transmitters and the second filter was a high pass filter set at 200 Hz to eliminate interference from power line harmonics. The signal was then fed to a 1/f response shaping amplifier. The feedback circuit of this Fairchild 709C unit contained a capacitance that gave a gain of 26 db at 10,000 Hz and a gain of 60 db at 200 Hz. This output was then fed to the six filter cards.

2.2.3 Filter Cards

Filter cards were provided for each of five preset frequencies and broadband. These cards filtered out signals of a certain frequency from the broadband spectrum. The selected signals were then detected, amplified and fed to the recorder at Poker Flat or the A/D converter at Bar 1. A sixth card (broadband) contained no filter and passed the whole spectrum to be recorded to show the total level of all signals in the receiver passband. Each card, except the broadband, contained an FS-20 filter unit, two 709C amplifiers and a dual diode minimum detector. The gain of the

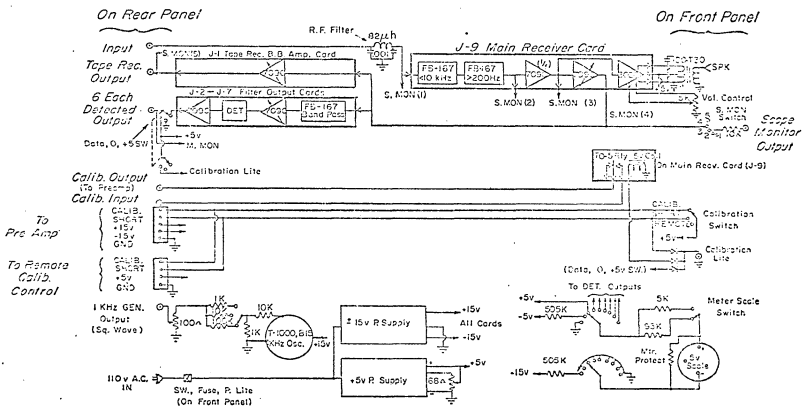

Figure 2.1b VLF receiver model 102

cards was set to 15 db to give outputs in the 0 - 1 volt region.

2.3 Method of Data Collection and Processing

The block diagrams in Figures 2.2 and 2.3 show the complete VLF system at Poker Flat and Bar 1, respectively. The data were collected on chart paper and on magnetic tapes. The time marks on the chart paper and magnetic tapes were provided from a local clock in the case of Poker Flat records and from a radio time standard station for Bar 1 records. Because the timing at Poker Flat relied on a local clock, time marks on the Poker Flat recorder were sometimes in error due to occasional power outages. The chart and tape records were calibrated automatically with a 1 kHz square wave signal of ten seconds duration once each hour. This calibration was found useful for recognizing gain variations. The absolute calibration is described in Section 2.4. Automatic switching to the calibrating signal was accomplished by relays controlled by the time source, which turned off the data and fed the calibration signal into the input of the preamplifier. Calibrations also served to put time marks on the chart recordings. The speed of the chart drive was 1 mm/minute for both stations. Tape recordings were made for the first two minutes after each hour at a speed of 7-1/2 inches per second.

The tape recorder was turned on at the beginning of the calibration sequence. As a result, the calibration tone appeared on the tape and served to delimit the different recording sequences. The operator who changed the tapes voice annotated the tape with the date and time of the day. The times of the recordings were determined by counting the calibration tones. The chart paper was taken off the recorder once every week and the times and dates were clearly printed on the records. The magnetic tape was changed once every day and was monitored on a day to day

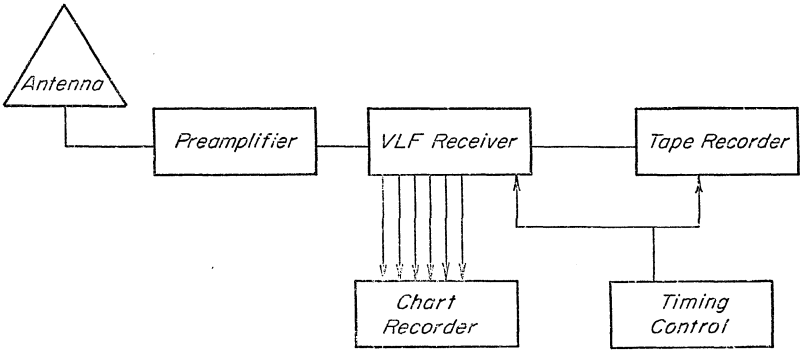

Figure 2.2 Block diagram for Poker flat, College VLF system

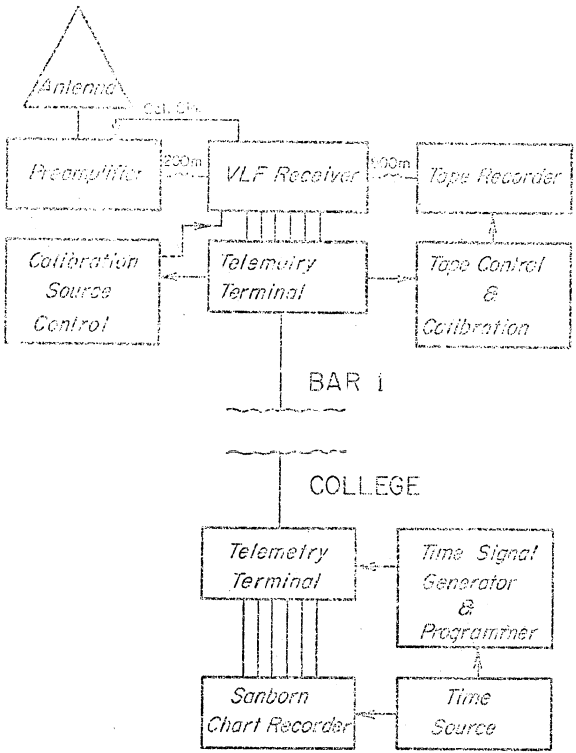

Figure 2.3 Block diagram for Bar 1 system

routine basis to identify the VLF emissions and also to spot check on the visual chart records. The tape recorder at Poker Flat was not operated during weekends.

In the case of Bar I observations, the data were sent to and recorded at College through a telemetry system. The system had a decimal A/D converter that converted voltages between 0 and 2 volts from the VLF receivers to numbers between 1 and 200. Each of the six channels of the detector outputs were sequentially sampled three times per second giving a 1 cps response on the chart recorder. A log book record was maintained for identification of any VLF emission on the chart record. The magnetic tapes also enabled identification of many emissions when aurally monitored throughout the course of these observations. A separate log book was established to report what had been heard from the tapes. From the magnetic tapes it was extremely easy to recognize chorus emissions because of their characteristic sound like the chirping of birds, but hiss could be identified only on a few occasions. Chart records, however, clearly indicated the hiss emissions.

2.4 Calibration and System Sensitivity

The purpose of this section is to describe the system calibrations that permit the interpretation of the chart records in terms of the incident field strength of the signal. The curves thus obtained are used for determination of the sensitivity of our ground VLF systems in terms of the incident field strength and estimate the threshold of detectable flux (watts $m^{-2}Hz^{-1}$). The voltage at the input of the preamplifier, V_m, corresponding to the voltage induced in the antenna, V_i, is a function of antenna and receiver characteristics and is given by:

$$V_m = \frac{R_r V_i}{\left[(R_r + R_a)^2 + (2\pi f L_a)^2\right]^{1/2}}, \qquad (2.1)$$

where L_a is the antenna inductance and R_r and R_a are resistances of the receiver input and antenna respectively. Equation (2.1) is obtained by neglecting the radiation resistance and ground losses. Values of R_r, R_a and L_a have been experimentally determined and are taken as 0.76 ohm, 0.1 ohm and 30 micro henries respectively. Substituting these values in equation (2.1), V_m can be determined in terms of V_i at each center frequency f.

Let E_o be the electric field strength of the signal incident on the antenna. Assuming the magnetic-vector is normal to the plane of the antenna for a monochromatic signal, the induced voltage V_i is related to the electric field strength E_o by

$$V_i = E_o h, \qquad (2.2)$$

where h is the so called effective height of the antenna. The effective height of the loop antenna can be obtained from the following relation:

$$h = \frac{2\pi}{\lambda} S n, \qquad (2.3)$$

where

n = number of turns in the loop = 1,

λ = wavelength of the signal

and

S = area of the loop = 41.8 m^2.

If the signal is assumed to be a white noise, the induced voltage V_i in a band Δf is given by

$$V_i = E_o h \sqrt{\Delta f} \quad . \qquad (2.4)$$

It is appropriate to consider the passband as equivalent to a rectangular passband of constant gain and a bandwidth of Δf where Δf is the 3 db

bandwidth of the actual system. From the calibration curves, the bandwidth at each receiver channel can be easily determined. Calibration curves for both models 101 and 102 have been drawn from the knowledge of DC output voltages from the filter cards for a fixed input voltage to the preamplifier and are shown in Figures 2.4 and 2.5 respectively. Full scale deflection on the Bar I (101) chart records corresponds to DC output voltage of 1 V, while full scale on the College (102) receiver corresponds to 5V DC. From equations (2.1) and (2.4) we get

$$E_o = \frac{V_m}{h\sqrt{\Delta f}} \left[\frac{R_r}{\left[(R_r + R_a)^2 + (2\pi f L_a)^2 \right]^{1/2}} \right]^{-1} \quad (2.5)$$

V_m can be determined in terms of chart deflections from the calibration curves at each receiver channel. Equation (2.5) then gives us the incident electric field strength as a function of deflection on the chart paper. The results are plotted in Figures 2.6 and 2.7 for receiver models 101 and 102 respectively. From the knowledge of E field corresponding to a certain deflection on the chart paper, the power flux of the signal P_o can be obtained and is given by the relation

$$P_o = \frac{E_o^2}{377} \text{ (watts } m^{-2} Hz^{-1}). \quad (2.6)$$

The sensitivity threshold of the receiver is defined to be the ambient noise level detected by the receiver. Computations of the threshold of detectable flux (Table 4.2) for VLF hiss events reported in Chapter IV and during periods of satellite VLF emission (Table 5.1) reported in Chapter V have been performed by using curves in Figures 2.6 and 2.7 with due regard

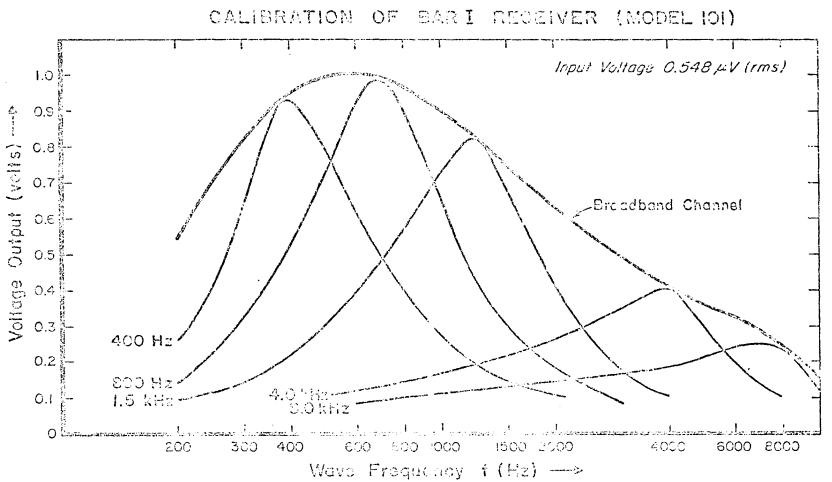

Figure 2.4 Calibration curves for various frequency channels for Bar I receiver (Model 101)

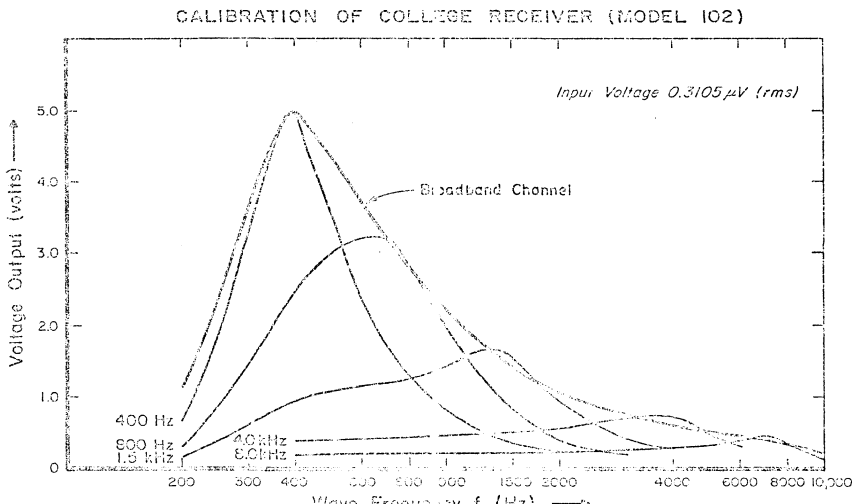

Figure 2.5 Calibration curves for various frequency channels for College receiver (Model 102)

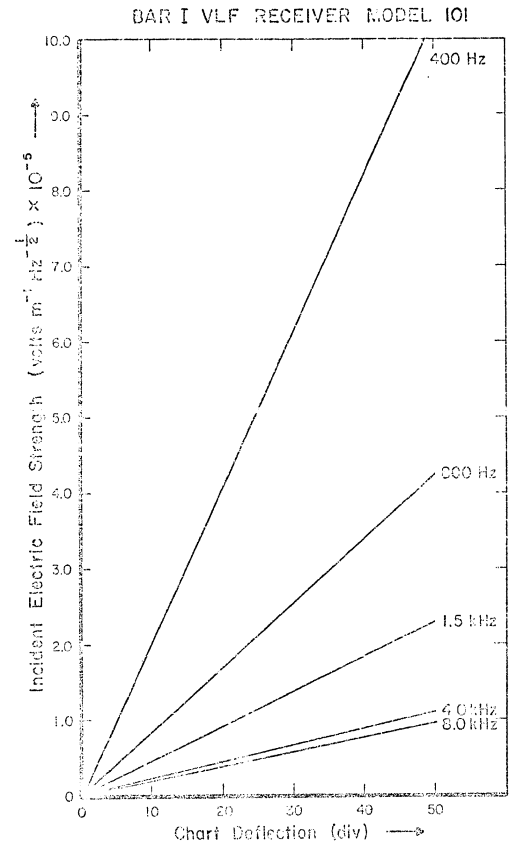

Figure 2.6 Curves showing the incident electric field strength of the signal at VLF center frequencies vs chart deflection for model 101 receiver

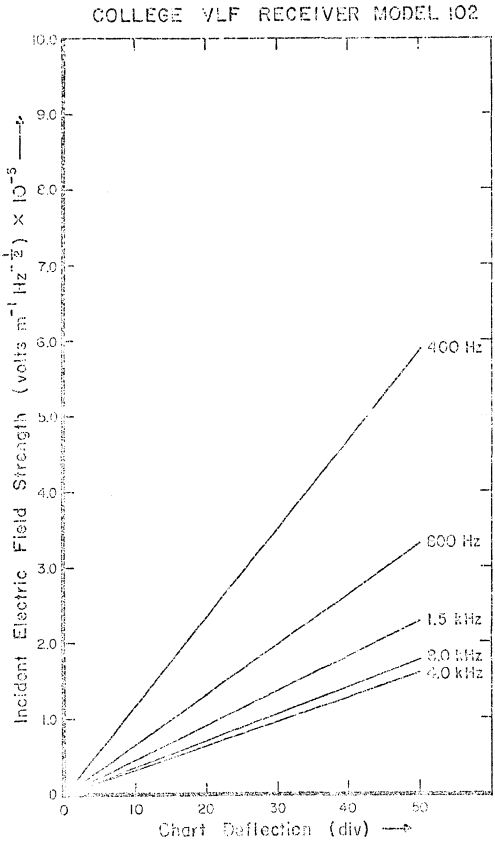

Figure 2.7 Curves showing the indident electric field strength of the signal at VLF center frequencies vs chart deflection for model 102 receiver

to the base level at each receiver channel established by the ambient noise. Sensitivity calculations are useful to determine whether the system is capable of detecting the emission of certain strength depending upon the ambient noise level at the time of the event.

CHAPTER III

MORPHOLOGY OF CHORUS EMISSIONS

3.1 Statistical Analysis

Very low frequency radio emissions in the range of 400 Hz to 8 kHz were observed frequently on the College and Bar I chart records and by listening to the magnetic tapes. Although various types of emissions were also contained in the received data, we were primarily concerned with hiss and chorus. It was relatively easy to identify chorus from the tapes because of the narrow frequency band which the human ear can readily discriminate, while hiss is difficult to discriminate on the tapes because of its broadband character which blends in with the other background noise. In addition, since hiss is relatively a short duration phenomenon in contrast to chorus, it often missed the tape recording interval. The recording of the VLF emissions on magnetic tapes was particularly useful for analysis of their time vs frequency relationships whereas the chart records provided a continuous monitoring of the data and gave information about the time of the event and its intensity, etc. Log book records of the VLF emissions for each station prepared from listening to the tapes and the spectral analysis from film records showed the following characteristics:

1. Spectral analysis from the recorded broadband noise points out that chorus occurs mostly in the range of 1 to 5 kHz and is, sometimes, also accompanied by an ELF hiss background which could be recognized from its characteristic sound of wind blowing through pine trees.

2. Chorus is usually a late morning phenomenon occasionally extending into the afternoon periods with a peak around 1100 hrs local

time averaged over all the months, whereas hiss usually occurs during the late evening hours.

3. Some seasonal variation of chorus is also apparent as seen from the histograms plotted for each month against local time and the magnetic activity index K_p in Figures 3.1 and 3.2 respectively for College data taken in 1967-68. The plots show that the maximum chorus activity on the surface of the earth is higher in the local winter months (September to April) compared to the summer months May to August), which possibly is due to the higher ionospheric electron density in the summer.

4. Figure 3.2 shows the % occurrence of chorus emissions as a function of K_p for the various months of the year. From the figure, it can be seen that the occurrence of chorus is rather independent of the level of geomagnetic activity. Figure 3.3 shows a plot of % occurrence frequency of chorus against local time for various K_p values. Except for $K_p = 0$, a definite diurnal variation of chorus emission can be seen, which is relatively independent of the value of K_p.

5. There appears to be a lack of occurrence of all VLF emissions in the early morning periods (0200-0600 150°WMT) with a few exceptions. One significant exception occurred during a great magnetic substorm on March 8, 1970. This was analyzed in detail (Srivastava and Swift, 1971) and is reproduced in Appendix A.

6. A summary report of VLF events for both College and Bar I, given in Table 3.1, indicated that occurrence frequency of VLF hiss events is much higher at Bar I than at College while the reverse is true for chorus and ELF hiss. Also the presence of VLF emission at one station does not appear to be correlated with its presence at the other station, i.e.,

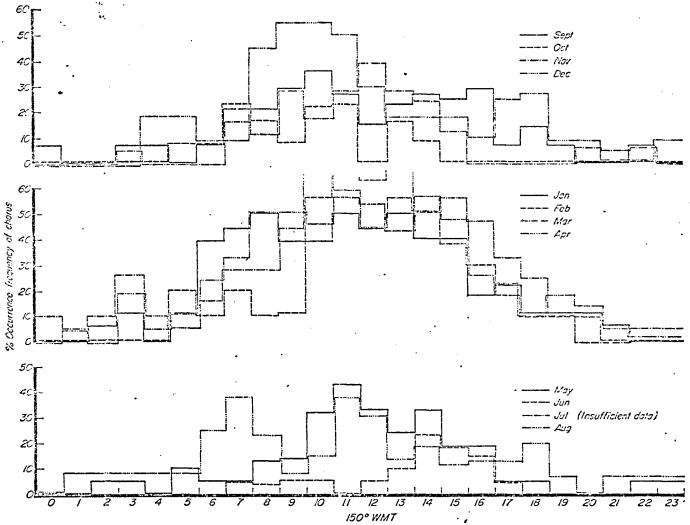

Figure 3.1 Histogram for % occurrence frequency of chorus for various months vs local time

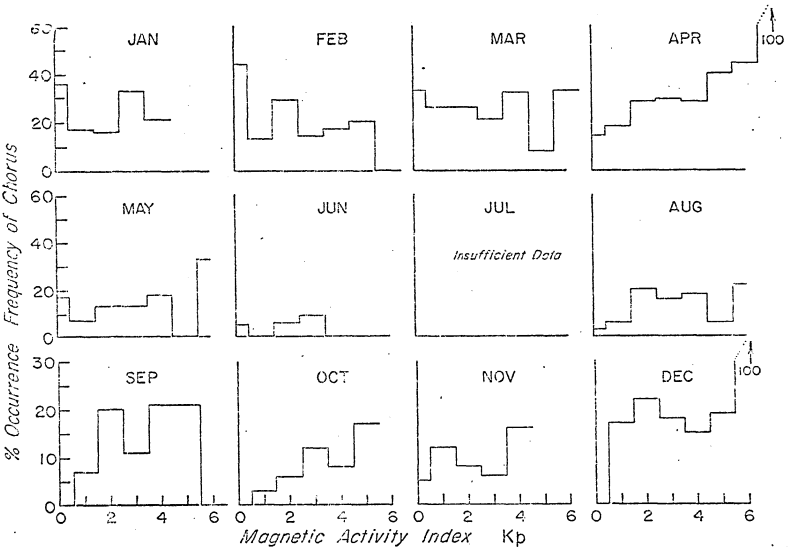

Figure 3.2 Histogram for % occurrence frequency of chorus for various months vs Kp

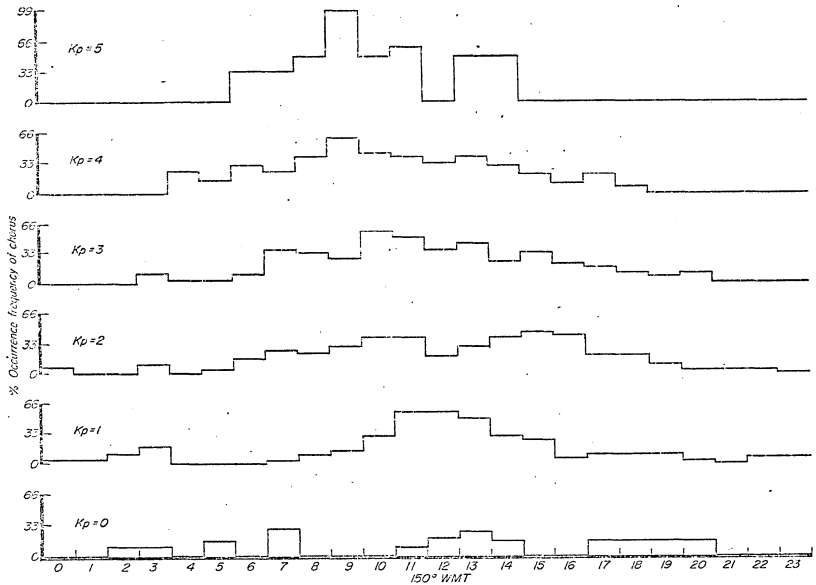

Figure 3.3 Histogram for % occurrence frequency of chorus vs local time for various Kp values

TABLE 3.1

Source of identif.	Poker Flat VLF Station: Period of observation	Total Events	Hiss or Chorus*	%Occurr#	Mode of identif.	Bar I VLF Station: Period of observation	Total Events	Hiss or Chorus*	%Occurr#	Mode of identif.
Log book	Aug 26, '69 to Jan 4, '71	86	Chorus 70 Hiss 16	81 19	By aurally monitoring the magnetic tapes	April 17, '70 to Jan 31,'71	43	Chorus 22 Hiss 21	51 49	By aurally monitoring the magnetic tapes
Chart records	April 20 '70 to Jan 4, '71	59	Chorus 31 Hiss 28	52 48	According to the time of their occurrence	April 17 '70 to Jan 31, '71	64	Chorus 11 Hiss 53	17 83	According to the time of their occurrence
Both Log book and chart records	Apr 20, '70 to Jan 4, '71	28	Chorus 24 Hiss 4	86 14	Events simultaneously present in the chart as well as heard on the tapes	Apr 17, '70 to Jan 31, '71	15	Chorus 7 Hiss 8	47 53	Events simultaneously present in the chart as well as heard on the tapes

* Few of the events contain both chorus and ELF hiss at the same time.

\# The % occurrence is with respect to the total number of events that have occurred during the period mentioned.

there is a lack of simultaneous occurrence for most of the emissions at the two VLF sites. There were very few examples of both stations recording the same VLF event. This indicates that either the emissions are localized in latitude or that different ionospheric conditions may prevail over the two stations on the same geomagnetic meridian or both.

The statistical analysis of chorus emission does not show any particularly noteworthy trends. If the occurrence of chorus depended strongly upon ionospheric electron density, then diurnal and seasonal variations would similarly reflect the amount of ionizing solar radiation incident on the ionosphere. However, Figure 3.1 shows peaks in the occurrence of chorus during the daylight hours but a seasonal minimum during the summer months. Russell et al. (1969) in their OGO 3 survey of ELF noise in the magnetosphere indicate a high frequency of occurrence in the 0600 to 1800 sector of the magnetosphere. Since the OGO 3 survey was taken well above the ionosphere, we may presume that the diurnal variations indicated in Figures 3.1 and 3.3 reflect more the variaiton in the conditions responsible for the generation of chorus emissions rather than variations in propagation conditions within the ionosphere. However, since chorus is generated deep within the magnetosphere, considerations of symmetry between the northern and southern hemispheres of the magnetosphere would indicate that a seasonal dependence of the generation of chorus is unlikely. This suggests that the seasonal dependence of chorus observations is controlled primarily by ionospheric propagation conditions.

The insensitivity of our chorus observations to magnetic activity suggests either that the two phenomena are not related or that the occurrence of chorus is controlled by two competing effects. The latter

possibility might result from chorus generation being enhanced during periods of high magnetic activity, and the ionosphere becoming more opaque to the transmission of ELF/VLF emissions during these same disturbed periods.

3.2 Latitudinal Variations

Analysis of chorus events recorded at College and Bar I during a period of observation from 19 April 1970 to 31 December 1970 has revealed a latitudinal variation of chorus activity as a function of K_p. This is indicated by Figure 3.4, which is a plot of % occurrence frequency of chorus against the magnetic activity index K_p for both College and Bar I on the same scale. It can be seen from Figure 3.4 that the number of chorus emissions per unit time for a particular value of K_p is much less at Bar I than at College. To draw Figure 3.4, we considered all the chorus events found by listening to the magnetic tapes from both the VLF stations during the same period of observation, in a time period of 0600-1600 150°WMT which is when chorus usually occurs. The % frequency was determined by using the relation $(N_c/N_o) \times 100$, where N_o is the total number of observations for a particular K_p in the time range as mentioned above and N_c is the total number of chorus events for the same K_p and time range.

A comparison of chorus events from College and Bar I was also made as a function of local time and is shown in Figure 3.5. The % occurrence frequency here was determined by summing up the number of observations and chorus events separately for the same time irrespective of the K_p value. Parallel variations in the frequency of chorus emissions against time for both stations can be seen in Figure 3.5, with an exception at 1000 hrs. As is apparent from Figure 3.5, both College and Bar I peak around 1200 hrs local time.

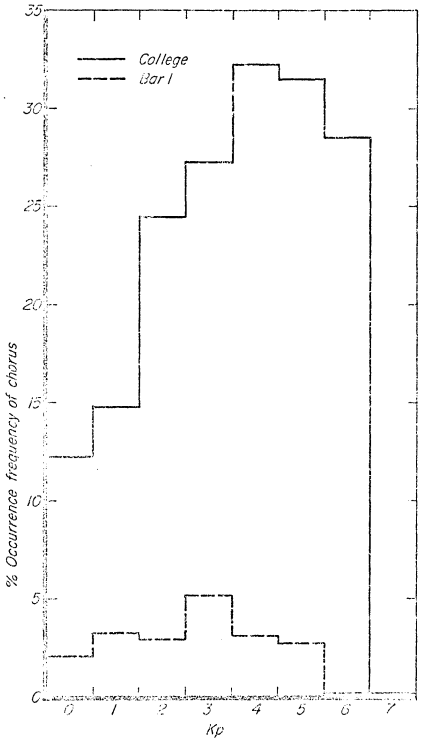

Figure 3.4 Histogram for % occurrence frequency of chorus against magnetic activity index Kp for College and Bar I VLF station

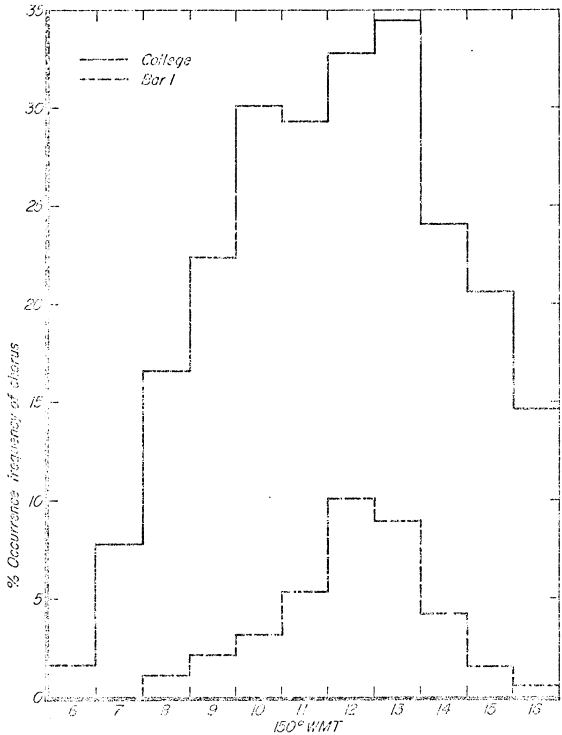

Figure 3.5 Histogram for % occurrence frequency of chorus against local time for College and Bar I VLF station

3.3 Results and Discussion

It is found from observations of chorus at College and Bar I that this discrete noise below approximately 4 kHz tends to decrease poleward of the auroral oval and occurs mainly on the dayside of the earth equatorwards of the central statistical region of auroral activity. It is also known experimentally through satellite observations that chorus emissions are correlated with energetic particle (> 40 kev electrons) precipitation in the daytime auroral zone atmosphere. Ground observations of chorus emissions are found to be inconsistent with the general level of magnetic activity as indicated by K_p index. This may be due to the ionosphere becoming more opaque to the transmission of ELF/VLF emissions during these same disturbed periods. However, it does not rule out the possibility that magnetic substorm control of chorus emissions and subsequent electron precipitation in the auroral zone atmosphere are related. The theory suggested by Swift (1968) that the energy source of chorus emissions and of consequent electron microbursts is the free energy associated with a loss-cone distribution in the ring current seems to adequately explain the morphology of chorus emissions.

Observations of VLF emissions by Injun 3 satellite (Gurnett and O'Brien, 1964) have shown that the amplitude of chorus has a marked latitude variation with a maximum at an L value of 5 (L is the distance in earth radii from the center of the earth to the point where a magnetic field line crosses the plane of the geomagnetic equator). Although our analysis of ground VLF emissions do not pertain to a similar study, latitudinal variation of chorus is quite apparent from the VLF data at two stations on the same geomagnetic meridian.

CHAPTER IV

VLF HISS AND THE VISUAL AURORA

Detailed morphological relationships between VLF hiss, observed at two ground auroral zone stations at College and Bar I, and aurora are investigated in association with all-sky camera data. A number of examples of VLF hiss bursts coincident with the overhead passage of auroral forms were observed and the case histories of a few individual events are described in this section (Figures 4.I to 4.II). The data chosen for intensive analysis cover the period from September to December 1970 which was the only period when both the VLF stations were functioning in conjunction with the operation of all-sky cameras (ASC) at College and Inuvik NWT. A few events during the winter months of 1969-1970, when only the College station was operating, were also studied. For the purposes of carrying out comparison studies, it should be mentioned that there was no all-sky camera operation at the Bar I VLF site. Therefore, ASC pictures from Inuvik, which is 301 km from Bar I and the closest station with an ASC, were used to observe aurora occurring overhead at Bar I, whose position on the Inuvik ASC pictures is indicated by means of a cross in Figures 4.3 and 4.4.

4.I Observations

During the four months of simultaneous operation, a total of I8 hiss events were recorded at College while the VLF station at Bar I recorded 25 hiss events. The details of this with respect to the visibility of aurora are summarized in Table 4.I. Hiss events as listed in the table were recognized primarily from the chart records since almost all of them occurred outside the two minute period after the hour

when the tape recordings were made. It is worthwhile to note from the table that the occurrence of cloudy nights, no operation or no film, and equipment problems, etc., do not rule out the possibility that the aurora was present during the VLF event.

Table 4.I clearly indicates, as is consistent with other studies (Morozumi, 1962; Jørgensen and Ungstrup, 1962; Harang and Larsen, 1965; Morozumi and Helliwell, 1966), that the presence of VLF hiss is generally associated with auroral activity overhead although sometimes aurora may not be observed because of cloudy sky conditions or instrumental failures, etc. There did not occur even one event during the present period of study that showed hiss without aurora. The converse, however, was not found to be true since there had been a few occasions during these four months where an intense display of rapidly moving auroral forms did not produce detectable hiss. This is completely analogous to a study of radio emission in the frequency range of 1 to 7 MHz by Parthasarthy and Berkey (1964) who attribute the emission to auroral electrons. Examples of auroral substorm activity at College with no indication of VLF hiss on the chart records are shown in Figures 4.9 - 4.11. Since ground reception of VLF signals is dependent on many factors such as the source of emission (i.e., type of particle precipitation causing both aurora and hiss), behavior of the ionosphere and propagation conditions in the medium, etc., the appearance of auroral forms seems to be a necessary but not a sufficient condition for the production of hiss.

We shall determine, from comparison of ground VLF hiss records with visual aurora as seen through the all-sky camera, the different features in both records under normally quiet and geomagnetically disturbed periods

by studying a few individual cases in detail. General relationship between riometer absorption and VLF hiss will also be studied.

TABLE 4.1

Description	VLF Station		Remarks
	College	Bar I	
Total hiss events*	18	25	As seen on chart records
Aurora present	8	7	Inuvik ASC was used for Bar I
	-	3	ASC clock stopped
Cloudy nights	6	9	
No photographic auroral data	4	6	ASC not operating

* These events are for the period September - December 1970.

4.2 Comparison Studies

While comparing the VLF data obtained at the two stations situated at different locations on the same geomagnetic meridian, this sample of events indicates that VLF hiss occurs more frequently along the poleward rather than equatorward edge of the auroral oval. This conclusion should be regarded as being rather tentative at this stage given the small statistical sample. Two of the most remarkable features seen on the College and Bar I hiss records are as follows:

1. Hiss events seem to occur more frequently at Bar I than at College. In most instances when hiss is present at College, it is not observed at Bar I and vice-versa. Of all the hiss events listed in Table 4.1 during the four month period, only three nearly simultaneous events with slight mismatch of timings were seen on both records. There was one occasion,

however, on November 25, 1970, when exact simultaneous occurrence was noticed. Unfortunately, this event could not be analyzed with respect to aurora because the College station was very cloudy, and the clock of the Inuvik ASC was not functioning.

2. Three examples of the events of auroral activity along with the substorm, found during the four month period when there is no VLF in the time interval of 1800-0100 150°WMT, are displayed in Figures 4.9 - 4.11. It is also found that sudden brightening of the auroral form or the overall brightening covering the entire field of view of the camera very often coincides with the peak hiss emission. Examples of this behavior for some of the hiss events are given later in the form of illustrations showing chart records of the hiss events and corresponding all-sky camera photographs.

Hiss records for two different dates, October 18, 1970 (0817-0823 UT) and December 14, 1970 (0739-0748 UT) from College, are shown in Figures 4.1 and 4.2. These two dates were selected for more detailed analysis because good VLF and all-sky camera data were obtained concurrently. Others were left out because the all-sky camera pictures for those dates had too much interference from moonlight or clouds. For the same reasons, the dates selected from Bar 1 records were November 10, 1970 (0526-0530 UT) and November 11, 1970 (0410-0413 UT) and are shown in Figures 4.3 and 4.4. Unfortunately, these four events did not occur within the two minute interval, after the hour, when a tape recording is made, however, they are distinct on the chart records. The all-sky camera pictures for corresponding stations for all events are shown above the hiss records.

Although all these events occurred during a period when it was

magnetically active, later examples (Figures 4.5 - 4.8) show hiss during no magnetic substorm. This shows that there is little or no correlation of VLF hiss with magnetic activity index Kp. All we can say is that the probability of observing the VLF emission is much higher when a geomagnetic disturbance occurs. The three-minute scaled values for the H-component of the magnetogram for each of the selected dates are plotted and shown in Part (c) of every figure. VLF data have also been compared with the 30 MHz riometer records. Magnitudes of riometer absorption in db at a few points during the time of each VLF event have been computed for this purpose. The summary is presented in Table 4.2. Threshold of detectable flux (watts $m^{-2}Hz^{-1}$) at each receiver channel where data is displayed in Figures 4.1 - 4.11 and the peak power flux of the event have also been calculated and are included in Table 4.2. VLF data are divided into three sets corresponding to the geomagnetic and auroral conditions during the occurrence of hiss events. There are four different hiss events considered in Set A which occurred during high geomagnetic and auroral activity. Set B is comprised of another four events which were present during magnetically quiet periods under relatively quiet auroral arc situation. Three cases have been included in the study as counter examples (Set C) where we do not find any VLF hiss event on the ground during periods of auroral and slight magnetic activity. Values of the sensitivity threshold for events in Set No. B, during the period when Lockheed receiver was in operation, were not computed since the calibrations for that receiver were not available. Set C is described in Section 4.5.

4.3 Description of Individual Events

The time resolution available for the hiss records is one minute for both College and Bar I whereas for all-sky camera records it is half

TABLE 4.2

Set No.	Date of hiss event observed on the ground	Period of VLF hiss event in (UT)	Observing ground VLF station	Threshold of detectable flux (watts $m^{-2}Hz^{-1}$) Rec.. Chan (kHz)		Peak Power flux of VLF data (watts $M^{-2}Hz^{-1}$)	Magnitude of riometer absorption in (db) during the time of event
A	Oct 18, 1970	0817-0823	College	0.8 1.5 4.0 8.0	6.6×10^{-16} 6.6×10^{-16} 2.4×10^{-16} 3.2×10^{-16}	4.2×10^{-14} 1.0×10^{-13} 4.4×10^{-14} 3.2×10^{-14}	Bad record (interference)
	Dec 14, 1970	0739-0748	College	1.5 4.0 8.0	4.5×10^{-15} 9.5×10^{-15} 2.9×10^{-15}	2.1×10^{-13} 1.1×10^{-13} 1.3×10^{-13}	0735 ∿ 0.34 0742 ∿ 4.8 0744 ∿ 2.0 0745 ∿ 1.6 0748 ∿ 3.0
	Nov 10, 1970	0526-0530	Bar 1	4.0 8.0	1.1×10^{-16} 9.5×10^{-16}	2.4×10^{-16} 2.4×10^{-16}	0530 ∿ 1.3
	Nov 11, 1970	0410-0413	Bar 1	4.0 8.0	1.1×10^{-16} 9.5×10^{-16}	2.4×10^{-16} 2.4×10^{-16}	0413 ∿ 0.34 0414 ∿ 1.25 0415 ∿ 2.4
B	Nov 20, 1969	0935-1100	College	—	—	—	—
	Dec 12, 1969	1126-1226	College	—	—	—	1224 ∿ 0.36 1226 ∿ 0.86 1230 ∿ 1.2
	Jan 5, 1970	0927-1008	College	—	—	—	—
	Feb 5, 1970	0956-1011	College	—	—	—	—
C	Oct 11, 1970	0600-1000	College	0.4 0.8 1.5 4.0 8.0	4.4×10^{-15} 5.0×10^{-16} 6.0×10^{-16} 2.0×10^{-16} 2.0×10^{-16}	—	0700-0800 ∿ 0.44 0800-0855 ∿ 0.8 0930 ∿ 0.25
	Nov 9, 1970	0700-1000	College	0.4 0.8 1.5 4.0 8.0	4.4×10^{-15} 2.6×10^{-16} 9.0×10^{-16} 2.0×10^{-16} 2.0×10^{-16}	—	0930 ∿ 0.17 0940 ∿ 0.25 0950 ∿ 0.53
	Dec 8, 1970	0600-1100	College	0.4 0.8 1.5 4.0 8.0	4.4×10^{-15} 1.0×10^{-15} 6.0×10^{-16} 1.6×10^{-15} 2.0×10^{-16}	—	Bad Record (Interference)

a minute for College and one minute for Inuvik. Because the timing at the College VLF site relied on a local clock, time marks on the College recorder were sometimes in error due to occasional power outages. All the timings hereafter will refer to universal time for describing the individual events.

4.3.1 October 18, 1970

Figure 4.1 shows this event, as seen through the all-sky camera pictures, which corresponds to a period of active aurora with large changes in intensity. Although there was some interference from moonlight and clouds, the auroral forms were still visible. The aurora actually started with a long, thin and faint arc at 0810:30 in the south-west sector of the picture and diffused in the next half minute. At 0812 again there appeared a faint glow in the same position becoming an arc in the next half minute which moved slowly westward. At 0813, the same arc became more apparent, became brighter at 0813:30 and 0814 it split into two arcs, moved towards the center of the all-sky camera picture and became brighter. At 0814:30 the sky became very bright with a bright form extending east-west and the activity appeared to be the most intense at this point. The peak hiss intensity appears to coincide with the maximum brightness of the auroral forms in the zenith and the onset of the negative bay. Thereafter, both the hiss and auroral intensities appear to diminish although the negative bay persisted for another twenty minutes. The most striking feature of this example is the simultaneous variation in the intensity of the aurora and the hiss emission. Absorption during this event could not be found because of the bad riometer record. However, the input power flux at the peak of this event exceeds the detectable

threshold flux by about two order of magnitude and the event becomes readily observable on the VLF channel records in Figure 4.1.

4.3.2 December 14, 1970

This event at College, Figure 4.2, is another good example which illustrates the occurrence of hiss emission immediately following a rapid brightening of the aurora. The ASC pictures at College show that aurora had been present from 0640. The first clear form appeared at 0712:30 in the south. During the next few minutes it moved poleward of the camera's zenith. At 0721:30, 0724 and 0724:30 there were several distinct forms that did not appear to brighten enough to be associated with the sudden impulsive start of the hiss emission. From 0739 to 0724, the aurora showed large fluctuation in intensity that faded out after 0742. Here the hiss emission started at 0739 coincident with the brightening and remained for about ten minutes. Comparison with the magnetogram indicated that the hiss occurred during the maximum epoch of the magnetic substorm. It can be seen from Table 4.2 that riometer absorption is present to a considerable extent during this event. In fact, the hiss emission starts during 0735-0742 when absorption grows from 0.3 to 4.8 db. The two, therefore, seem to be positively correlated in the beginning, but hiss practically vanishes after 0748 where absorption is 3.0 db and continues further. Table 4.2 indicates that the peak power flux for this event is of the order of 10^{-13} watts $m^{-2}Hz^{-1}$ which makes it likely that the emission had been quite strong to sustain heavy riometer absorption or had penetrated the ionosphere outside of the riometer antenna beam.

4.3.3 November 10, 1970

This hiss record from Bar 1, Figure 4.3, can be seen on the 4000 and

8000 Hz channels. We have used the all-sky camera records from Inuvik to check on auroral conditions during this event. A thin long auroral form aligned east-west in the southern sky could be seen to appear around 0510 and remained very quiet at the same location until 0525. In the very next minute at 0526, coincident with the onset of hiss event, the form split into two arcs moving rapidly poleward and accompanied by a sudden brightening. The brightening sequence continued from 0529 to 0532 after which the auroral display became patchy and inactive until it ended at 0542. One thing to note here is that at 0527 a westward traveling surge also started along with the northward motion of the aurora and filled the entire field of view within three to four minutes. The hiss event began at 0526 and lasted until 0530. This event suggests that the westward traveling surge Inuvik to Bar I was associated with the emission of VLF hiss. It is significant that the hiss event began somewhat in advance of the poleward expansion of the auroral forms.

4.3.4 November 11, 1970

Figure 4.4 shows this event at Bar I beginning at 0410 which could be seen only on the 4000 Hz channel. It was again a short duration event, and was not very intense. The Inuvik ASC pictures showed once again the auroral forms appearing at 0407 in exactly the same fashion as the situation had developed on the previous day. At 0410 again the westward traveling surge appeared, became intense at 0411 and 0412 and at 0413 the entire aurora started moving north as it did on November 10, 1970. At 0414 it started becoming diffuse and from 0415 onwards the aurora became a thin form again, aligned east-west but this time in the northern sky. After a while this form moved to the south but this activity did not produce any

hiss. For this event again the occurrence of hiss on the chart record corresponds very well with the auroral brightening sequence. The small magnetic bay at 0412 appears to coincide rather well with the hiss emission. It should be noticed from Table 4.2 that the power flux of events on both November 10, 1970 and November 11, 1970 is 2.4 x 10^{-16} watts $m^{-2}Hz^{-1}$ whereas the threshold of detectable flux is 1.1 x 10^{-16} and 9.5 x 10^{-16} watts $m^{-2}Hz^{-1}$ at 4.0 and 8.0 kHz channels repectively. Since the signal power flux is more than the threshold at 4.0 kHz and less at 8.0 kHz channel, the events are observed on the 4.0 kHz channel but are relatively invisible on the 8.0 kHz channel in Figures 4.3 and 4.4. Although, Bar I riometer records are not available for these events, College records show little or no absorption. However, the riometer records from Inuvik NWT indicate that after the absorption values reached 1.3 and 1.25 db on November 10 and November 11, 1970 respectively, the VLF emissions had completely vanished.

All examples given above indicate that before and during periods of intense auroral brightening, the auroral and the hiss intensities tend to show a simultaneous variation but the hiss intensities drop practically to zero after the brightening sequence is over. The most interesting feature to note is that in all four cases the occurrence of hiss corresponds to a motion of east-west aligned auroral arcs from south to north, i.e., the brightening of the arc is followed by its rapid poleward expansion. This is also the time when the sharp onset of a negative change in the horizontal component of the earth's magnetic field is observed in the region where the brightened arc is located and also in the region swept by its poleward motion (Akasofu, 1966). Since all these four events took place either just before or during the expansive phase of the magnetic substorm, it appears that the impulsive character or the sudden onset of auroral hiss occurs at the time of brightening and

stays for a short time during the poleward expansion phase of the substorm.

4.4 Hiss During Quiet Periods

The selected hiss events observed during winter months of 1969-70 at College in association with the College all-sky camera pictures during relatively quiet periods are November 20, 1969 (0935-1100 UT); December 12, 1969 (1126-1226 UT); January 5, 1970 (0937-1008 UT) and February 5, 1970 (0956-1011 UT) and are shown in Figures 4.5 - 4.8. It is to be noted from their magnetograms that there is no apparent substorm activity during the period that VLF hiss is reported but the all-sky camera pictures do show auroral activity. In almost all cases the auroral forms were seen to appear on the northern horizon stretching east-west. There was not much movement but intensity fluctuations were noticed. These figures do, however, indicate that VLF hiss can be received on the order of 500 km from the field lines where the emission is generated. In these examples, it is also worth noting that the hiss emission was not accompanied by any obvious magnetic disturbance. Even the magnetograms from Inuvik and Barrow which are at higher latitude than College did not indicate any particular substorm activity at the time of the recorded hiss event. It is indicated from Table 4.2 that examples of VLF hiss on November 20, 1969, January 5, 1970 and February 5, 1970 do not show any riometer absorption. However, the particular event on December 12, 1969 does have some riometer absorption. Figure 4.6 shows that hiss is present from 1126 to 1226 along with some development of a small negative bay around 1215 and some brightening of the auroral arc which moves towards zenith at 1220. While there is no absorption from 1126 to 1222 during the event, it becomes apparent from 1222 onwards with values of 0.86 db at 1226 and 1.2 db at 1230. The

example does not indicate any peak to peak correspondance between VLF hiss and riometer absorption but shows complete cesession of hiss after absorption reaches a value of 0.86 db at 1226. This event is contradictory to the event of December 14, 1970 where VLF hiss is observed during riometer absorption of 4.8 db which tends to show that there is no consistent relationship between VLF emissions and riometer absorption. However, the fact that the events occurred under different ionospheric conditions point out that the propagation of VLF emissions through the ionosphere under different auroral and geomagnetic activity plays an important role in establishing the proper limits to observing VLF emission on the ground.

Gurnett and Frank (1972) and Gurnett (1966) have published comparisons between VLF hiss and auroral electron precipitation. It is pointed out that the equatorial boundary of the hiss zone and the precipitation zone appear to coincide to within a degree or two of latitude at an altitude of about 2000 km. It is also known that at VLF frequencies the ray path can only deviate 19° from the field line (Stix, 1962). From the fact that the ray energy direction or the ray path is highly collimated about the magnetic field line, a simple calculation permits one to show that the VLF hiss propagating from 2000 km down to auroral heights at 100 km above the earth could be observed equatorward about 6° in latitude from the field line where it was observed by the satellite. The extent of latitude roughly corresponds to about 680 km over the earth's surface. Therefore, an interesting question is whether the hiss observed in the events displayed in Figures 4.5 - 4.8 could have propagated from the source directly to the receiver or whether the hiss must have propagated down the field line and then through the earth-ionosphere waveguide to

the receiver. Since the receiver is less than 680 km from the field lines which pass through the auroral forms in Figures 4.5 - 4.8, we conclude that the observed hiss could have propagated directly from the source region, assuming it is above 2000 km.

4.5 Counter Examples

For all of the hiss events observed during periods in which aurora could be seen, aurora was always observed. This naturally raises the question of whether there are intense auroal displays when hiss is not observed. Figures 4.9 - 4.11 show examples in which intense auroral activity appeared overhead accompanied by magnetic substorm activity and in which no hiss was observed. Table 4.2 indicates the presence of some amount of absorption during these events. Since the auroral and magnetic substorm activity shown in these examples was similar to the conditions shown in Figures 4.1 - 4.4, it is likely that hiss was also generated during the events shown in Figures 4.9 - 4.11. Moreover, the VLF data taken by the INJUN 5 satellite (Gurnett and Frank, 1972; Gurnett, private communication) indicate that hiss is almost always present on the auroral oval above the ionosphere. This leads us to conclude that the controlling factor in whether or not hiss is observed, is the propagation condition in the ionosphere.

4.6 Conclusions

Analysis of auroral and hiss events at College and Bar I has very clearly established a general relationship between the two. It has been shown that although auroral events may not necessarily accompany hiss events on the ground due to several factors involved in the intervening propagating medium, VLF hiss is invariably associated with aurora. This

may be due to the same precipitating particles responsible for both hiss and auroral light. The examples of correlation between occurrences of VLF hiss and auroral activation are sufficiently convincing to believe that there does exist a causal connection between them. Contradictory examples, however, point out to the importance of propagation of VLF emissions through the ionosphere and indicate that the signals may be completely deflected to different regions. Therefore, the controlling influence, in determining whether the emissions come to the ground, is the propagation path followed by the signal under different ionospheric conditions. There is, however, no consistent relationship found between VLF emissions and the riometer absorption but in cases of corresponding hiss and auroral substorm activity, the peak hiss emission usually occurs at the time of brightening of the auroral forms after which absorption usually tends to increase. Comparison studies between VLF hiss observations at the two stations indicate a lack of simultaneous occurrence for most of the emission. This suggests that the emissions are localized in latitude, and that propogation of a hiss signal in the earth-ionosphere waveguide is not an important factor in determining whether it would be received. It is found from ground observations that VLF hiss tends to maximize poleward of the auroral oval. Since there is a gradual decrease of the soft energy electrons going from auroral zone to lower L values in the outer Van Allen zone which contains energetic electrons, the decrease in the number of hiss events equatorward of the oval seems to be in agreement with the decrease in flux for the soft paticle precipitation for lower L-values.

It is also seen under disturbed conditions that auroral hiss occurs at the time of brightening of the auroral forms and remains present for a

short time during the poleward expansion phase of the substorm. It may be during this time that the intense precipitation of soft electrons takes place correlating with the production of hiss and may also move poleward of the oval along with the poleward expansive phase of the auroral substorm.

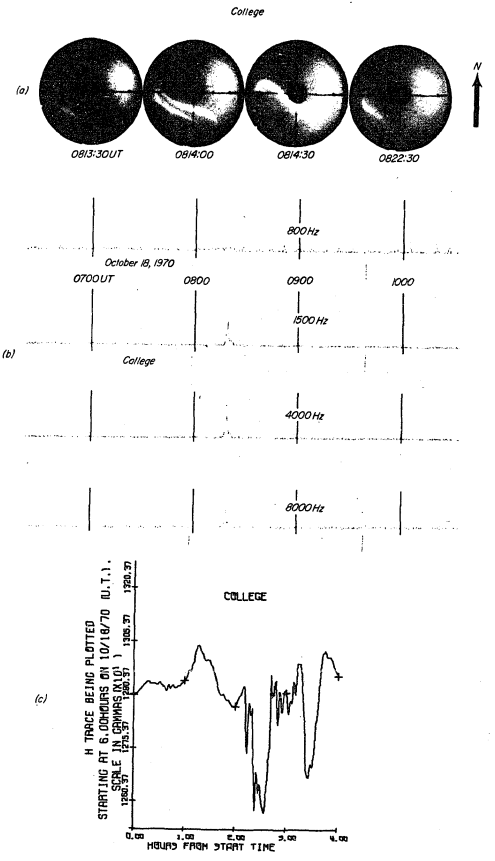

Figure 4.1

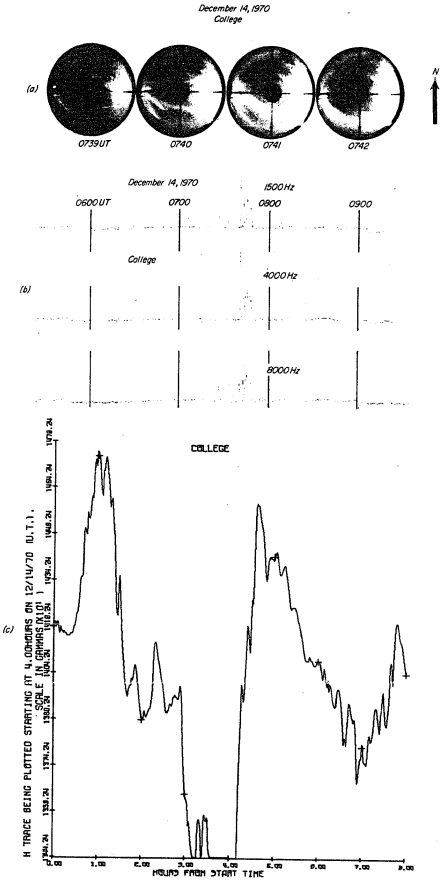

Figure 4.2

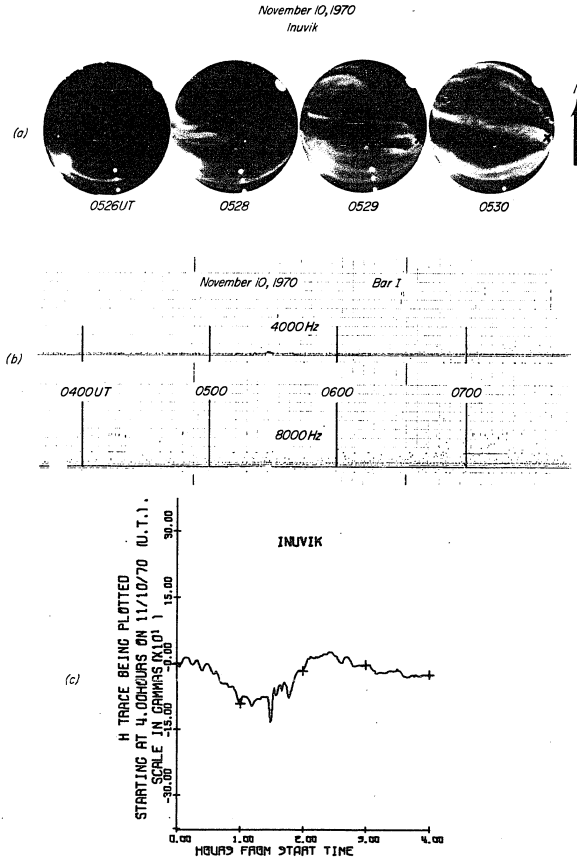

Figure 4.3

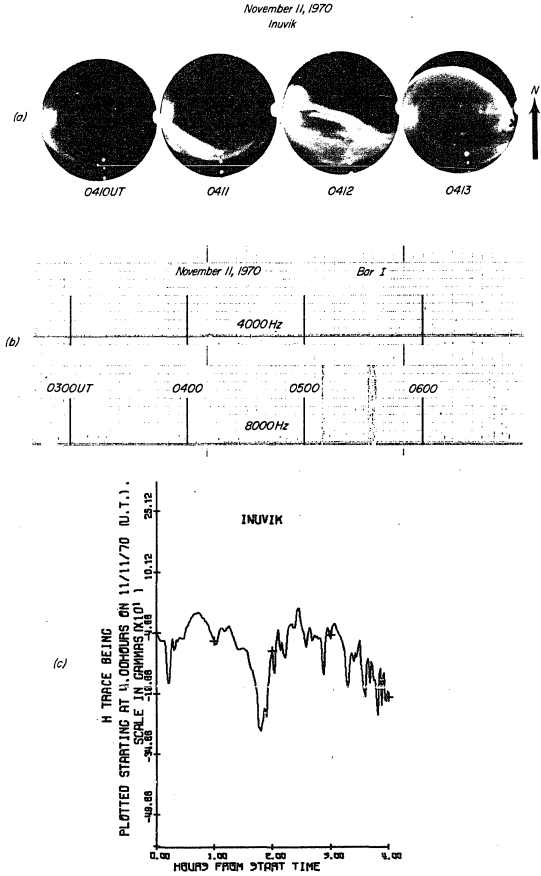

Figure 4.4

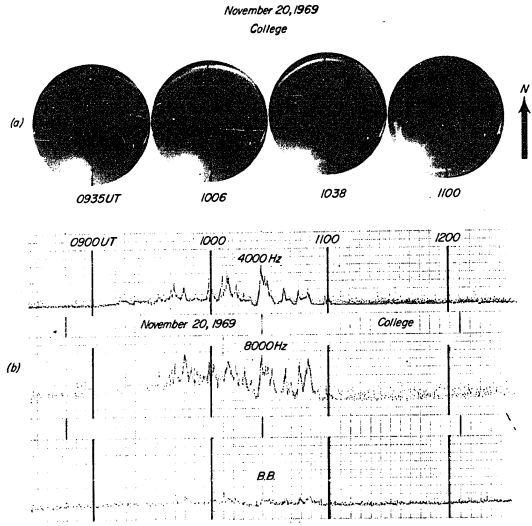

Figure 4.5

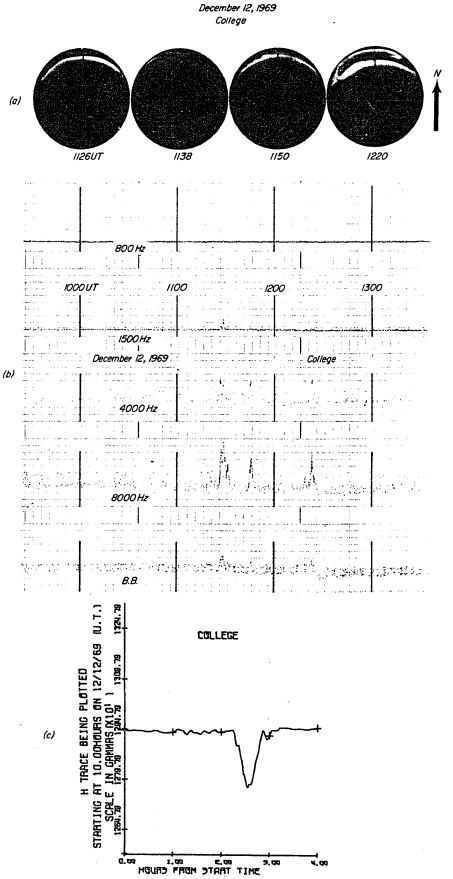

Figure 4.6

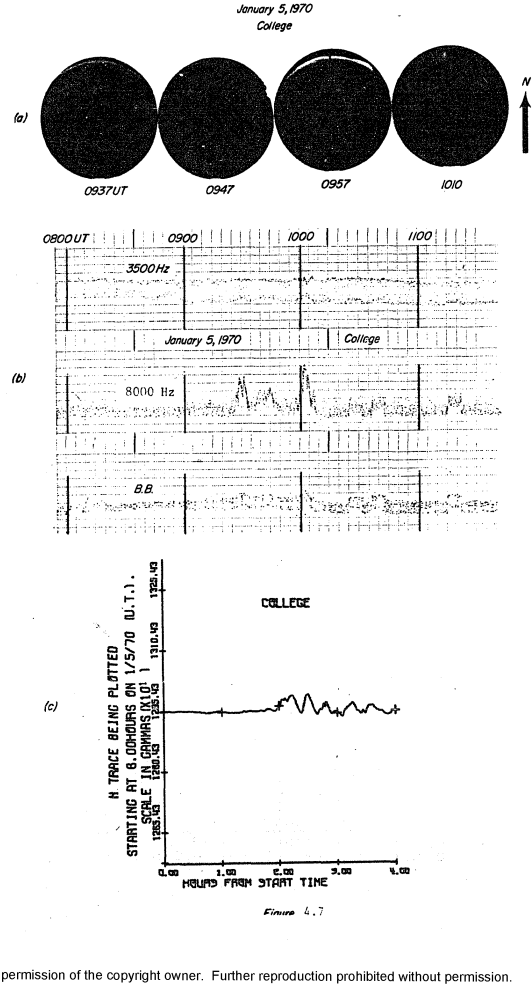

Figure 4.7

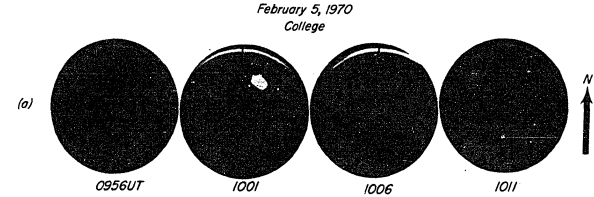

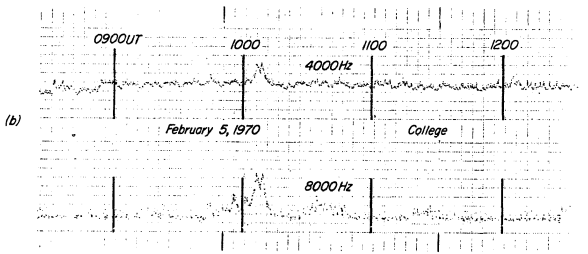

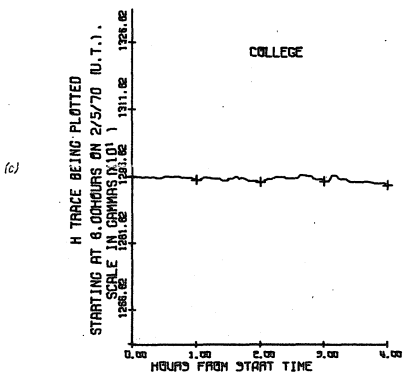

Figure 4.8

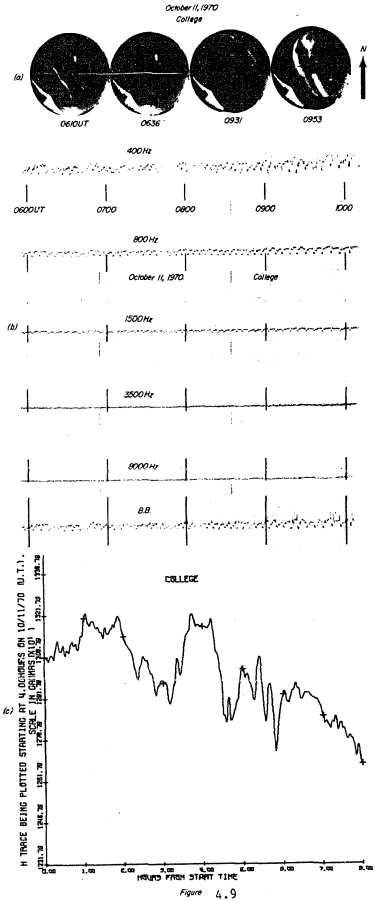

Figure 4.9

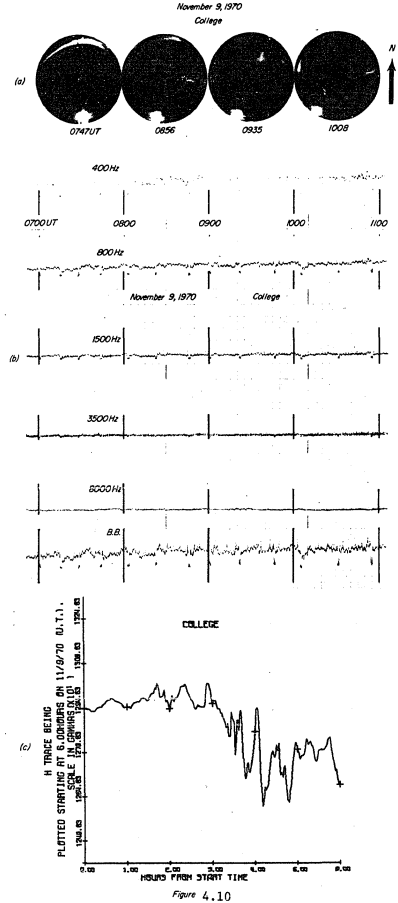

Figure 4.10

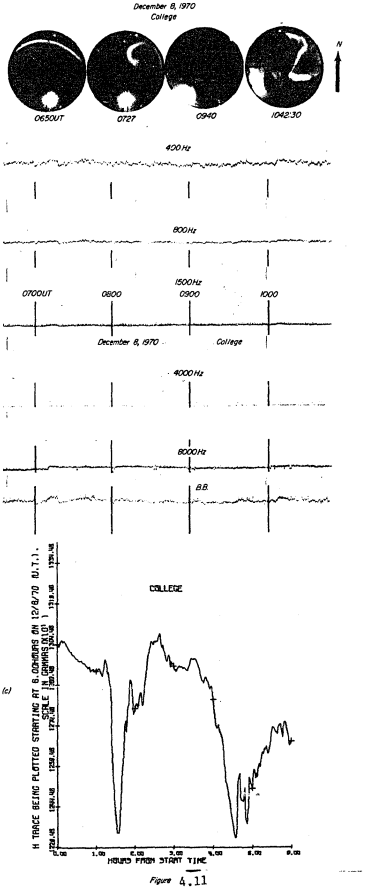

Figure 4.11

CHAPTER V

COMPARISON BETWEEN SATELLITE AND GROUND DATA

5.1 Introduction

Satellite studies of VLF emissions, most notably by the University of Iowa with their low altitude polar orbiting satellites Injun 3 and Injun 5 (Gurnett and O'Brien, 1964; Gurnett, 1966, Gurnett et al., 1969), have shown that VLF emissions are present in much greater abundance in the magnetosphere than on the ground. The absence of many of these emissions on the ground could well be explained in terms of reflection of the signals back to the magnetosphere (Cartwright, 1964; Thorne and Kennel, 1967; Lyons and Thorne, 1969; Russell et al., 1969 and Dunckel and Helliwell, 1969). At other times, however, depending upon the propagation characteristics of the medium, the VLF signals traveling along, or in a narrow cone about, the field line penetrate through the magnetospheric and ionospheric barriers without being reflected or absorbed and reach the earth's surface to be detected by the ground VLF station. Intensities of these emissions on the ground are found to be lower by about two to three orders of magnitude than at the satellite altitudes above the ionosphere.

In fact, there have not been enough simultaneous ground and satellite observations in the past to prove the correspondence, if there is any, and comparison studies are available only in a very few cases. Rocket studies of Iversen et al. (1967) and Cartwright (1963) do, however, indicate a complete lack of correspondence between simultaneous measurements of VLF emissions on a rocket and on the ground. The same conclusion was reported by Gurnett (1966) for two cases where comparison was available, namely that the VLF hiss observed in the ionosphere via the Injun 3 satellite is not

necessarily observed on the ground. We have tried to compare the VLF events at College and Bar I with the Injun 5 satellite observations, and the comparisons are given in Table 5.I for the month of May 1970 where data from both sources were simultaneously available.

5.2 Satellite Observations through Injun 5

Injun 5 satellite data were kindly provided by Dr. Donald A. Gurnett (private communication, 1972) from the University of Iowa. Times of satellite passes over College and Bar I in a rectangular cross-section of the magnetosphere from $\lambda \pm 4.5^{\circ}$ in invariant latitude and $\phi \pm 4.5^{\circ}/\cos\lambda$ in invariant longitude are listed in Table 5.I for the month of May 1970. This cross-section of the magnetosphere roughly corresponds to a magnetic flux tube which intersects the ionosphere at 110 km within the field of view of an all-sky camera. The least distance as measured on the earth's surface between the points where Injun 5 field line passes through the 110 km level and the ground station during the event, is also given in Table 5.I. Distance calculations were made by Prof. D. W. Swift (private communication, 1972) while at the University of Iowa, for all the satellite passes included in Table 5.I. Although there were several satellite passes over College and Bar I in the month of May, we have included only those passes in Table 5.I for which the satellite VLF events were present. Sensitivity threshold calculations for ground VLF receiver corresponding to date of event were also made and are indicated in the table wherever available. Since Bar I riometer had not been operated, absorption values for events at Bar I are obtained from Inuvik riometer records.

Table 5.I clearly shows that most of the events observed by the Injun 5 satellite are not found on the ground, except for one occasion on

TABLE 5.1

Ground VLF Station	Date of Event	Satellite Pass #	Time of Sat. crossing in (UT)	Event Present		Threshold of detectable flux (watts $m^{-2}Hz^{-1}$)	Riometer absorption in (db)	Least distance between Injun 5 field line at 110 km & ground station (km)
				Satel. Rec.	Grnd. Rec.			
College	May 11, 1970	7792	0856-0901	yes	no	——	0	445
Bar I	May 11, 1970	7792	0858-0903	yes	yes	1.0×10^{-15}	0	268
Bar I	May 20, 1970	7906	1611-1613	yes	no	9.5×10^{-16}	Bad record	634
College	May 21, 1970	7919	1751-1758	yes	no	——	0	235
Bar I	May 23, 1970	7943	1710-1716	yes	no	9.5×10^{-16}	0	66
College	May 23, 1970	7943	1713-1716	yes	no	——	0	482
Bar I	May 27, 1970	7992	1752-1754	yes	no	5.0×10^{-16}	0	688
College	May 27, 1970	7992	1753-1757	yes	no	——	0	279

May 11, 1970 when the hiss event on ground at Bar I was identified to be the same as observed on the satellite records, the remaining seven satellite VLF events did not appear on the ground. There were, however, many events observed on the ground in May 1970: 14 at College and 6 at Bar I at times other than the satellite crossings. These events could not be analyzed with satellite data because the posirion of the satellite did not happen to be within the magnetic flux tube of these stations.

As observed from the satellite data for the event of May 11, 1970 and shown in Figure 5.1, VLF emission is present from 0900-0902 UT with a peak at 0900:30 UT. The satellite traverses an altitude range from 1850 to 1950 km and a geomagnetic latitude range from +60° to +65° within the event time slot. Satellite coordinates at the peak emission are 72° INV and 21.5 MLT which correspond to the corrdinates of a typical VLF hiss event as reported by Gurnett (1966). The peak electric field strength of the signal at 7.35 kHz is of the order of 5.0×10^{-8} volts^2/Hz. This gives a power flux of 9.6×10^{-13} watts $m^{-2}Hz^{-1}$. The corresponding ground event at Bar I shown in Figure 5.2 occurs from 0856-0900 UT with a peak at 0858 UT. The emission can be seen on the 8 kHz channel and is of the order of 3.0×10^{-15} watts $m^{-2}Hz^{-1}$. It is apparent from the two power flux measurements at nearly the same frequency that the ground event is weaker than the satellite event approximately by two orders of magnitude. The energy loss is ascribed to attenuatuion in the lower ionospheric layer. There was no magnetic activity on this particular day as seen from the magnetograms of Bar I, College and Ft. Yukon. In this respect, this event could be termed as a quiet day event.

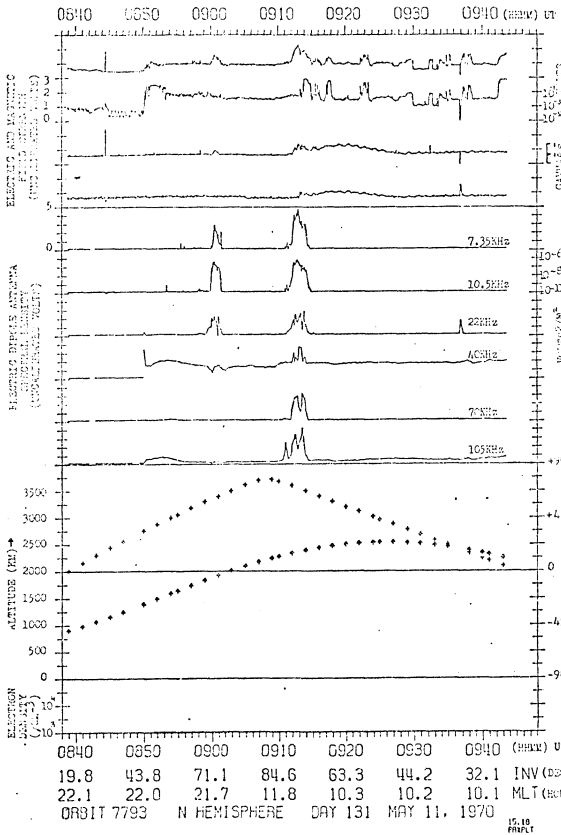

Figure 5.1 Satellite record of VLF emission on May 11, 1970

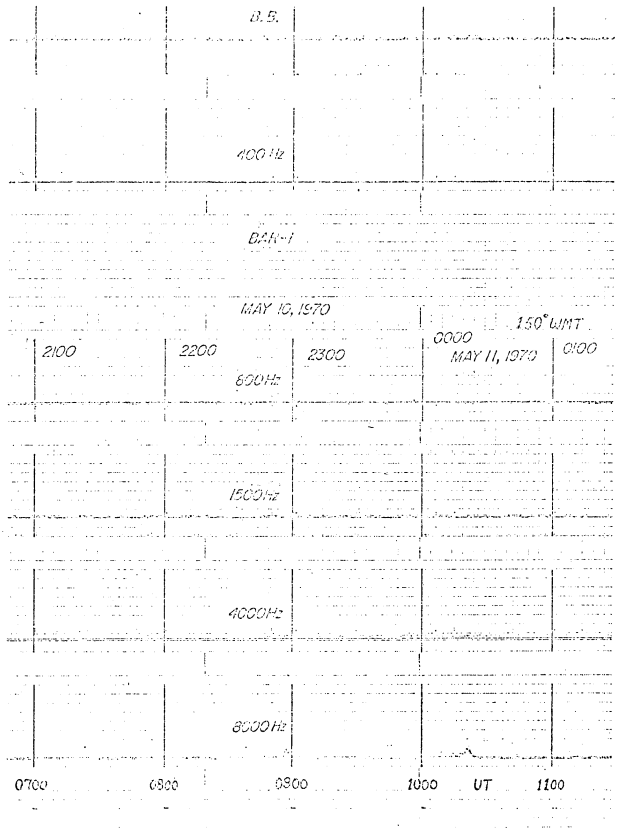

Figure 5.2 VLF hiss event at Bar I ground station on May 11, 1970

5.3 Discussion

Although simultaneous ground and satellite data were available only for one month, the comparison of the two data has clearly revealed a very definite lack of VLF events on the ground. Since we did not observe seven of the eight satellite VLF events on the ground, the question remains as to what really happened to these signals. Did the signals reflect back to the magnetosphere or did they simply disappear in the ionosphere due to collisional attenuation? Table 5.1 indicates that the 30 MHz riometer records did not show any indication of absorption during times of satellite events over College and Bar I. Therefore, if the input power flux due to the event remains above the threshold of detectable flux for the ground VLF system, the event should be observed on the ground VLF records. However, the lack of collisional absorption, as measured by the riometer, is only one of several conditions required for the propagation of VLF signals to the ground. There may be other attenuation losses in the propagation medium which restrict the VLF/ELF emissions to reach the ground.

Computations to be presented later show that the actual region, which determines whether or not signals can be observed on the ground, occurs in the 60 to 125 km altitude range. It is in this region that the attenuation due to defocussing of signal rays could be extensive depending upon the zenith angle of the phase normal direction with which the signals are incident at 125 km. We shall also try to see if the reflection of VLF signals in the magnetosphere or ionosphere exerts any controlling influence on their observability on the ground. These theoretical studies will be described in the following chapters.

CHAPTER VI

VLF RAY TRACING IN A MODEL IONOSPHERE

6.1 Need for Ray Tracing

The very-low-frequency natural emissions, hiss and chorus, have been observed at many auroral zone ground stations in both hemispheres for a long time. These emissions are of interest there because they correlate strongly with many of the manifestations of the auroral zone phenomena such as auroral optical emissions and particle precipitation into the auroral zone atmosphere (Gurnett and O'Brien, 1964; Gurnett, 1966; Oliven and Gurnett, 1968; Gurnett and Frank, 1972) and may, themselves, be manifestations of plasma instabilities in the magnetosphere and ionosphere. Similarly, whistler related studies and observations have been conducted on the ground mainly at mid-latitude stations, since whistlers are not so common at high latitudes. A unique problem, however, which would not have been visualized by ground observations alone, grew increasingly important with the advent of artificial satellites when the VLF payload aboard the series of Injun, OGO and Alouette satellites started observing and recording a variety of VLF emissions. This included hiss, chorus, plasmaspheric hiss and lower hybrid resonance bands, etc., most of which could not be accounted for by the ground VLF records. Unfortunately, there have not been enough simultaneous ground and satellite observations but, as it is reported in Chapter V, whenever the comparison was available, the satellite event could not be identified from records of the ground VLF station. It became quite clear through many satellite observations that there is an apparent lack of VLF events on the ground comapred to those which are present in the magnetosphere.

It was natural to believe at first that reflection or complete

absorption of VLF signals, in the course of their propagation to the earth from the emitting source, play the important role of main obstacles causing non-reception of VLF signals on the ground. VLF ray path computations have been performed to investigate this problem on a theoretical basis. Ray tracing technique, when used for this purpose, presents an important analytical method for studying the behavior and propagation of electromagnetic waves through an inhomogeneous and anisotropic medium, such as the ionosphere and the magnetosphere, and will be described in the following analysis.

It is known that energy associated with electromagnetic waves in an anisotropic medium does not, in general, travel in the direction of the wave normal but in a different direction which we call the ray direction, and the trajectory of this energy flow is known as the ray path. The difference between the wave normal vector and the direction of energy flow depends on the magnitude of the refractive index and its functional dependence on the wave normal angle relative to magnetic field direction. Ray paths for an electromagnetic disturbance at very low frequencies can be determined by assuming that the medium is slowly varying or that the WKB solution is valid (Budden, 1961). Carrying out ray path computations, however, necessitates certain assumptions which become desirable due to the complicated nature of the medium involved. Most significant of these assumptions are the initial conditions of the ray path which relate to the location of the source of VLF emissions. This is discussed in Section 6.3. Since VLF ray paths are strongly dependent upon the plasma properties of the medium such as the electron density and static magnetic field, it is also essential to choose an appropriate model to describe the

ionosphere. We have assumed a diffusive equilibrium model for electron and ion density and a centered dipole geomagnetic field. The validity of the assumptions will be discussed later. Ray paths for a variety of VLF frequencies, initial altitude, latitude and wave normal angles are then computed for this model.

6.2 Earlier Studies vs Present Study

VLF ray tracing computations have been conducted by several workers in the past for various models of the ionosphere and with different approaches to determination of ray paths. Booker (1936, 1938, 1949) developed a wave packet method where the direction of the ray path is the direction of motion of a wave packet disturbance. It was shown that from the variation of the Booker quartic with electron density and incident angle, that it is possible to construct the ray path for the wave packet. This method was further improved by Millington (1951, 1954). A very important Poynting vector approach to ray tracing was developed by Poeverlein (1948, 1949, 1950) who assumed a plane stratified and non-absorbing model ionosphere and graphically constructed the index of refraction surface (a plot of the index of refraction vs wave normal angle). The two-dimensional graphical method of Poeverlein was extended to three dimension by Mullaly (1955). It was Hines (1951d) who concluded that for a non-absorbing medium, both the Booker-Millington wave packet method and the Poeverlein-Mullaly Poynting vector approach give the same direction of energy flow. Weinberg (1962) has applied the eikonal method to wave propagation in anisotropic inhomogeneous media and has discussed in detail the problem of computing ray paths in the ionosphere. The equations to determine ray trajectory and some geometrical relations for

ray tracing in inhomogeneous media are also discussed by Stix (1962).

There have been many ray tracing computations in the past in connection with the whistler studies. The first calculation of whistler ray paths in a model ionosphere using a graphical method was performed by Maeda and Kimura (1956) who developed a theory based on Fermat's principle and used the quasi-longitudinal approximation to the whistler index of refraction, and horizontal stratification of an electron ionosphere. Yabroff (1961) published whistler ray path calculations which used the exact expression for the refractive index and also included the curvature of the ionosphere, although he assumed an ionosphere composed of electrons only. These ray tracings were based on the magneto-ionic theory of propagation as applied to a monotonically decreasing distribution of electrons in the magnetosphere and predicted that the ray paths may be asymmetric with respect to the equatorial plane, a characteristic which did not favor the explanation of the long-continuing echoes of whistlers. Smith (1960) described a propagation mechanism involving field-aligned ducts which did explain many of the observed propagation features of whistlers. Ray paths have also been calculated including the effect of dominant ions in the upper ionosphere (Hines, 1957; Kimura, 1966; Shawhan, 1966; Walter, 1969 and Cerisier, 1970).

In our computations of VLF ray paths, we have considered predominantly an O^+ ionosphere in the absence of collisions. Contribution due to H^+ ion is taken as negligible in the ionosphere but becomes increasingly important in the magnetosphere because of the drop in O^+ density. The present study, however, does not consider the propagation of VLF waves through the magnetosphere trapped in ducts which are field-aligned electron

number density inhomogenities. VLF wave propagation in the medium is assumed to be in the whistler mode where the wave frequency is well below the electron cyclotron frequency but greater than the ion gyro frequency. The use of a digital computer is made to determine the VLF ray paths by using a set of differential equations derived by Walter (1969) which exactly correspond to the set of equations given by Haselgrove (1955).

6.3 Initial Condition of the Ray Path

Although the real mechanism for the generation of VLF emissions, which would also indicate the source location is not clearly understood (Gallet and Helliwell, 1959; Dowden, 1963; Gurnett and O'Brien, 1964; Swift, 1965; Kennel and Petschek, 1966; Thorne and Kennel, 1967; Swift, 1968; Jørgensen, 1968; Lim and Laaspere, 1972), we have proceeded to compute VLF ray paths according to two possible source locations which will be described below.

Information obtained from experiments using satellite-borne receivers indicate the following: 1. Observations of Injun 3 (Gurnett, 1966) and Injun 5 (Gurnett and Frank, 1972) show that the auroral zone VLF hiss is observed near and on the poleward side of the trapping boundary for energetic electrons (E > 40 kev) in a zone typically about 7° wide in latitude and centered on 72° INV at local midnight. 2. It is observed (Gurnett and Frank, 1972) that near and poleward of electron (E > 40 kev) trapping boundary, VLF hiss is associated with intense fluxes ($\sim 10^9$(cm^2 sec ster)$^{-1}$) of precipitating low energy electrons with energies on the order of 100 ev to a few kev. 3. VLF hiss is generally observed to be

propagating down the geomagnetic field line from a generation region above the satellite. 4. Gurnett and Frank (1972) also report that the electron energy spectrum in the local evening is characterized by inverted V precipitation events and shows considerable evidence of acceleration and heating caused by quasi-static electric fields parallel to the geomagnetic field (Frank and Gurnett, 1971). All these satellite observations suggest that the precipitated soft electrons in the auroral zone atmosphere near and poleward of the electron (> 40 kev) trapping boundary may be the cause of generation of VLF hiss above the satellite altitude.

In view of the fact that Injun 5 invariably observed VLF hiss in the altitude range of 1700-2400 km (Gurnett et al., 1969), we are led to believe that VLF hiss should be generated above this altitude. We also noticed in Chapter IV that no VLF hiss events have been observed beyond roughly 600 km from the visible aurora. If this fact is combined with the satellite observations and it is also assumed that the direction of energy flow at VLF frequencies is columnated to a maximum angle of 19° about the field line (Stix, 1962), the altitude range for hiss generation is limited to somewhere between 2500-3000 km. In the following, therefore, the first set of VLF ray path computations envisages the ray paths starting from a representative altitude of 3000 km and at an invariant latitude of 69° where a localized point source of VLF emissions is assumed.

VLF noise measurements in the magnetosphere through low altitude satellites (Barrington et al., 1963; Jørgensen, 1968; Gurnett and O'Brien 1964; Scarf et al., 1968 and Taylor and Gurnett, 1968) are not necessarily completely representative of the distribution of signals throughout the

entire magnetosphere. For example, Dunckel and Helliwell (1969) have described the occurrence, intensity and spectra of emissions observed by OGO I satellite at frequencies below the local electron gyro-frequency. Their data cover geocentric distances from 2 to 24 earth radii. The spectra resemble those observed on the ground and include hiss, random chorus, periodic chorus and triggered emissions and are observed at much higher L values. The broadband noise resemble the auroral hiss observed at ground stations. For this reason computations of ray path have been made to see whether these emissions can reach the ground. The spectral features of these emissions indicate that the region of production is located close to the equatorial plane of the magnetosphere. OGO I observations fit rather well with the suggestion of Thorne and Kennel (1967) that VLF noise in the whistler mode is produced in the equatorial plane of the magnetosphere resulting from a plasma instability. Kennel and Petschek (1966) have established this instability by considering the pitch-angle diffusion of the particles into the loss cone and their eventual precipitation into the atmosphere. The experimental evidence supporting the Kennel and Petschek instability theory is provided by the correlation observed between the occurrence of 40 kev electron precipitation and VLF chorus (Oliven and Gurnett, 1968) and the correlation between soft electron precipitation and VLF hiss (Gurnett and Frank, 1972).

VLF signals generated near the magnetic equator at higher L values propagate towards the earth in the two hemispheres following approximately the magnetic field lines; but these signals may never even penetrate to low altitudes due either to reflection or absorption or both. To study

VLF wave propagation in the magnetosphere, we have performed a second set of VLF ray path computations. The location of the VLF source emissions for this set is assumed at the 40 kev electron trapping boundary at L = 6.0 in the equatorial plane of the magnetosphere.

6.4 Computational Procedure

There is always a unique ray path produced for a particular model ionosphere and for a unique set of initial conditions ($\vec{k}_o$, $\vec{r}_o$) where k_o and r_o are the initial wave number and position of the signal. We have tried to exhibit families of ray paths by variations of a five parameter set which consists of a frequency, an initial altitude, an initial latitude, an initial wave normal angle and a model ionosphere. For a given family of curves, four of these parameters are held constant while the fifth parameter is varied.

As it is pointed out in Section 6.3, two sets of computations of VLF ray paths have been performed depending upon the initial conditions of the ray path which is concerned with the source location. For the first set of computations, the wave normal angle with respect to the vertical, δ, is taken in the range 0° to $\pm$ 90° at 10° interval and the VLF frequencies considered are 1.0, 4.0 and 8.0 kHz. The ray paths are terminated after reaching an altitude of 125 km from the surface of the earth. Since the validity of the ray path calculations breaks down below 125 km and attenuation due to electron collisions becomes important, a different computational method has to be used in the 60-125 km altitude range. The results of these calculations will be presented later. Ray path computations for second set is performed for wave normal angles relative to magnetic field direction, ψ, in the range 10° to 30° at 1.0 and 4.0 kHz.

Both sets of computations are repeated for quiet and disturbed model ionospheres.

A centered dipole geomagnetic field with a magnetic induction of 0.32 gauss at the earth's surface on the equator is assumed. The propagation medium is taken to be constituted of a plasma of electrons and two positive ions, namely: O^+ and H^+ in a diffusive equilibrium situation. Ray paths are calculated in two dimensions in a magnetic meridian plane and are plotted in terms of geocentric altitude and magnetic latitude over a spherical earth of 6372 km radius. The exact expression for the phase refractive index in the cold plasma approximation is used. The electron density models are assumed to be only radially dependent and the distribution of constituents in the model ionosphere is assumed to be smooth so that the ray paths represent the non-ducted and non-scattered behavior of ray paths in the VLF range.

6.5 Description of the Models

Two different models corresponding to the quiet-time and disturbed conditions of the high latitude ionosphere have been used for our ray path computations. Electron density and the ion composition are specified at a reference altitude of 400 km and the diffusive equilibrium model used in the program calculates the density and the composition above the reference altitude. Below 400 km level, however, the electron density is very sensitive to the diurnal, seasonal and solar cycle variations. Hence, the electron density values below 400 km are taken from the appropriately chosen profiles in slabs of 25 km and are put into the program.

The quiet and disturbed ionosphere electron density profiles are

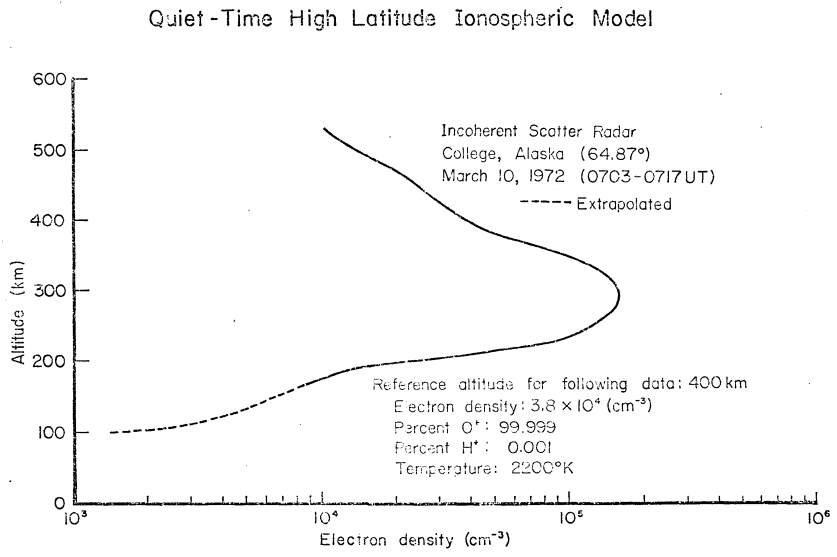

Figure 6.1 Quiet-time ionospheric model

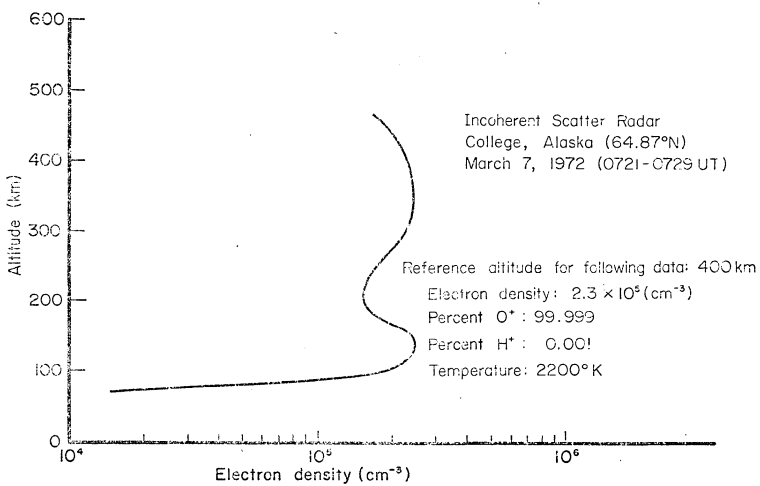

Figure 6.2 Disturbed ionospheric model

shown in Figures 6.1 and 6.2 respectively. The profiles are obtained from observations of the incoherent scatter radar at Chatanika near College, Alaska. The quiet and disturbed models correspond to very quiet and disturbed geomagnetic conditions on March 10 and March 7, 1972 respectively. The O^+ ion is considered to be predominant at 400 km. The percentage composition of the two ions at 400 km is assumed to O^+ = 99.999%, H^+ = 0.001%. Electron and ion temperatures in our model are assumed to be the same and is taken as 2200° K at 400 km. The radar operation at College is sensitivity limited and cannot observe electron densities below $10^4(cm^{-3})$. However, the electron densities for the quiet model are extrapolated to 100 km where it is matched with the value given by Deeks (1966) under normally quiet situations.

6.6 Ray Tracing Equations

Assuming that the propagation is confined to a meridian plane, where the parameters such as the density and static magnetic field of the medium are known at each point, only a set of three differential equations is necessary to determine the position of the wave packet. These differential equations are the time variation of the geocentric distance and the latitude of the wave packet plus the time variation of an angle that gives the wave normal direction.

Based on the concept of group velocity, the two-dimensional ray tracing differential equations in polar coordinates as obtained by Walter (1969) are as follows:

$$\frac{dr}{dt} = \frac{c}{\mu}(\text{Cos } \delta - \text{Tan } \alpha \text{ Sin } \delta), \tag{6.1}$$

$$\frac{d\theta}{dt} = \frac{c}{r\mu}(\text{Sin } \delta + \text{Tan } \alpha \text{ Cos } \delta), \tag{6.2}$$

$$\frac{d\delta}{dt} = -\frac{c}{\mu^2}\left(\frac{\partial \mu}{\partial r}\,\mathrm{Sin}\,\delta - \frac{1}{r}\frac{\partial \mu}{\partial \theta}\,\mathrm{Cos}\,\delta\right) - \frac{c}{r}\,\mathrm{Sin}\,\delta, \tag{6.3}$$

where

r and θ - polar coordinates of the ray path,

μ - phase refractive index,

α - angle between wave normal and the energy flow direction,

δ - angle between wave normal and the radial vector

and
$$\mathrm{Tan}\,\alpha = -\frac{1}{\mu}\frac{\partial \mu}{\partial \psi}, \tag{6.4}$$

where ψ is the angle between the wave normal and the magnetic field vector. The angles in relation to polar coordinate system are shown in Figure 6.3.

To solve the set of equations (6.1) to (6.3), it is necessary to determine the phase refractive index as well as its partial derivatives with respect to r, θ and ψ. Assuming the cold plasma approximations, the phase refractive index is given by the equation (Stix, 1962):

$$A\,\mu^4 - B\,\mu^2 + C = 0, \tag{6.5}$$

with solutions given by

$$\mu^2 = \frac{B \pm F}{2A}, \tag{6.6}$$

where

$$A = S\,\mathrm{Sin}^2\psi + P\,\mathrm{Cos}^2\psi, \tag{6.7}$$

$$B = RL\,\mathrm{Sin}^2\psi + PS\,(1 + \mathrm{Cos}^2\psi), \tag{6.8}$$

$$C = PRL, \tag{6.9}$$

$$F^2 = B^2 - 4AC. \tag{6.10}$$

and

$$S = \frac{1}{2}(R + L), \tag{6.11}$$

$$R = 1 - \sum_i X_i \frac{1}{1 + Y_i}, \tag{6.12}$$

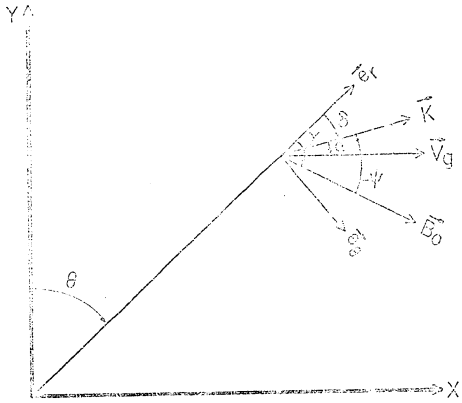

Figure 6.3 Angles in relation to polar coordinate system

$$L = 1 - \sum_i X_i \frac{1}{1 - Y_i}, \tag{6.13}$$

$$P = 1 - \sum_i X_i, \tag{6.14}$$

$$X_i = \left(\frac{f_{oi}}{f}\right)^2, \tag{6.15}$$

$$Y_i = \frac{f_{Hi}}{f}, \tag{6.16}$$

where

f_{oi} = plasma frequency of the ith ion,

f_{Hi} = gyro frequency of the ith ion,

f = wave frequency.

The diffusive equilibrium model given by Angerami and Thomas (1963) is assumed here. For this model electron density, N_{De}, is given by:

$$N_{De}(z) = N_{eb}\left[\sum_i \alpha_{ib}\, e^{-z/Hi}\right]^{\frac{1}{2}}, \tag{6.17}$$

where z is the geopotential height given by

$$z = r_b\,(1 - \frac{r_b}{r}). \tag{6.18}$$

r_b is the reference geocentric distance at which the electron density N_{eb} and the ion percentage α_{ib} are specified. The scale height of the ith ion is H_i given by:

$$H_i = \frac{k\,T}{m_i\, g_b}, \tag{6.19}$$

where g_b is the acceleration due to gravity at r_b, k is the Boltzmann constant, T is temperature in degrees Kelvin and m_i is the mass of the ith ion. The electron gyro frequency for a centered dipole is given by:

$$f_{He} = f_{Heo}\left(\frac{r_E}{r}\right)^3 \quad (1 + 3\,\mathrm{Cos}^2\,\theta)^{\frac{1}{2}}, \qquad (6.20)$$

where f_{Heo} is the electron gyro frequency at the dipole equator ($\theta = 90°$) at the earth's surface and r_E is the earth's radius.

6.7 Method of Digital Computation

The program used for our VLF ray path computations has been described in detail by Walter (1969) and is used here with certain modifications to suit our particular problem. It consists of a main program where the values of the parameters are originated to start the integration of the ray tracing differential equations and four sub-routines that carry the bulk of the load of providing the densities of the plasma components, printing the output of the program and a procedure to solve a system of N first order differential equations using a fourth order Adam's predictor-corrector method etc. The computer program is prepared in FORTRAN IV for an IBM computer 360/40.

Plot subroutines are written for both sets of computations and are included in the program for the purposes of plotting the results. Ray paths, thus obtained under different conditons, are shown in Figures 6.4 - 6.15. Ray path characteristics and their behavior in the propagating medium are discussed in the next chapter.

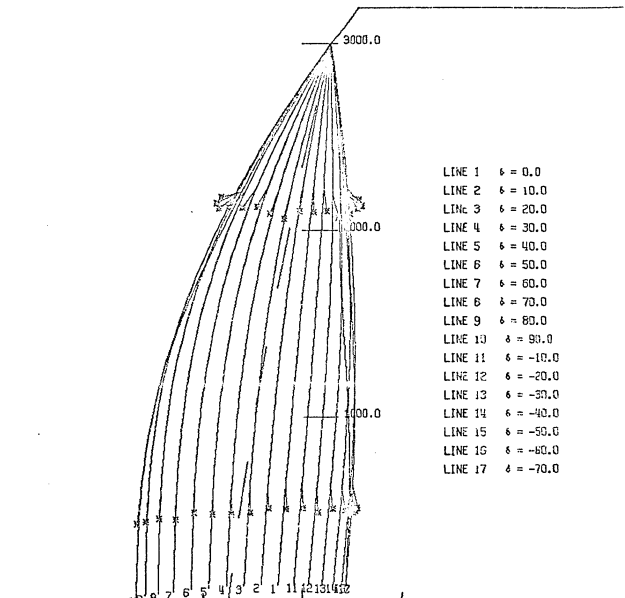

INITIAL LATITUDE = 64.00 FREQUENCY = 1.0 KHZ
RAY PATHS CALCULATED FOR WAVE PACKETS AT VARIOUS INITIAL WAVE NORMAL ANGLES STARTING AT 3000. KM. AND DOWNG DOWN TO FINAL ALTITUDE NEAR 100. KM. A DIPOLE FIELD LINE THROUGH THE STARTING POINT IS SHOWN FOR REFERENCE. ARROWS INDICATE THE WAVE NORMAL DIRECTIONS.

Figure 6.4

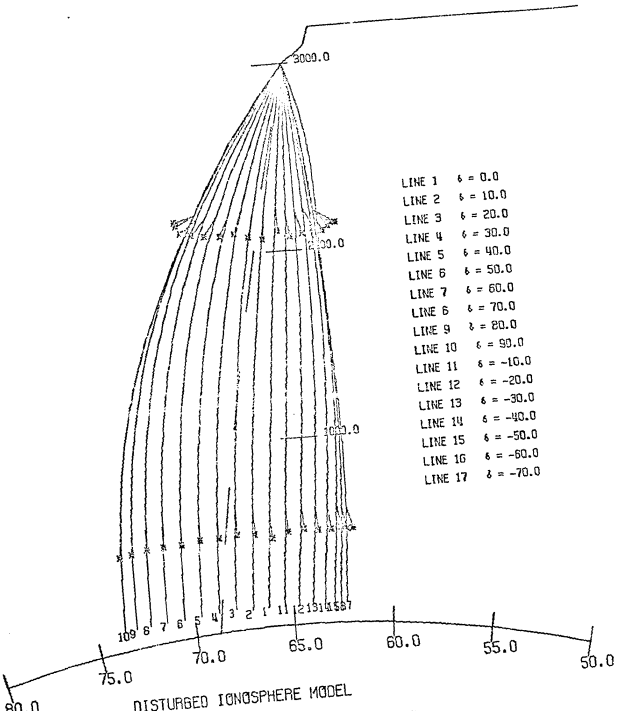

Figure 6.5

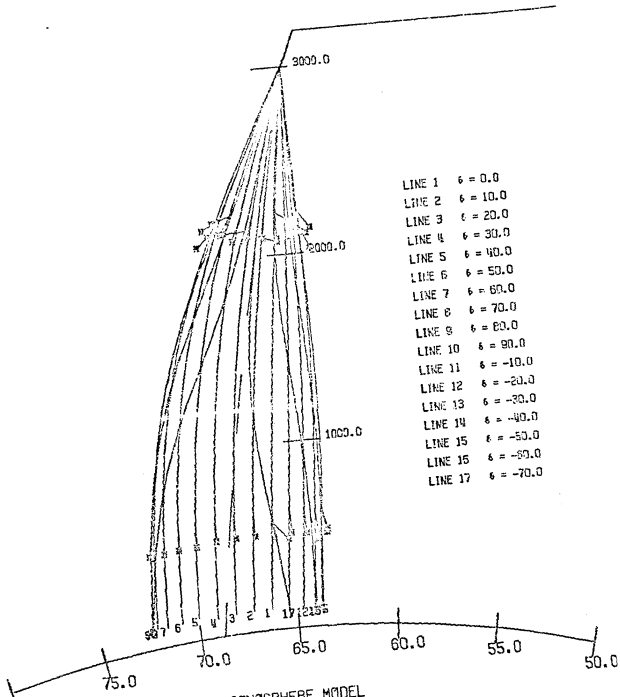

Figure 6.6

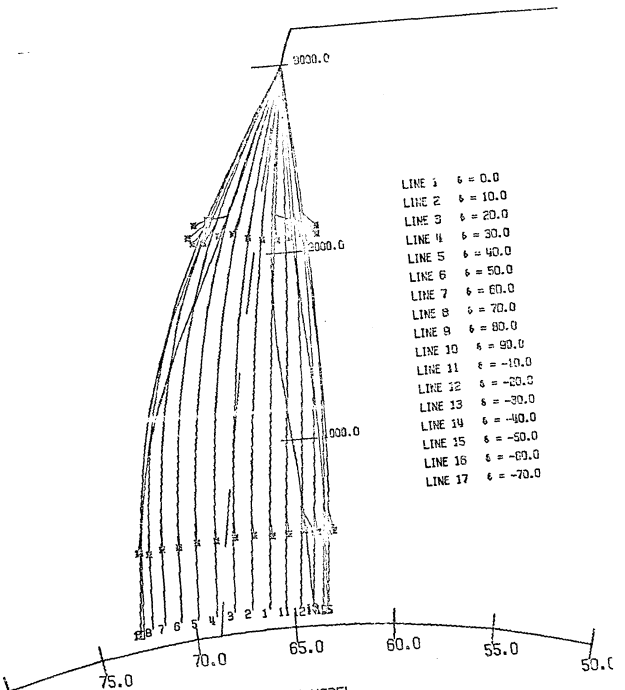

Figure 6.7

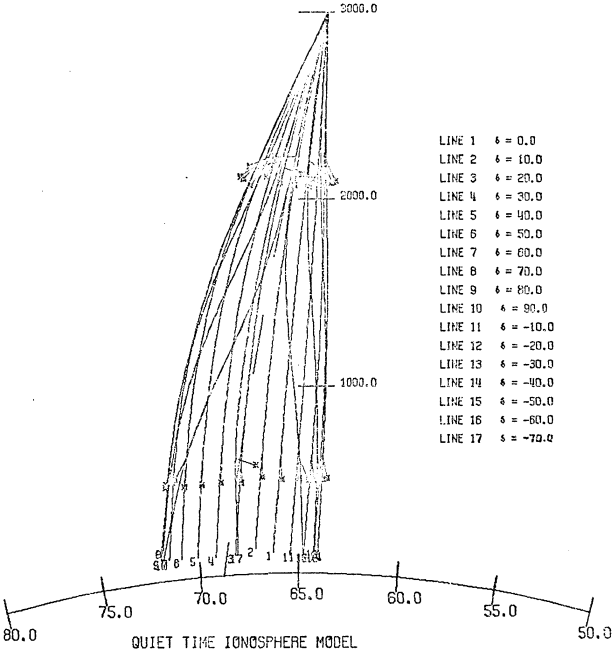

INITIAL LATITUDE = 64.00 FREQUENCY = 8.0 KHZ
RAY PATHS CALCULATED FOR WAVE PACKETS AT VARIOUS INITIAL WAVE NORMAL ANGLES STARTING AT 3000. KM. AND COMING DOWN TO FINAL ALTITUDE NEAR 100. KM. A DIPOLE FIELD LINE THROUGH THE STARTING POINT IS SHOWN FOR REFERENCE. ARROWS INDICATE THE WAVE NORMAL DIRECTIONS.

Figure 6.8

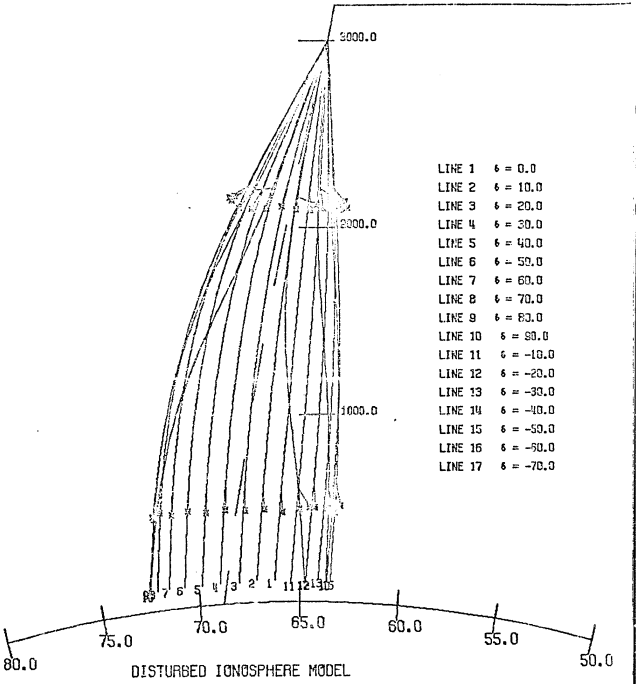

DISTURBED IONOSPHERE MODEL

INITIAL LATITUDE = 64.00 FREQUENCY = 8.0 KHZ
RAY PATHS CALCULATED FOR WAVE PACKETS AT VARIOUS INITIAL WAVE NORMAL ANGLES STARTING AT 3000. KM. AND COMING DOWN TO FINAL ALTITUDE NEAR 100. KM. A DIPOLE FIELD LINE THROUGH THE STARTING POINT IS SHOWN FOR REFERENCE. ARROWS INDICATE THE WAVE NORMAL DIRECTIONS.

Figure 6.9

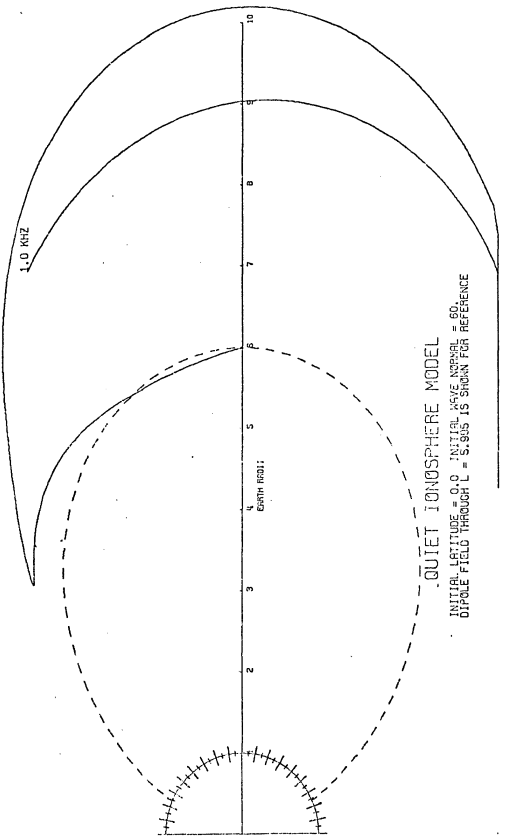

Figure 6.10

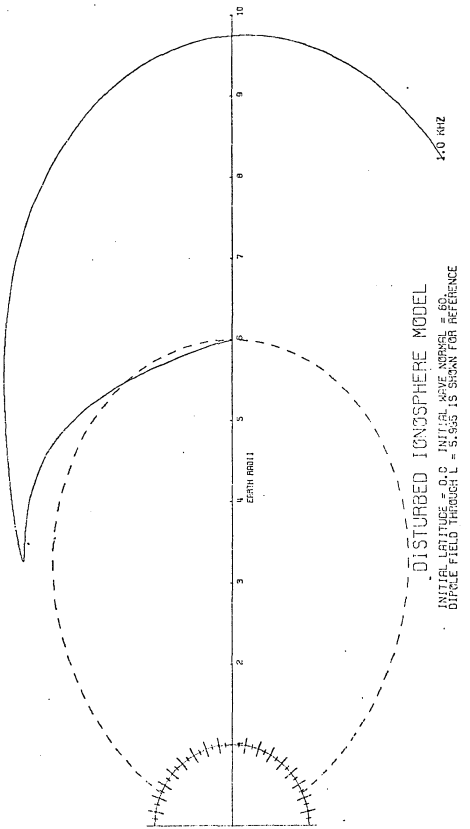

Figure 6.11

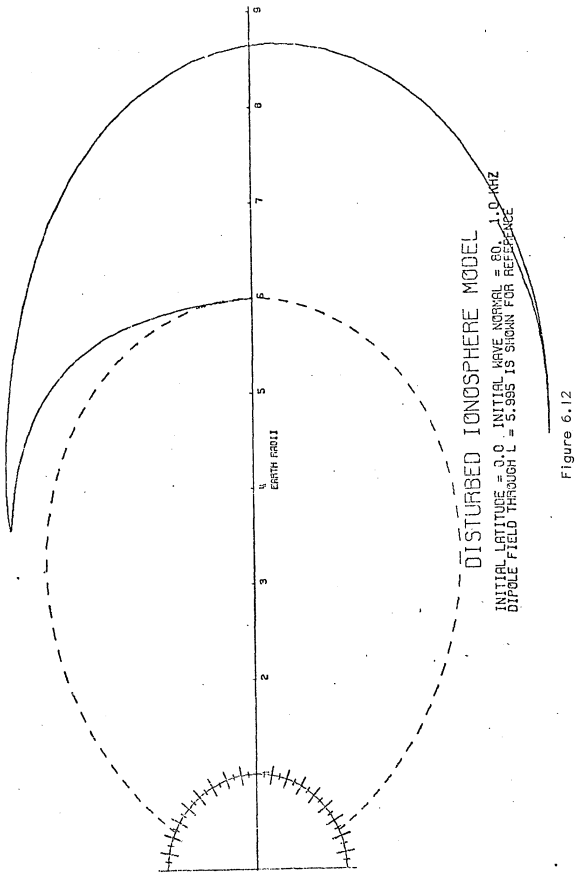

Figure 6.12

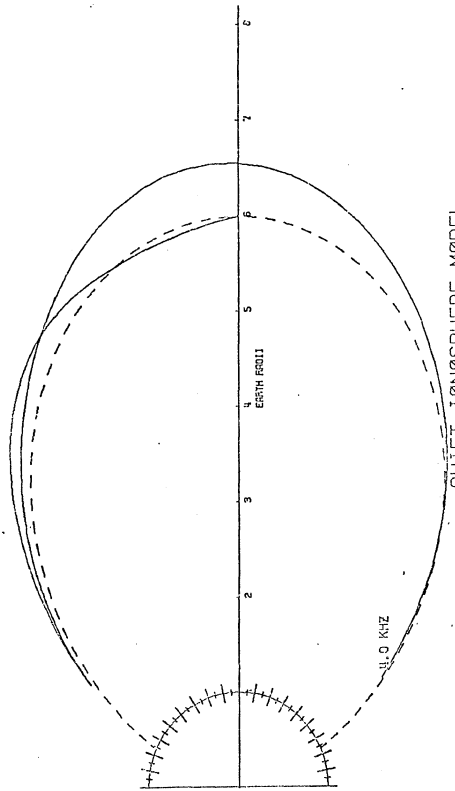

Figure 6.13

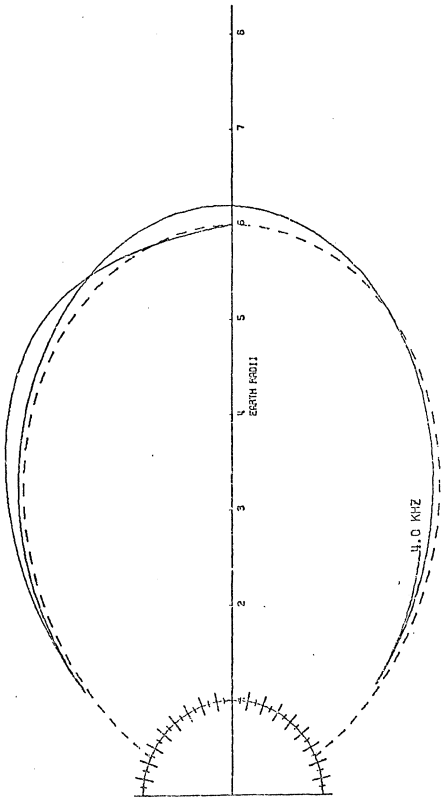

Figure 6.14

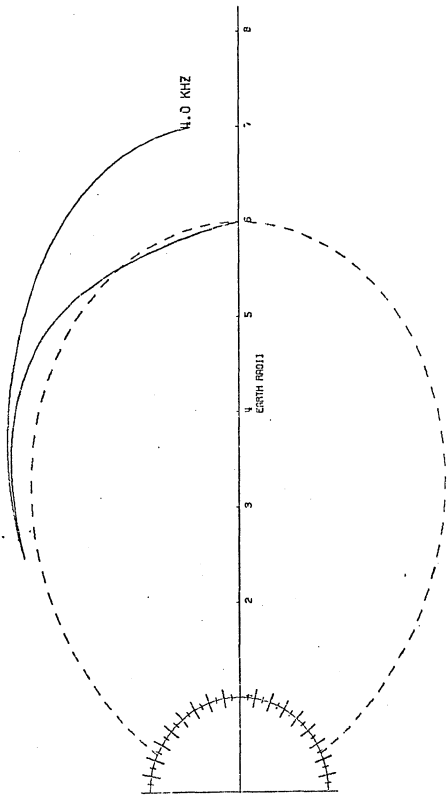

Figure 6.15

CHAPTER VII

INTERPRETATION OF RAY PATH BEHAVIOR

7.1 Behavior of Ray Paths for Calculations of Set No. I

Families of ray paths for wave packets starting from a fixed point source assumed above the Injun 5 satellite altitude have been plotted for a variation in the initial wave normal angles relative to the vertical, frequency and the electron density model. Ray paths for VLF signals, thus obtained, are displayed in Figures 6.4 - 6.9 and reveal several characteristics of the propagation of VLF waves in the magnetosphere and ionosphere. A dipole field line through the starting point is shown for reference and arrows along the ray paths indicate the wave normal directions for signals propagating downwards. It is clearly seen from Figures 6.4 - 6.9 that ray paths, for identical initial conditions but for different wave normal angles do not follow the same path and that none of these paths follows exactly the field line that passes through the starting point. It is indicated that ray paths with negative wave normal angles, ψ, come equatorward of the field line whereas rays with positive wave normal angles move poleward of the field line. However, the extent to which the rays go either side of the field line is limited in range as seen from the bending of the signal rays with high initial wave normal angles towards the field line.

The latitudinal spread of ray paths at 1.0, 4.0 and 8.0 kHz up to 125 km seem to be concentrated to within a range of $< \pm 6°$ from the latitude at which the field line through the starting point meets the earth's surface. This latitudinal spread on the earth's surface roughly corresponds to a distance of $\sim$ 600 km from the field line. Since we do not observe any

hiss events to more than 600 km from the visual aurora, the above observation seems to suggest that emissions with all possible wave normal angles from the source would be observed on the ground provided there is no divergence of ray paths below 125 km level towards the horizontal. However, it is found from computational results in the lower ionosphere (see Chapter VIII) that signals between the 125 km level and the ground do tend to deviate further from the vertical. This suggests that there is only a small cone of initial wave normal angles about the field line within which the signals would be received on the ground. The signals outside this cone of angles would be reflected back to the magnetosphere from the 125 to 60 km level in the ionosphere. Even the signals within the cone of angles that are received on the ground are highly attenuated due to divergence of ray paths in the low ionosphere.

Ray tracing computations performed for a span of initial wave normal angles reveal qualitatively the same physical picture for both quiet and disturbed models. Quantitative differences do, however, exist for the two ionospheric models. Ray paths usually take their place according to variations in the electron density, wave normal direction relative to magnetic field direction and the curvature of the field line; but the calculations do not give any indication that the VLF signals are reflected in the 3000 to 125 km altitude range. It should be noticed from Figures 6.6 - 6.9 that the ray paths at 4.0 and 8.0 kHz do not monotonically deviate away from the field line for increasing initial wave normal direction, δ. These ray paths with higher initial wave normal angles in the beginning rather turn inward close to the field line, thus, crossing the ray paths for lower values of initial δ and diverge again from the field line as it comes closer to the earth.

If, at any time, the initial wave normal vector is perpendicular to the magnetic field, there is obviously no downward propagation. This can be seen for signals with initial wave normal angles $\delta > -80°$. Results of the first set of computations will be considered again in Chapter VIII, where these ray paths are further extended from 125 km to the ground. Meanwhile, ray path computations of the second set which refer to the propagation from the equatorial plane will be considered now.

7.2 Propagation at an Angle to the Field

Before we go into the discussion of the behavior of ray paths for the second set of computations, it will be worthwhile to see at what cone of wave normal angles about the field line in the equatorial plane, VLF waves are most likely to be generated.

Whistler mode waves become unstable by pitch-angle anisotropies in the distribution of electrons in Doppler-shifted cyclotron resonance with the waves (Kennel and Petschek, 1966). The condition for this resonance is (Stix, 1962):

$$k_{\parallel} v_{\parallel} = \omega + n \Omega; \qquad (7.1)$$

$$n = -\infty \text{ ----- } -1, 0, +1, +2, \text{ -----},$$

where $k_{\parallel} = k \cos \psi$ is the component of the wave vector parallel to the earth's field, $v_{\parallel}$ is the parallel velocity, ω is the wave frequency, n is any non-zero integer and Ω is the electron cyclotron frequency. For the cyclotron harmonics ($n \neq 0$), the sign of the contribution of each resonance to the growth rate is given by the anisotropy. When $n = 0$, $k_{\parallel} v_{\parallel} = \omega$ is the condition for Landau resonance which gives a damping contribution to the energy exchange between particles and waves corresponding to Landau damping for an electron distribution that decreases

monotonically with energy. The magnitude, and thus, the relative importance of each resonance, is given by a coefficient which depends on the angle between the wave vector and the field as well as anisotropy and number of resonant particle at each resonance. Specific plots of the growth rate $\gamma(\psi)$ as a function of wave normal angle have been given by Kennel (1966) and Kennel and Petschek (1969) for an electron velocity distribution appropriate to a turbulent plasma. It is indicated by these plots that if the energy spectrum of the particles is hard enough, cyclotron interactions are important over a significant cone of angles whereas for a softer spectrum, the unstable cone shrinks rapidly. For an electron spectrum ($\frac{dJ}{dE} \propto \frac{1}{E^{2-3}}$), typically found in the magnetosphere (McDiarmid et al., 1963), the wave is unstable for $\psi \leq 40°$ (Kennel and Thorne, 1967). We have, therefore, computed ray paths for second set assuming $\psi = 10° - 30°$ for both models. These ray paths are shown in Figures 6.8 - 6.13.

7.3 Interpretation of Results for Calculations of Set No. 2

Ray paths for this set of computations have been plotted (Figures 6.10 - 6.15) where only the nightside of the earth is shown in the figures. The earth radii in the equatorial plane are numbered. A dipole field line through L = 6.0 is shown for reference. The results indicate that signals at VLF frequencies, originating in the equatorial plane at L = 6.0, are reflected back to the magnetosphere. We also find that as one considers higher frequency waves, the point at which the reflection takes place moves closer to the surface of the earth. Thus, low frequency waves are reflected long before reaching the ionosphere. We do not find the qualitative physical picture of the ray paths to be greatly "model dependent", i.e., reflection of the signals can be seen for both the models

except that minor quantitative differences do exist. Successive reflections of the VLF signals from one hemisphere to the other seems to indicate that the waves are quasi-trapped. This quasi-trapping is, however, rather incomplete since the waves do tend to move to somewhat high L values as they approach the earth and would, on reflection, again move out further. Thus on each reflection, the waves move to a slightly higher L-shell. This general outward migration of the waves to a higher L-shell on each reflection has also been seen by Kimura (1966) in his ray tracing calculations using an entirely different electron number density model. The general picture, therefore, that the VLF signals are reflected in the magnetosphere, seems to be independent of the model used.

It may be useful to compare VLF ray paths of second set with the variation of lower hybrid resonance frequency (f_{LHR}). For a multicomponent plasma, the lower hybrid resonance frequency (Smith and Brice, 1964; Cerisier, 1970) is given by

$$\frac{1}{f_{HLR}^2} = \left(\frac{1}{f_{oe}^2} + \frac{1}{f_{He}^2}\right) \frac{m_p}{m_e} M_{eff}, \tag{7.2}$$

where f_{oe} and f_{He} are the electron plasma and gyro frequencies respectively, m_p and m_e are the masses of the proton and electron respectively. M_{eff} is the effective weighted mean mass of the ions given by

$$\frac{1}{M_{eff}} = \sum_i \alpha_i / m_i , \tag{7.3}$$

with α_i being the fraction of the positive ion density occupied by the

ith ion species. The lower hybrid resonance frequency is very sensitive to the variation of electron density and ion composition and its altitude profile for the two selected models is shown in Figures 7.1 and 7.2 for comparative studies.

For propagating waves, the wave normals of the signals usually turn under the combined influences of the gradient of the magnetic field and the curvature of the field lines. In other words, the angle, ψ, between the wave normal vector and the magnetic field increases and finally it becomes almost perpendicular to the field lines close to the resonance cone. The lower hybrid resonance frequency (f_{LHR}) is very small at greater distances in the equatorial plane and the resonance cone always exists when the propagations frequency is above the f_{LHR}. Now at the same time, the descending VLF wave traverses the region where ψ increases as the altitude lowers, the lower hybrid resonance frequency also gradually increases. When it reaches the altitude where the lower hybrid resonance frequency passes the wave frequency, ψ becomes equal to $\pi/2$. At this time the refractive index becomes infinitely large and the wave energy is reflected upwards.

Figure 7.3a schematically shows the path of energy of a typical whistler mode wave. For clarity the separation between the descending and ascending parts of the path are exaggerated but, in reality, they may be almost overlapping. Figure 7.3b permits a better understanding of the process of reflection; it is shown there for the various points marked in Figure 7.3a, which is the axial cut of the refractive index surface (plot between refractive index and wave normal angle) about the magnetic field. The ray direction is always at right angles to this surface.

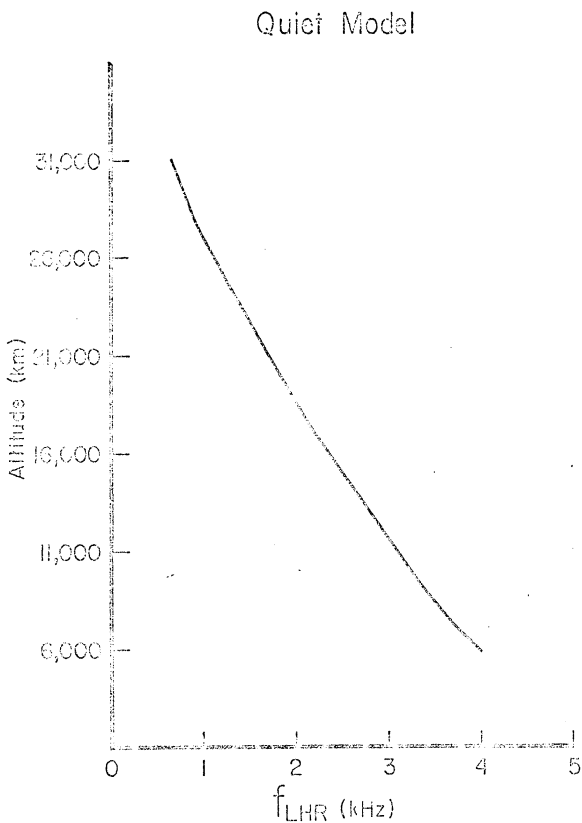

Figure 7.1 Variation of lower hybrid resonance frequency with altitude for quiet model

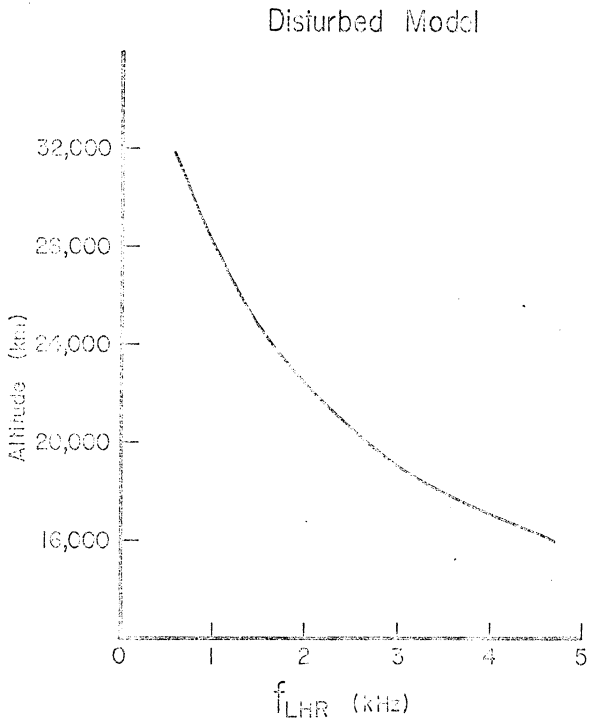

Figure 7.2 Variation of lower hybrid resonance frequency with altitude for disturbed model

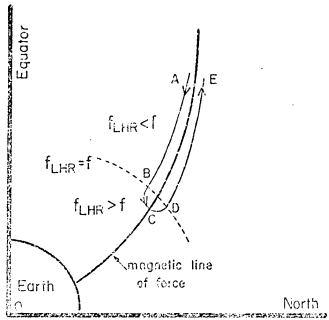

Figure 7.3a Path of energy of a typical whistler mode wave

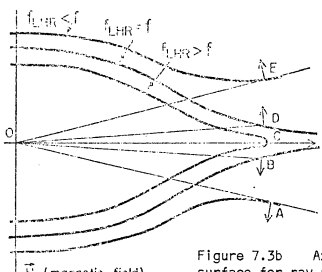

Figure 7.3b Axial cut of refractive index surface for ray path in Figure 7.3a

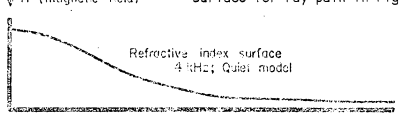

Figure 7.3c Typical refractive index surface plotted from computational results for a 4.0 kHz signal under quiet conditions

Figures 7.3a and 7.3b represent schematically how the whistler mode waves are reflected when the lower hybrid frequency exceeds the wave frequency. A typical refractive index surface plotted from computational results for a 4 kHz signal and quiet model is shown in Figure 7.3c.

7.4 Summary and Discussion

VLF ray path computations in the present study have been performed to understand some of the basic features of whistler-mode VLF wave propagation in the magnetosphere and ionosphere. Ray tracing was done principally to reveal why VLF/ELF emissions are comparatively rare events on the ground but are very common at satellite altitudes. Equations, as originally developed by Haselgrove (1954) to work with a digital computer and obtained for two-dimensional ray tracing in a meridian plane by Walter (1969), have been used for this purpose. Computations were divided into two sets depending upon the initial conditions of the ray path corresponding to two different source locations for VLF/ELF emissions. For the first set of computations, wide-band auroral hiss is assumed to be produced around 3000 km altitude level in the auroral zone atmosphere. The source of VLF/ELF emissions for the second set was considered to be situated in the equatorial plane of the magnetosphere outside the plasmapause at L = 6.0 in the auroral zone. The reason for conducting computations of the second set is due to some similarity between auroral hiss observed at ground stations and the broadband noises observed by the high altitude OGO I satellite (Dunckel and Helliwell, 1969).

Computational results indicate that VLF emissions, originating at 3000 km in the auroral zone with almost any wave normal direction relative to magnetic field less than $\pm \pi/2$, should be found down to the 125 km

altitude level under both quiet and disturbed conditions. The region below 125 km, which may account for the loss of VLF signals due to reflection or attenuation losses due to divergence of signal rays from the vertical and collisional absorption or both, will be considered in the next chapter. VLF signals starting from the auroral zone region in the equatorial plane are found to be reflected back much before reaching the ionosphere. Hence, these signals will never be observed on the ground.

Ray tracing studies have been carried out under certain assumptions which, although they make an already complicated problem a litte more simple to work with, are not strictly valid for a more realistic approach to conditions present in the magnetosphere. For example, the order estimates of electron density using a diffusive equilibrium model (Angerami and Thomas, 1963) seem to be higher at far distances from the earth in the equatorial plane than measured values. However, this depends upon the electron density values chosen at the reference altitude of 400 km. The diffusive equilibrium model does not account for the observed knee (abrupt decrease in magnetospheric ionization density) at about 4 R_E, the position of which changes during periods of changing magnetic activity and local time (Carpenter, 1966; Angerami and Carpenter, 1966). Also the ducts, which are field-aligned electron number density inhomogeneties present in the magnetosphere, are not a feature of this model. In this sense, the assumption of diffusive equilibrium model used in our computations presents only a simplified ionization density (in the magnetosphere) smoothly decreasing with increasing radial distance from the earth. The magnetosphere, for our computations, is assumed to be permeated by a static magnetic field represented by the centered dipole configuration which is not too bad an

approximation up to 6 R_E during quiet periods. Beyond that the configuration and content of the magnetosphere is dominantly controlled by the solar wind, convection electric field ($\vec{E} \perp \vec{B}$), etc.

CHAPTER VIII

GROUND OBSERVATIONS OF EMISSIONS IN RELATION TO IONOSPHERIC ABSORPTION

8.1 Introduction

From the preceding ray tracing computations of the first set (for VLF signals originating at 3000 km and coming down to an altitude of 125 km) it has been found that there is no indication of any reflection of VLF signals. The attenuation of signals also does not seem to play any major role above 125 km and thus they could not be lost completely. It was, therefore, initially assumed that the VLF signals produced in the auroral zone atmosphere should be observable on the ground. This is possible provided there is no attenuation of the signals below 125 km and that their intensities remain above the threshold of detectable flux for the ground VLF system. However, the calculations to be presented in this chapter show that the actual region, which determines whether or not the signals can be observed on the ground, occurs in the 60 to 125 km altitude region. There could be heavy attenuation losses in the region below 125 km due to divergence of ray paths towards the horizontal, collisional absorption and even reflection of the signal before it comes out from the exit point of the ionosphere at 60 km. All of these attenuation losses will now be considered in this chapter.

First, it is quite apparent that because of the rapid depletion of electrons in the lower ionosphere, the refractive index drops from $n >> 1$ at 125 km to $n = 1$ below the ionosphere. This causes the wave normal angle of the signal to increase appreciably from the vertical as it comes down and emerges from the ionosphere. Since the ray directions

are found to be very close to wave normal directions in this region, the VLF ray paths too tend to deviate away from the vertical in a similar fashion. Therefore, there always exists a limiting wave normal angle at the top of the lower ionosphere beyond which the wave normals could be deviated to more than $\pi/2$, before emerging from the ionosphere, resulting in signal reflection. Secondly, even for signals that do come to the ground, there is always, in addition to collisional absorption, additional attenuation due to divergence of signal ray paths. This is because when the signal propagates downward from the top of the lower ionosphere, the linear separation between the ray path and the vertical becomes greater. We can determine the attenuation due to divergence of ray paths in the following way: Since the source function of VLF emissions is not known, we assume that the source is uniform along the east-west direction, i.e., it is a cylindrical line source corresponding to the length of an auroral arc and that it emits isotropically. A pair of rays in the meridian plane will tend to be separated further apart as they proceed earthward. Then the signal power flux at the ground is reduced by the ratio of linear separations between ray paths at satellite altitude and the ground even if there is no dissipation of power in the D region due to collisions. This is usually the spatial power loss which could be converted into db corresponding to different areas of incident power flux at two height levels. Since, the actual power absorbed in the D region due to collisional loss is always present, it is then added to the spatial power loss caused by the divergence of ray paths.

Computations have been performed to extend the ray paths from 125 km to the earth using the WKB method and to determine the absorption in that region. Results of VLF wave propagation in the lower ionosphere will then

be related to the reflection and absorption processes.

8.2 Wave Normal Calculations in the Lower Ionosphere

In general, there are four different propagating magneto-ionic modes in the ionosphere which represent two upward propagating ordinary and extraordinary and two similar downward propagating modes; they have propagation constants given by the roots of Booker quartic equation (Budden, 1961). These modes have been studied by Swift (1962) who developed equations for VLF radio wave propagation in the ionosphere using the quasi-longitudinal approximation in which the propagation equations appeared as four first order linear differential equations coupled by gradients in electron density and collision frequency. In our analysis, however, attention will be restricted to only one mode for penetrating wave and its behavior as it travels obliquely through the horizontally stratified anisotropic ionosphere in the presence of geomagnetic field and electron collisions.

Let us adopt the coordinate system as shown in Figure 8.1. The magnetic field B_o is confined to the x - z plane and is inclined at an angle δ to the x-axis. The electron density and collision frequency is to vary only in the z-direction. The direction of propagation is denoted by the vector $\vec{T}_k$ at an angle ψ to the z-axis and with an azimuthal angle ϕ. The wave normal angle θ between the direction of wave normal and direction of geomagnetic field can then be determined by taking the scalar product of $\vec{T}_k$ and $\vec{B}$ and is given by

$$\text{Cos } \theta = - \text{Cos } \psi \text{ Sin } \delta + \text{Sin } \psi \text{ Cos } \delta \text{ Cos } \phi. \qquad (8.1)$$

The complex propagation constant in a uniform magneto-ionic medium is obtained from Appleton-Hartree formula (Ratcliffe, 1959) and is given by

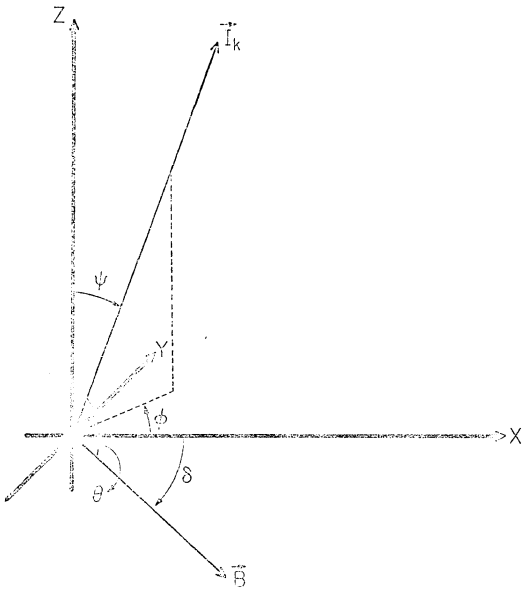

Figure 8.1 Coordinate system

$$k = \frac{\omega}{c}\left[1 - \frac{X}{1 - iZ - \left[\frac{Y_T^2}{2(1 - X - iZ)}\right] \pm \sqrt{\left[\frac{Y_T^4}{4(1 - X - iZ)^2}\right] + Y_L^2}}\right]^{\frac{1}{2}} \quad (8.2)$$

where

$$X = \left(\frac{\omega_N}{\omega}\right)^2,$$

$$Y = \frac{\omega_H}{\omega},$$

$$Z = \frac{\nu}{\omega},$$

$$\omega_N^2 = \frac{4\pi N_e e^2}{m_e} \quad \text{(square of the angular plasma frequency)},$$

$$\omega_H = \frac{e B_o}{m_e c} \quad \text{(angular electron gyrofrequency)},$$

m_e = mass of electrons in gm,

e = electron charge in e.s.u.,

N_e = electron density in cm^{-3},

B_o = magnetic induction of the earth's field in gauss,

ν = electron collision frequency

$\omega = 2\pi f$ (angular wave frequency),

$Y_L = Y \cos \theta$,

$Y_L = Y \sin \theta$,

θ = angle between directions of propagation and geomagnetic field,

and

c = velocity of light.

Let us now consider a plane boundary in the x-y plane located at z_1. Let the propagation constant at $z < z_1$ by k^i and at $z > z_1$ be k^{i+1} corresponding to one propagating mode. Snell's Law requires that the

condition of propagation that must be satisfied at all levels in the ionosphere is

$$k^i \text{ Sin } \psi^i = \frac{\omega}{c} \text{Sin } \psi_o, \tag{8.3}$$

where ψ_o is the zenith angle of the wave below the ionosphere. We shall now be interested in determining angle ψ at all levels in the ionosphere, which is not trivial, as k is an irrational function of Sin ψ. However, in practice, as pointed out by Swift (1962), a simple iterative solution for Sin ψ can be found. For example, if Sin ψ^i is known and it is desired to find Sin ψ^{i+1}, then we let Sin ψ_l^{i+1} be the lth step in the iterative process described by the equation

$$\text{Sin } \psi_l^{i+1} = \frac{\frac{\omega}{c} \text{Sin } \psi_o}{k^{i+1} (\text{Sin } \psi_{l-1}^{i+1})}, \tag{8.4}$$

where

$$\text{Sin } \psi_o^{i+1} = \text{Sin } \psi^i$$

and this simple iteration converges in a very few steps. It is pointed out (Swift, 1962) that as a wave penetrates the D region of the ionosphere, some of the energy is converted into other modes, which results in the process of reflection, while some of the energy is dissipated by electron collisons with neutral particles. We have also obtained an estimate of attenuation for the penetrating wave by computing attenuation coefficients of the WKB solution for the propagating mode as a function of the angle of incidence. The attenuation is given by:

$$\exp - \left[\int_o^z I_m (k \text{ Cos } \psi) \, dz \right], \tag{8.5}$$

where I_m denotes the imaginary part. The total attenuation is then given by:

$$A_{db} = 8.7 \left[\int_o^z I_m (k \text{ Cos } \psi) \, dz \right]. \tag{8.6}$$

The total absorption, suffered by the signal due to collisions only, is expressed in db and is integrated over the entire height range from 125 km to below the ionosphere by using the trapezoidal rule.

8.3 Assumptions of Various Parameters

We have used equations (8.1) to (8.4) to determine the zenith angle of the phase normal ψ at each 5 km interval starting from below the ionosphere and up to 125 km. Collisional attenuation is also determined for the same height range using equation (8.5). For this purpose, we appropriately choose the electron density profiles for both the quiet and the disturbed conditions of the nighttime ionosphere and a collision frequency profile representing the lower ionosphere. These profiles are shown in Figure 8.2. N_e-h profiles considered for computations under quiet and disturbed conditions are due to Deeks (1966) and Ungstrup (1971) respectively. It should be pointed out that the electron density values at 100 km level for both models come to a very close agreement with the values observed by the incoherent scatter radar operated near College, Alaska. However, the limitations of the scatter radar do not permit us to use its N_e-h profile for the D region of the ionosphere. It can be noticed from Figure 8.2 that both N_e-h profiles and ν-h profile have been extrapolated to the region where electron density becomes unity for the sake of completeness of lower ionospheric regime. Computations have been done from 60 to 125 km for quiet model and from 40 to 125 km for disturbed model. This includes the entire lower ionospheric regime where collisional absorption is present. However, the results indicate that there is no appreciable divergence of the signal rays below 75 km for quiet model and below 60 km for disturbed model. The collision frequency profile is taken from Parthasarathy and Berkey (1965).

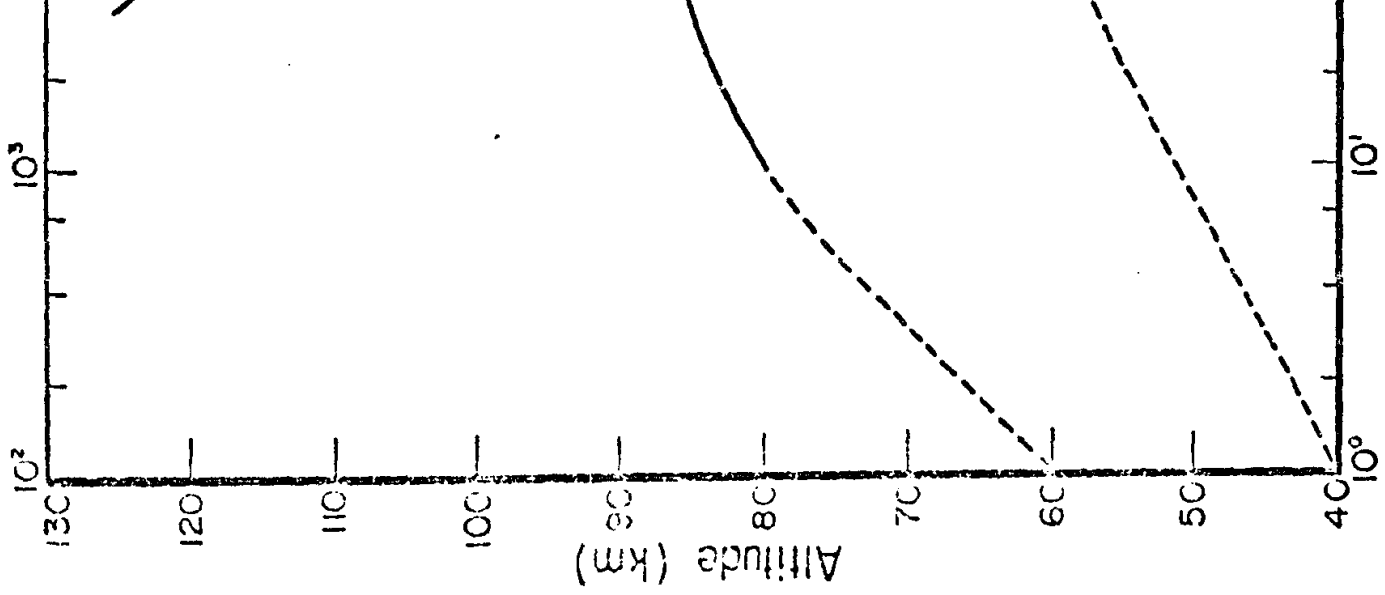

Figure 8.2 E

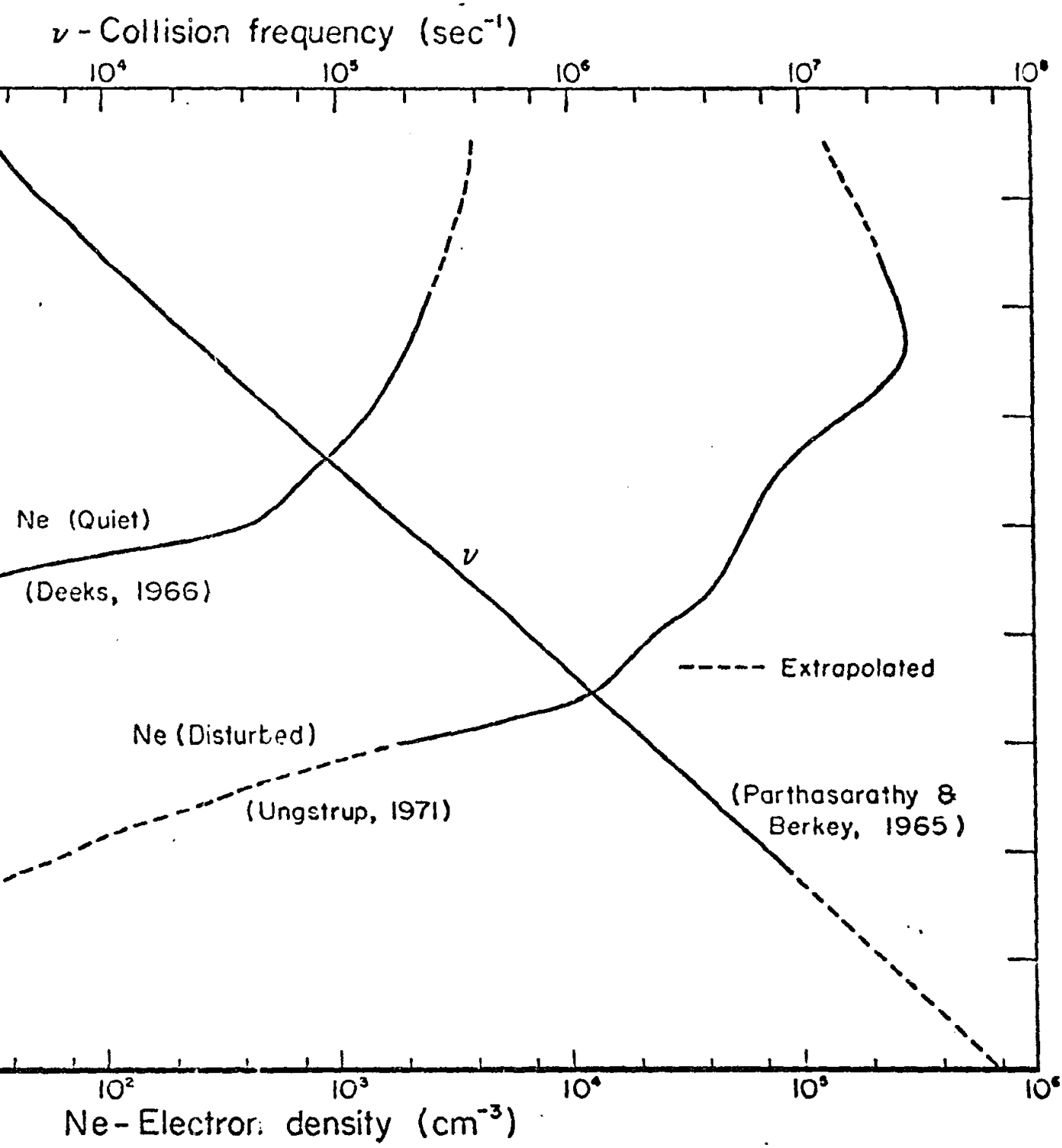

lectron density and collision frequency altitude profiles

We assume for our computations, a constant magnetic field strength of 0.57 gauss, a dip angle of 77° corresponding to high latitude station (College) and propagation frequencies of 1.0, 4.0 and 8.0 kHz in the VLF range. A range of incident wave normal angles from the vertical (ψ_o) at the bottom of the ionosphere, to vary from 10° to 90° in intervals of 10°, is considered. We then compute all emergent angles at each fixed ionospheric level for a given ψ_o. This process is repeated for three different azimuthal angles ϕ = 0°, 90° and 180°. Then, from the proper knowledge of wave normal angles at 125 km from earlier ray tracing computations, VLF ray paths can be easily extended from 125 km to the ground.

Due to the complexity of computations involved, a computer program is written in FORTRAN IV for an IBM computer 360/40. The emergent angles at each ionospheric height level have been determined using Snell's law formulation for each given incindent angle below the ionosphere. Total collisional absorption (db) in the lower ionosphere has also been determined at VLF frequencies by computing attenuation coefficients of the WKB solution for the propagating mode. A full generalized expression for propagation constant is used for these purposes. Results are summarized in Table 8.1 and Table 8.2 for quiet and disturbed models respectively. For comparing VLF absorption with riometer records, absorption at 30 MHz has also been computed for vertically incident waves using the same models. 30 MHz absorption is mentioned at the bottom row of Tables 8.1 and 8.2 for quiet and disturbed conditions respectively.

8.4 Signal Reflection in the Lower Ionosphere

It can be noticed from Tables 8.1 and 8.2 that, at a wave frequency of 4.0 kHz typical of VLF hiss, the limiting value of wave normal angle

TABLE 8.1

QUIET MODEL

Azimuthal angle of phase normal in (degrees)	Zenith angle of phase normal at 60 km in (degrees)	Zenith angle of phase normal at 125 km in (degrees) for wave frequency in (kHz)			Total absorption in (db) from 60 to 125 km for wave frequency in (kHz)		
		1.0	4.0	8.0	1.0	4.0	8.0
0	10	0.69	1.36	1.90	0.26	0.57	0.90
	20	1.35	2.68	3.74	0.34	0.91	1.59
	30	1.97	3.90	5.44	0.46	1.40	2.53
	40	2.54	5.0	6.97	0.62	2.0	3.66
	50	3.02	5.95	8.27	0.80	2.68	4.95
	60	3.41	6.71	9.33	0.99	3.43	6.37
	70	3.70	7.27	10.10	1.18	4.22	7.86
	80	3.88	7.62	10.57	1.34	5.03	9.10
	90	3.93	7.73	10.73	1.40	5.43	9.31
90	10	0.69	1.37	1.91	0.23	0.44	0.63
	20	1.36	2.69	3.76	0.26	0.58	0.94
	30	1.98	3.93	5.50	0.33	0.88	1.54
	40	2.55	5.05	7.07	0.44	1.33	2.41
	50	3.04	6.02	8.42	0.58	1.90	3.49
	60	3.43	6.81	9.51	0.75	2.56	4.74
	70	3.73	7.38	10.32	0.92	3.28	6.16
	80	3.90	7.74	10.81	1.06	4.0	7.65
	90	3.97	7.86	10.97	1.12	4.42	8.65
180	10	0.69	1.37	1.92	0.20	0.33	0.42
	20	1.36	2.71	3.79	0.21	0.34	0.44
	30	1.99	3.96	5.56	0.23	0.44	0.64
	40	2.56	5.11	7.17	0.28	0.67	1.12
	50	3.06	6.10	8.56	0.37	1.07	1.94
	60	3.46	6.90	9.70	0.49	1.63	3.02
	70	3.76	7.50	10.53	0.65	2.30	4.32
	80	3.94	7.86	11.05	0.78	2.99	5.75
	90	4.0	7.98	11.22	0.84	3.40	6.74

Absorption at 30 MHz for vertical incidence = 0.002 db

TABLE 8.2

DISTURBED MODEL

Azimuthal angle of phase normal in (degrees)	Zenith angle of phase normal at 60 km in (degrees)	Zenith angle of phase normal at 125 km in (degrees) for wave frequency in (kHz)			Total absorption in (db) from 40 to 125 km for wave frequency in (kHz)		
		1.0	4.0	8.0	1.0	4.0	8.0
0	10	0.12	0.24	0.34	7.47	14.48	20.11
	20	0.24	0.48	0.67	7.54	14.71	20.53
	30	0.35	0.70	0.98	7.62	15.01	21.1
	40	0.45	0.89	1.26	7.72	15.38	21.83
	50	0.54	1.06	1.50	7.84	15.82	22.71
	60	0.60	1.20	1.70	7.98	16.33	23.73
	70	0.65	1.31	1.84	8.13	16.90	24.83
	80	0.69	1.37	1.93	8.38	17.46	25.93
	90	0.70	1.39	1.96	8.38	17.99	26.69
90	10	0.12	0.24	0.34	7.44	14.36	19.89
	20	0.24	0.48	0.67	7.47	14.46	20.09
	30	0.35	0.70	0.98	7.52	14.64	20.42
	40	0.45	0.89	1.26	7.59	14.89	20.90
	50	0.54	1.07	1.51	7.68	15.21	21.54
	60	0.60	1.21	1.70	7.79	15.6	22.32
	70	0.66	1.31	1.85	7.92	16.08	23.25
	80	0.69	1.37	1.94	8.06	16.65	24.35
	90	0.70	1.39	1.97	8.16	17.14	25.40
180	10	0.12	0.24	0.34	7.41	14.24	19.68
	20	0.24	0.48	0.67	7.41	14.23	19.65
	30	0.35	0.70	0.98	7.42	14.29	19.77
	40	0.45	0.90	1.27	7.46	14.42	20.02
	50	0.54	1.07	1.51	7.53	14.63	20.43
	60	0.60	1.21	1.71	7.61	14.92	21.0
	70	0.66	1.31	1.86	7.72	15.30	21.73
	80	0.69	1.38	1.94	7.84	15.79	22.67
	90	0.70	1.39	1.97	7.94	16.25	23.66

Absorption at 30 MHz for vertical incidence = 0.46 db

ψ from the vertical, beyond which the signal could be reflected back to the ionosphere, is 7.7° for quiet model and 1.4° for disturbed model. This means that there does exist a cone of wave normal angles within which the signals starting from the emitting source could propagate to the ground. However, any signal starting with a phase normal outside this cone would be reflected back from the D region of the ionosphere and such signals would not be observed on the ground. It can be readily seen from Table 8.2 that this cone of angles at 125 km is very small under disturbed conditions. As a result, the signals cannot reach the ground unless they are close to vertical incidence at 125 km. Wave normal angles relative to the field-direction at 3000 km which correspond to the cone of zenith angles of phase normal at 125 km have also been determined and will be discussed in Section 8.6.

Wave normal computations in the lower ionosphere do not show any significant difference in the cone of angles with variations in azimuthal angle. The limiting value of the zenith angle of phase normal, however, varies with the frequency directly and increases to 10.7° at 8.0 kHz whereas it is only 3.9° at 1.0 kHz under quiet conditions. Values of ψ at 125 km under disturbed conditions for 90° emergent angle are 0.7°, 1.4° and 2.0° at 1.0, 4.0 and 8.0 kHz respectively. A typical example to show how the divergence of ray path takes place in the lower ionosphere has been plotted from computational results at a wave frequency of 4.0 kHz under quiet conditions. This is shown in Figure 8.3 for an incident angle of 6.7° at 125 km which is found to emerge from the ionosphere at 60°. As mentioned in Section 8.1, VLF signals within the cone of angles which are not reflected from the lower ionosphere suffer a heavy spatial attenuation due to

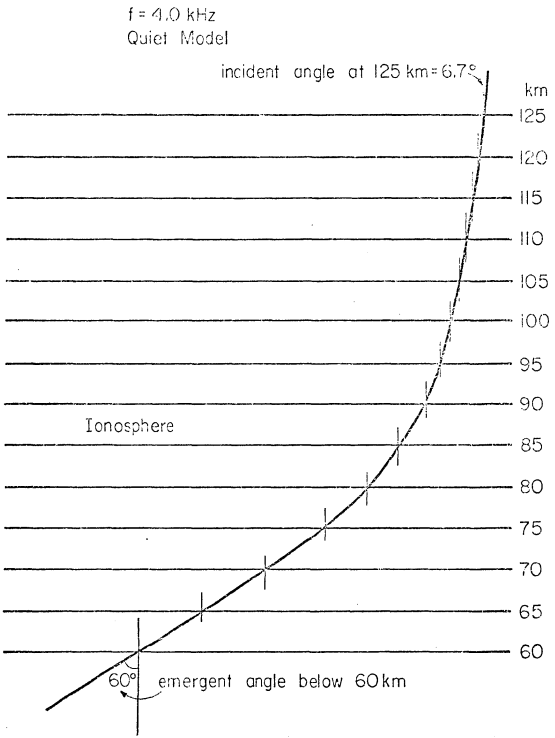

Figure 8.3 Schematic representation of divergence of ray path in the lower ionosphere for a 4.0 kHz VLF signal under quiet conditions

their ray path deviation from the vertical. This will be presented in the next section.

8.5 Attenuation due to Divergence of Ray Paths

We shall now consider a more important aspect of the problem and determine the extent of attenuation due to the defocussing of signal rays in the lower ionosphere. A representative VLF signal at 4.0 kHz, propagating through the quiet nighttime ionosphere to the ground, is again chosen for the sample analysis. Let us consider that the signal is incident at the 125 km level at each of five different wave normal angles; 3.9°, 5.0°, 5.6°, 6.7° and 7.3° from the vertical and mark these ray paths as 1, 2, 3, 4 and 5 respectively. These angles are chosen because they come out below the ionosphere with angles of 30°, 40°, 50°, 60° and 70° from the vertical whose propagation paths can be easily traced out from present computational results. Knowledge of initial wave normal angles for these signal rays at the emission source can be obtained from Figure 8.4 which gives a linear plot of wave normal angles from the zenith at 3000 km and 125 km. Figure 8.4 is obtained from results of ray path computations of Set No. 1. It is found that the signal rays from 1 through 5 have the source emission angles of 39.4°, 46.2°, 50.2°, 56.3° and 60.0° respectively. The propagation paths for these signal rays in the lower ionosphere are traced from results in Table 8.1 and are shown in Figure 8.5. Figure 8.5 clearly indicates a significant divergence of signal rays from the vertical by the time they arrive at the ground. It should be pointed out that the distances between rays 1 through 5 have been obtained from their respective separations obtained in previous computations and are plotted to scale.

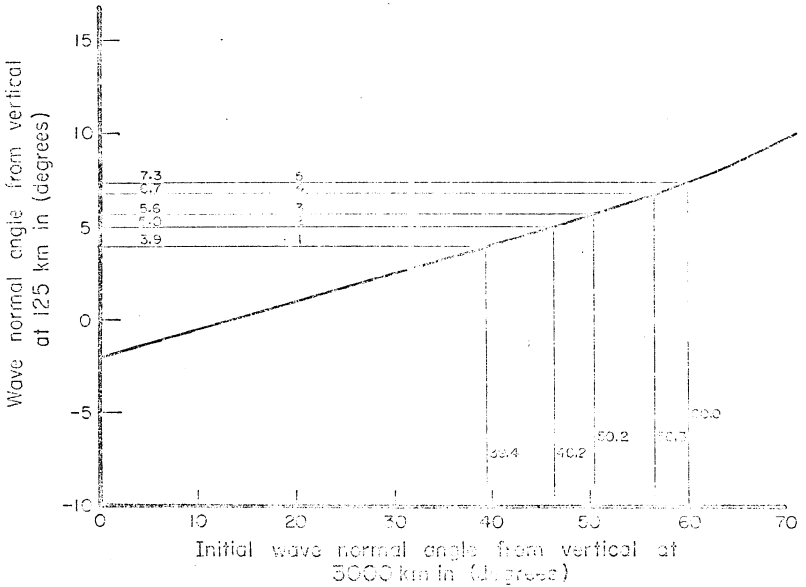

Figure 8.4 Plot between initial wave normal angles at 125 and 3000 km altitude levels

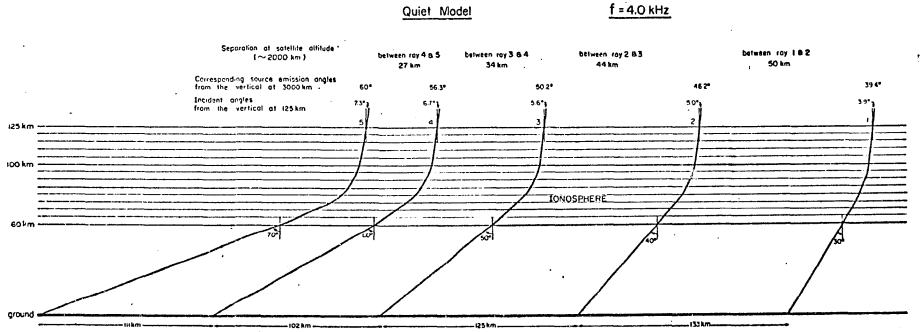

Figure 8.5 Propagation paths of a 4.0 kHz signal in the lower ionosphere with different zenith angles of phase normal at 125 km during quiet conditions

TABLE 8.3

Ray Path Nos.	Zenith angle of phase normal at the source point in (degrees)	Zenith angle of phase normal at 125 km in (degrees)	Zenith angle of phase normal at emergence from 60 km in (degrees)	Linear displacement between signal rays at ground in (km)	Linear displacement between signal rays at satellite altitude in (km)	Spatial attenuation due to divergence of signal ray paths in (db)	Collisional attenuation between signal ray paths in D region in (db)	Total attenuation of a 4.0 kHz signal for quiet model in (db)
1	39.4	3.9	30	133	50	4.25	1.70	5.95
2	46.2	5.0	40	125	44	4.53	2.34	6.87
3	50.2	5.6	50	102	34	4.77	3.05	7.82
4	56.3	6.7	60	111	27	6.13	3.82	9.95
5	60.0	7.3	70					

We shall now be interested in determining the attenuation due to divergence between ray paths 1 and 2, 2 and 3 and so on. This is done by assuming that the signal originally starts from the source with wave normal angles at 39.4°, 46.2°, 50.2°, 56.3° and 60.0° respectively. It is now relatively easier to determine the linear displacement between corresponding signal rays at the ground and at the satellite altitude of ∿ 2000 km where Injun 5 observed many VLF emissions. The corresponding displacements between two signal rays at the ground and at satellite altitude can be converted into spatial power loss in db for a cylindrical source by using the relation

$$A_{db} = 10 \log \frac{P_G}{P_S} = 10 \log \frac{L_G}{L_S}, \qquad (8.7)$$

where L_G and L_S correspond to the linear separations at ground and satellite altitude respectively. Absorption results for a 4.0 kHz VLF signal under quiet conditions are shown in Table 8.3.

Attenuation due to divergence of ray paths between two signal rays and total attenuation are then plotted in Figure 8.6 against the distance of ray paths from the foot of the magnetic field line from the source. It is clearly indicated from Figure 8.6 that the attenuation of the signals increases rapidly beyond about 500 km from the foot of the field line and may eventually become infinite for distances greater than about 600 km. Such distances correspond to signals generated at high initial wave normal angles.

In order to compare the attenuation of VLF signals with the riometer records, we have also made some theoretical estimate of the ratios between the abosrption of VLF signals and 30 MHz riometer absorption for the vertical incidence case. The absorption ratios can be calculated from the results

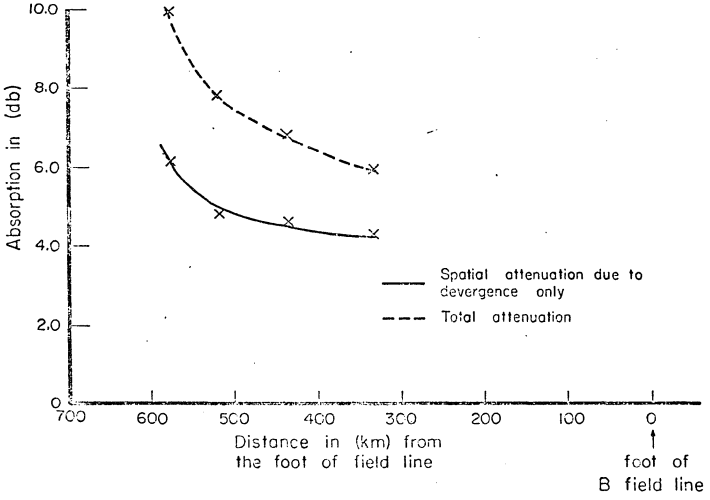

Figure 8.6 Spatial and total attenuation of a 4.0 kHz VLF signal for quiet conditions

in Table 8.1 and 8.2 for the quiet and disturbed conditions respectively. It is estimated that during the disturbed conditions, a 4.0 kHz VLF signal would suffer an absorption which is thirty times as high as the absorption suffered by a 30 MHz signal. Since the absorption ratio (A_{VLF}/A_{30MHz}) is proportional to $N_e^{-1/2}$, the ratios under quiet ionospheric conditions are found to be higher than the ratios during disturbed conditions. The theoretically derived absorption ratios indicate the extent of VLF signal attenuation and indicate the inconsistencies in the relationship of VLF emissions to the 30 MHz riometer absorption.

8.6 Summary and Discussion

Our wave normal calculations using Snell's law formulation indicate that VLF waves at 4.0 kHz, incident at 125 km with zenith angles of the phase normal, ψ_i, outside the range ± 7.7° and ± 1.4° under quiet and disturbed conditions respectively, would be reflected back from the lower ionosphere. These limiting angles at 125 km correspond to typical values of wave normal angles from the magnetic field direction at the source location.

We find that the extension of ray paths obtained from the earlier ray tracing computations of Set No. 1 to the results of wave normal calculations from 125 km to the ground indicate the following: For the quiet model, a 4.0 kHz signal starting from the source with initial wave normal angle relative to field direction of 46° comes to 125 km with a zenith angle of phase normal of 7.2°. On the other hand, the same signal starting with initial wave normal angle of 56° comes to 125 km with an angle of 8.2° and would be reflected, according to results in Table 8.1, before coming out of the ionosphere. Hence, a 4.0 kHz signal, starting from 3000 km with wave normal angle relative to field direction of more than about 50°,

cannot be received on the ground under quiet conditions. A similar analysis for disturbed model reveals that the signal has to be quite close to the field line at the source (< 10° for a 4.0 kHz signal) to escape reflection in the lower ionosphere.

For the plasma density model assumed in our computations, the cone of wave normal angles relative to magnetic field direction at 3000 km within which the VLF signals should be received at the ground have been determined from comparison of computational results and are shown in Table 8.4.

TABLE 8.4

Ionospheric Model	VLF wave frequency in (kHz)	Cone of zenith angle of phase normal at 125 km beyond which signal is reflected from lower ionosphere in (degrees)	Cone of corresponding wave normal angles relative to magnetic field direction at 3000 km in (degrees)
Quiet	1.0	± 3.9	-25 to +36
	4.0	± 7.7	-45 to +50
	8.0	± 11.0	-55 to +55
Disturbed	1.0	± 0.7	-3 to +8
	4.0	± 1.4	-6 to +10
	8.0	± 2.0	-13 to +16

It becomes quite apparent through computations in the lower ionosphere that there is a definite cone of wave normal angles of the wave which are permited to be transmitted to the ground. All other wave normals of the wave lying outside this transmission cone are trapped in the lower ionosphere and cannot exit to the earth-ionosphere cavity.

Table 8.4 indicates that high frequencies find a wider cone of angles that can be received on the ground and that the cone of wave normal angles becomes much smaller under disturbed conditions.

Even within the cone of wave normal angles, the signal rays diverge from the vertical and this divergence of signal ray paths towards the horizontal in the lower ionosphere is found to be mainly responsible for VLF signal attenuation. This attenuation appears to be even much larger than the absorption caused by collisions in the ionosphere. The total absorption, due to the sum of two attenuation losses, is found to increase rapidly beyond about 500 km from the foot of the field line passing through the source at which VLF emissions are generated. It, therefore, seems very likely that the auroral hiss, generated at altitudes from where the foot of the field line at the earth's surface is greater than about 500 km from the ground receiver, will be heavily attenuated. For vertical incidence in the ionosphere, theoretical studies of absorption ratios at 30 MHz riometer and VLF frequencies indicate that absorption of a 4.0 kHz signal under disturbed conditions is about 30 times as high as riometer absorption. These ratios are helpful for comparing attenuation of VLF emissions with the 30 MHz absorption as indicated by riometer records. Based on theoretical studies in the lower ionosphere, a conclusion can be drawn that many auroral hiss events can be observed at or above the auroral altitudes but are either reflected from, or heavily attenuated in, the lower ionosphere.

CHAPTER IX

GENERAL DISCUSSION AND CONCLUDING REMARKS

9.1 Summary of Results and Comments

Observations and analysis of VLF emissions, especially of VLF hiss, chorus and ELF hiss have been presented in this dissertation. Examples of events, indicating relationships of ELF/VLF emissions with the manifestations of auroral substorm phenomena, were studied using all-sky camera data, magnetic and 30 MHz riometer records. VLF data, for this purpose, were collected from two auroral zone ground stations at Bar I and College located on the same geomagnetic meridian (within and on the equatorward edge of the auroral oval) for almost a year and a half. Hiss and chorus events at College and Bar I were identified both by aural monitoring of magnetic tapes and from chart records. Although many VLF events were obtained on the ground during the period of observation, it represented only a small fraction of VLF emissions that might have been present in the auroral zone ionosphere. This has been shown by comparison of one month of Injun 5 satellite data with the ground VLF data which indicates a definite scarcity of VLF events on the ground. It became quite apparent that most of the emissions were restricted by the propagation medium from arriving at the ground VLF station.

The propagation of VLF signals in an inhomogeneous and anisotropic medium, such as the magnetosphere and ionosphere, has also been investigated. Considerable effort has been made to understand the causes for the rarity of VLF emissions at the ground level. Principal causes that exert controlling influences on the observability of VLF emissions on the ground have been determined from theoretical studies. This is done by

applying the ray tracing technique as originally developed by Haselgrove (1954) and obtaining the VLF ray paths for non-ducted whistler mode VLF wave propagation. In this chapter, we shall endeavor to relate and combine the results of observational analysis with the results obtained from theoretical studies to present a self-consistent picture of VLF and ELF emissions.

9.1.1 Chorus Emissions

It is seen from our ground observations that the narrow band chorus emission below about 4 kHz is primarily a day-time phenomena and extends from morning to late afternoon hours with a peak around 1200 hours local time. The period from 0200-0600 150° WMT is found to be relatively free from VLF emissions with a few notable exceptions where both chorus and ELF hiss are found to occur.

The most important result pertaining to the observations of chorus on the ground, is its absence in the late evening hours and its rarity in the 12 hour period centered on midnight. Chorus emissions and plasmaspheric ELF hiss, generated in the equatorial plane of the magnetosphere, have also been observed through high altitude satellites OGO 1, 3 and 5 (Russel et al., 1969; Dunckel and Helliwell, 1969 and Thorne et al., 1973). Russel et al. (1969) have reported the similarity between OGO 3 observations of steady noise and the bursts to that of the observed ELF hiss and chorus at lower altitudes respectively. Also, they do not observe VLF emissions in the night sector auroral zone of the magnetosphere. Through observations of OGO 1, Dunckel and Helliwell(1969) have described the occurrence, intensity and spectra of satellite emissions at frequencies below the local electron gyro frequency. Their observations give strong

support to the Kennel and Petschek (1966) mechanism of electron cyclotron instability in the equatorial plane.

We have conducted some ray path computations for VLF/ELF signals generated in the equatorial plane of the magnetosphere due to the similarity of satellite events with those observed on the ground. Ray path computations for VLF signals at 1.0 and 4.0 kHz starting at L = 6.0 from the equatorial plane revealed that they are reflected well before reaching the ionosphere and almost decisively establish that emissions from the equatorial plane cannot reach the auroral altitudes. Explanation of reflection mechanism is already provided in Section 7.3. Results derived from VLF ray path computations at greater distances about the reflection process are found to be relatively independent of the model. It is seen that more important than the plasma density variations in the deep magnetosphere is the fact that the wave normals turn under the combined influences of the curvature of the field lines and the gradients of the magnetic field. A separate computation for signals in the ELF/VLF range, starting from within the plasmapause at L = 3 and L = 5 was also performed to see if the mid-latitude chorus produced in the equatorial plane of the magnetosphere could come to the ground. The results, however, again indicated that these are also reflected back to the equatorial plane. It is, therefore, clear that although the spectra of emissions generated at the equatorial plane and observed by OGO 1 and OGO 3 within and outside the plasmapause may resemble ground chorus and ELF hiss, we find that these emissions are more or less trapped in the magnetosphere at altitudes $\geq 1\ R_E$ and cannot reach the ground.

On the other hand, theoretical computations for low altitude emissions

indicate that VLF/ELF emissions originating at 3000 km could be observed on the ground. Details of these computations will be discussed in the next subsection. Thus, all the dayside chorus events observed on the ground ought to have originated in the low altitude (a few thousand km) auroral zone in the dayside magnetosphere. In the context of ground observations, therefore, although the mechanism of chorus generation does not seem to be incompatible within the loss-cone instability theory of Swift (1968), however, it does not rule out the possibility that the emissions observed by high altitude satellites are generated by Kennel and Petschek (1966) mechanism in the equatorial plane.

The question, however, still remains why chrous at the ground level is rarely observed in the night sector. This has, in fact, been raised by Swift in his 1968 paper where he discusses a number of factors which might inhibit the development of his loss-cone instability. However, in connection with the ring current belt, the plausibility of the Bar I and College field lines extending deep into the plasmasheet rather than into the "proton ring current" region that Swift discusses, must also be considered. Such a severe stretching of field lines in the dark side of the magnetosphere has been suggested by Reid and Parthasarathy (1966), Parathasarathy and Reid (1967) and Frank (1971). Absence of night sector chorus would, therefore, also depend upon the topology of the B-lines in the night side auroral zone. If the topology of the field line is the basis, chorus events would be equally frequent in the night side at meomagnetic latitude < 60° because such field lines decisively map into the "proton ring current" belt.

The diurnal variation of chorus shows a close similarity to the

variation of the flux of trapped (i.e., with pitch angle $\tilde{\sim}$ 90°) $\geq$ 40 kev electrons at $\tilde{\sim}$ 2000 km. Frank, Van Allen and Craven (1964) have analysed this flux with respect to local time and noticed that the diurnal variation of this flux maximizes around local noon at 68° geomagnetic latitude and symmetrically decreases towards the midnight meridian (Figure 9.1). (Note that the magnetic local noon in Figure 9.1 corresponds to $\tilde{\sim}$ 1300 hours local time). The flux numbers in Figure 9.1 indicate that the flux is greater at noon than at night by an order of magnitude. We notice from our ground observations of chorus that a similar order of magnitude difference exists between noon and night hours (Figure 3.1) which reveals a close phenomenological association of chorus with the $\geq$ 40 kev electron flux. The observed $\geq$ 40 kev flux (Figure 9.1) is also notably anisotropic, i.e., whether in the dayside or in the nightside sector the trapped flux is more than an order of magnitude greater than the precipitated flux (i.e., with pitch angle $\tilde{\sim}$ 0°). On the other hand, the diurnal variation of the precipitated flux also maximizes around local noon for geomagnetic latitude less than 68°. A conclusion can, therefore, be drawn that the chorus emission observed at the ground level in the auroral zone is favored by the existence of large and anisotropic flux or the precipitated flux of $\tilde{>}$ 40 kev electrons at $\tilde{\sim}$ 2000 km. Since chorus is generated within the magnetosphere, considerations of symmetry between northern and southern hemispheres of the magnetosphere would indicate that a seasonal dependence of the generation of chorus is unlikely. This suggests that any seasonal dependence of chorus observations on the ground is controlled primarily by ionospheric propagation conditions.

Comparison of chorus events observed on the ground with the magnetic

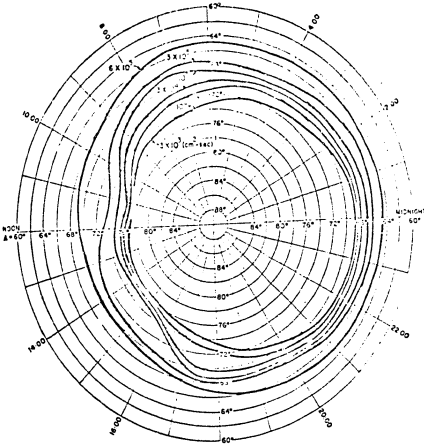

The median omnidirectional intensities of trapped electrons ($E \geq 40$ kev) measured at low altitudes with Injun 3 as displayed in a Λ local time coordinate system.

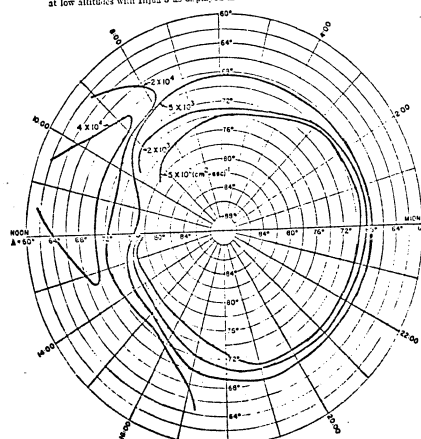

The median omnidirectional intensities of electrons ($E \geq 40$ kev) precipitated into the atmosphere as displayed in a Λ local time coordinate system.

Figure 9.1

activity index K_p, are not found to be as consistent as expected. This may be due to several competing effects influencing the observation of chorus emissions at the ground level. First, that the generation of chorus is enhanced during periods of high magnetic activity and secondly that the ionosphere becomes more opaque to the transmission of ELF/VLF emissions during these same disturbed periods. A third possibility is that the trapping boundary moves equatorward of the station during the hours of high K_p. We may also note that the simultaneous appearance of VLF emissions on both College and Bar I records are not observed. This suggests that the emissions may be localized in latitude and that the propagation of VLF signals in the earth-ionosphere waveguide is not an important factor in determining whether they should be observed on the ground.

In summary, we have seen from the preceding discussion of chorus that these emissions observed on the ground are the low altitude emissions. Chorus emissions are also generated in the equatorial plane of the magnetosphere by the Kennel and Petschek mechanism but are most decisively unable to reach the ground. During large magnetic inflation when the plasma moves to lower L-shell, chorus could also be seen to geomagnetic latitude less than 60°. The diurnal variation of chorus in the auroral zone seems to be related to the $\geq$ 40 kev trapped and anisotropic electron flux.

9.1.2 Hiss Emissions

The wide band VLF hiss is observed in the auroral zone mainly in the late evening hours or around local midnight and is found to be closely related to the visual auroral. Several examples of strong correlation between the occurrences of VLF hiss at the ground level and auroral activation have been found with the help of all-sky camera data. Some of these

examples are presented in Chapter IV which show that there does exist a close connection between the two. This may be due to the same precipitating particles being responsible for both hiss and auroral light. Swift (1965) suggested that auroral hiss may be caused by the well known two-stream instability associated with sufficiently strong currents flowing parallel to the magnetic field. On the other hand, it is also reported that strong whistler mode VLF emissions may be produced in the equatorial plane of the magnetosphere by wave amplification process and which, in turn, lead to pitch angle scattering of electrons by these waves (Kennel and Petschek, 1966; Thorne and Kennel, 1967). This scattering is a case of pitch angle diffusion of particles into the "loss cone" for eventual precipitation into the auroral zone atmosphere. However, we have already seen that such VLF signals would be reflected back to the equatorial plane well before reaching the ionosphere. It, therefore, seems reasonable to believe that VLF hiss events observed at the ground level and by low altitude satellites Injun 3 and Injun 5, are low altitude emissions and may have been produced by the mechanism proposed by Swift (1965). It is not clear, however, in Swift's paper whether there is a preferred altitude at which this instability arises. Kindle and Kennel (1971) have proposed that electrostatic ion cyclotron waves can be unstable to field-aligned currents comparable to those expected in the auroral zone. Gurnett and Frank (1972), through Injun 5 observations, have associated the VLF hiss events with the inverted V precipitation events of soft electrons which shows a considerable evidence of acceleration and heating of electrons. According to their results, the down coming VLF hiss is generated above the Injun 5 altitude $\tilde{\sim}$ 2000 km.

It should also be noted that some VLF hiss events have been recorded at quiet times when there were no obvious instabilities inferred by the behavior of visual aurorae. Another mechanism is "cerenkov radiation" for the production of hiss (Ellis, 1957; Jørgensen, 1968; Lim and Laaspere, 1972). This mechanism does not, however, seem to be able to account for the observed intensities of hiss emissions.

Corresponding examples of auroral hiss and substorm activity show that hiss is present for a short time coincident with the movement of auroral forms in the beginning stages of auroral breakup. The peak hiss emission occurs at the time of the brightening of the auroral forms. After the breakup, absorption usually tends to increase due to intense ionization and hardening of particle spectra and the hiss intensities practically drop to zero. However, this is not always true and hiss emission may continue for some more time showing positive correlation with absorption. This is where the relationship between VLF hiss and the riometer absorption is sometimes found to be inconsistent. Our ground observations have also indicated that hiss events are more frequently observed at Bar I than at College. This may be partly accounted by the following interpretation. Poleward expansion is, to a large extent, determined by the motion of the visual aurora which is a manifestation of low energy electron precipitation and has been reported by Akasofu (1966) to occur during the expansive phase of the substorm. The production of VLF hiss is also found to be correlated with the precipitation of low energy electrons (Gurnett and Frank, 1972). A poleward moving auroral form would, therefore, cause more hiss emission poleward rather than equatorward of the oval.

Some contradictory examples have been observed where auroral events did not lead to any hiss events at the ground level. Since VLF data taken by the Injun 5 satellite indicates that hiss is almost always present on the auroral oval above the ionosphere, it is concluded that the controlling factor, as to whether or not hiss is observed on the ground, is the propagation condition in the ionosphere. The result of observational studies that the propagation conditions in the ionosphere are generally responsible for restricting many VLF emissions at or above the auroral altitudes, prompted us to perform the ray path computations.

Ray path computations indicate that the near-auroral zone VLF signals (assumed to start from 3000 km) originating with almost any wave normal angle relative to the magnetic field direction propagate down from 3000 km to 125 km (if the initial wave normal vector is perpendicular to the magnetic field, there is, however, no downward propagation). There has been no indication of any reflection of VLF signals in the above altitude range. The latitudinal spread of all the ray paths at 125 km seems to be confined to within a range of $< \pm 6^{\circ}$ about the foot of the source field line. In short, the examples of auroral and hiss events at College and Bar I have clearly established a general relationship between the two. Although auroral events may not necessarily be accompanied by observation of hiss on the ground due to several factors involved in the intervening propagating medium, VLF hiss is almost always associated with the aurora and is present in the ionosphere (> 125 km) above the auroral oval. However, since the refractive index changes rapidly below 125 km and becomes unity at the boundary of the lower ionosphere, the above ray paths have been further extended to the ground

to see the effect of the lower ionosphere on the accessibility of VLF signals to the ground level.

9.1.3 Discussion of the Observability of Hiss and Chorus on the Ground

Computations below 125 km have been done by assuming horizontally stratified lower ionosphere and by applying Snell's law to determine the emergent wave normal angles at each specified ionospheric level. It has been found from calculations that the actual region which determines whether or not signals can be observed on the ground, occurs in the 60 to 125 altitude region.

Computations performed in the lower ionosphere (60-125 km) have shown that VLF signals may suffer total internal reflection beyond a certain limit of incident wave normal angles at 125 km. Reflection of VLF signals in the lower ionosphere is caused by the divergence of signal ray paths towards the horizontal. The limiting values of the zenith angles of phase normal which produce reflection of VLF signals at the boundary of the lower ionosphere, have been obtained for both the quiet and disturbed conditions of the ionosphere. To quote an example, the cone of angles beyond which a 4.0 kHz VLF signal would be reflected within the lower ionosphere, is found to be $\pm$ 7.7° and $\pm$ 1.4° (at 125 km) for quiet and disturbed conditions respectively. These angles, however, represent a different set of initial wave normal angles at the source location. For the assumed plasma density variations in the magnetosphere, the corresponding initial wave normal angles relative to the field direction for the same signal at 3000 km are found to be within -45° to +50° for the quiet ionosphere and -6° to +10° for the disturbed one. The cone of wave

normal angles at other VLF frequencies are given in Table 8.5. Since, the cone of angles to escape reflection of VLF signals becomes much smaller during disturbed conditions, it is apparent that although more VLF emissions are likely to be generated during disturbed conditions, it is equally important that the chances of reflection of the signal also increase considerably.

A separate computation of VLF ray paths was also performed from 125 km to 6000 km. This was done for wave normal angles at 125 km that turn into 90° at the lower boundary of the ionosphere. It was observed from these computations that the wave normal angles at 6000 km are smaller than the corresponding angles at 3000 km and get increasingly closer to the field line. However, if the plasma density configuration in the magnetosphere, i.e., the refractive index is varied, the wave normal angles assume different values at 6000 km. For example, a larger contribution from O^+ constituent is found to decrease the refractive index and thus, the cone of wave normal angles that would propagate to the ground increases. The increase in the cone of wave normal angle for increased O^+ contribution would tend to maximize the particle density even in a small horizontal cross-section above the auroral oval. This would anticipate more heating and instability necessary for the production of hiss. In general, however, starting from 125 km, the wave normal vector is initially pulled away from the vertical toward $\vec{B}_o$ by the effect of the gradient in the magnetic field. The refractive index variation due to vertical gradient of the plasma density then becomes a controlling factor, causing further tilting of the wave normal toward $\vec{B}_o$.

Computations in the lower ionosphere show that even those signals

which are within the allowed cone of wave normal angles and manage to come to the ground, diverge from the vertical. The divergence of ray paths from the vertical increases for signals with higher zenith angles of phase normal at 125 km. VLF signals are also attenuated due to the divergence of signal ray paths in a meridian plane. This attenuation can be specified by the ratio of linear separations between any pair of ray paths at the satellite altitude and at the ground and have been determined for representative ray paths. This spatial attenuation appears to be even larger than the absorption caused by the electron-neutral collisions in the ionosphere during quiet conditions. The total attenuation, due to the sum of the two attenuation losses, is found to increase rapidly beyond about 500 km from the foot of the field line passing through the source at which the VLF emissions are generated. In conclusion, many of the near-auroral zone VLF events are frequently either reflected by, or heavily attenuated in, the lower ionosphere and these losses in the lower ionosphere are the principal causes for the rarity of hiss and chorus emissions at the ground level.

9.2 Discussion of Errors and Approximation and Recommendations for Future Work

There have been a number of approximations and assumptions inherent in our observational and theoretical work which should be considered at this point. Although certain approximations have been made in the theoretical computations to simplify the otherwise complicated problem, they may have introduced certain inaccuracies in the analysis. These are described below and relevant suggestions to improve upon measurements and calculations have been proposed for future work.

First of all, in connection with the operation of a ground VLF system for continuous recording, we find that it is of utmost importance to maintain a reliable time base for VLF data. We found that the timings of our Bar I observations which were provided by a time standard station have been quite accurate. On the other hand, since our College data had relied on a local clock and suffered from a chronic problem of power outages, the timings were found to be wrong once in a while. Any suspected timing on the College record was, however, corrected by spot checking of records on a day to day routine basis. The need for a time standard station through telemetry network is, therefore, quite apparent. Time confusion due to power outages could be avoided by providing mechanical operation of chart recorder. The basis for this suggestion arises from the several instances when the VLF emissions were recorded around a breakup event. Whether these emissions were a few minutes before, or exactly at, or a few minutes after the breakup cannot be determined without the necessary confidence in the time marks. Such accuracies are more readily available in mechanically driven recorders rather than the electrically driven ones.

Another handicap in the observations of VLF events on the ground has been the sensitivity of the ground VLF system and the fluctuation width of the system noise level to register weak VLF events. VLF emissions are heavily attenuated in the ionosphere and are much less intense on the ground than they are at the source location. In this respect, it seems very likely that we may have missed to record several weak emissions with our VLF system on the ground, thus affecting the statistical studies. We shall only point out here that the future observations should aspire

to improve the S/N ratio by at least an order of magnitude, e.g., by a better choice of field station site.

Our theoretical studies of VLF ray path computations have been performed by assuming the diffusive equilibrium model for plasma density variations in the magnetosphere. This was done by specifying electron and ion compositions at the reference altitude of 400 km. Using this model, therefore, the densities at higher altitudes > 400 km depended upon the parameters chosen at 400 km altitude level. Basic calculations of ion densities in a multicomponent exosphere (see Whitten and Poppof, 1971) using a diffusion process indicates that the concentration of the heavier constituent (O^+) decreases with increasing altitude whereas the lighter ion (H^+) concentration increases with altitude until it dominates the composition. Therefore, instead of considering a complete O^+ atmosphere, we have adjusted the percentage ion composition at 400 km to yeild a predominant O^+ atmosphere to about 3000 km. We have not used the diffusive equilibrium model below 400 km simply because neither the ionization nor the recombination rates could be ignored. Values of electron density at less than 400 km are taken from selected N_e-h profiles for quiet and disturbed conditions of the ionospehre and are fitted into the ray tracing program.

The diffusive equilibrium model, as we find, does not provide completely satisfactory electron densities along field lines deeper into the magnetosphere because, for example, it ignores the E fields perpendicular to B field lines. This model also seems unable to predict the observed knee in the plasmasphere or the presence of ducts threading into the magnetosphere and in itself is a subject of further investigation.

However, the conclusion derived from our ray path computaions, which are performed for the non-ducted whistler mode VLF wave propagation, retain their validity.

The magnetosphere in our computations is assumed to be permeated by a static magnetic field represented by the centered dipole which is not too bad an approximation to 6 R_E during quiet times. Beyond that the configuration and content of the magnetosphere is dominantly controlled by the solar wind, convection electric fields ($\vec{E} \perp \vec{B}$) etc. It is, therefore, suggested that a probable improvement on the ray path computations could be made in future by using a more realistic model for the geomagnetic field.

It should be recognized that we have mapped the ray paths on the basis of one-dimensional ionosphere, i.e., with electron density varying only in the vertical direction and not in the north-south or east-west direction at any altitude. It is suggested that the horizontal gradients in electron densities should also be considered for future VLF related work. A much more realistic effort would require allowance for variations at least in the north-south directions.

REFERENCES

Akasofu, S.-I., Electrodynamics of the magnetosphere: Geomagnetic storms, Space Science Rev., 6, 21-143, 1966.

Angerami, J. J. and D. L. Carpenter, Whistler studies of the plasmapause in the magnetosphere, 2. Electron density and total tube electron content near the knee in magnetospheric ionization, J. Geophys. Res., 71, 711-725, 1966.

Angerami, J. J. and J. O Thomas, The distribution of ions and electrons in the earth's exosphere, Tech. Rept. No. 4, SEL-63-110, Radio Science Lab., Stanford University, Stanford, California, December 1963.

Barrington, R. E., J. S. Belrose and D. A. Keeley, Very low frequency noisebands observed by Alouett I satellite, J. Geophys. Res., 68, 6539-6541, 1963.

Booker, H. G., Oblique propagation of electromagnetic waves in a slowly-varying non-isotropic medium, Proc. Roy. Sec., 155A (885), 235-257, 1936.

Booker, H. G., Propagation of wave packets incident obliquely upon a stratified doubly refracting ionosphere, Phil. Trans. Roy. Soc., 237 A (781), 411-451, 1938.

Booker, H. G., Application of magneto-ionoinic theory to radio waves incident obliquely upon a horizontally stratified ionosphere, J. Geophys. Res., 54, 243-274, 1949.

Brice, N. M. and R. L. Smith, Lower hybrid resonance emission, J. Geophys. Res., 70, 71-80, 1965.

Brice N. M., Morphology of elementary magnetospheric substorms, CSUAC 94, Cornell University, Ithaca, New York, June, 1967.

Budden, K. G., Radio waves in the Ionosphere, Cambridge University Press, Cambridge, England, 1961.

Carpenter, D. L., Whistler studies of the plasmapause in the magnetosphere. I. Temporal variations in the positions of the knee and some evidence on plasma motions near the knee, J. Geophys. Res., 71, 693-709, 1966.

Cartwright, D. G., Rocket observations of very low frequency radio noise at night, Planet. Space Sci., 12, 11-16, 1963.

Cerisier, J. C., Propagation perpendiculaire au voisinage de la frequence de la resonance hybride basse, Plasma Waves in Space and Laboratory, American Elsevier Publishing Co., New York, Vol. 2, 487-521, 1970.

Deeks, D. G., D-region electron distributions in middle latitudes deduced from the reflection of long radio waves, Pro. Roy. Soc. London, A 291, 413-437, 1966.

Dowden, R. L., VLF emissions from the exosphere, Res. Rep. Iono. Prediction Services, Australia, 1963.

Dunckel, N. and R. A. Helliwell, Whistler mode emissions on the OGO I satellite, J. Geophys. Res., 74, 6371-6385, 1969.

Ellis, G. R., Low frequency radio emission from aurora, J. Atmos. Terr. Phys., 10, 303, 1957.

Frank, L. A., Plasma in the earth's polar magnetosphere, J. Geophys. Res., 76, 5202-5219, 1971.

Frank, L. A. and D. A. Gurnett, Distribution of plasmas and electric fields over the auroral zones and polar caps, J. Geophys. Res., 76, 6892-6846, 1971.

Frank, L. A., J. A. Van Allen and J. D. Craven, Large diurnal variations of geomagnetically trapped and of precipitated electrons observed at low altitudes, J. Geophys. Res., 69, 3155-3167, 1964.

Gallet, R., Geophysics, the earth's environment, Gordon and Breach, Science Publishers, 1962.

Gallet, R. M. and R. A. Helliwell, Origin of "very-low-frequency" emissions, R. Res. Nat. Bur. Stds., 63D, 21-27, 1959.

Gurnett, D. A., Private communication, 1972.

Gurnett, D. A. and B. J. O'Brien, High latitude geophysical studies with satellite Injun 3, 5, very-low-frequency electromagnetic radiation, J. Geophys. Res., 69, 65-89, 1964.

Gurnett, D. A., Satellite study of VLF hiss, J. Geophys. Res., 71, 5599-5615, 1966.

Gurnett, D. A., G. W. Pfeifer, R. A. Anderson, S. R. Mosier and D. P. Cauffman, Initial observations of VLF electric and magnetic fields with the Injun 5 satellite, J. Geophys. Res., 74, 4631-4648, 1969.

Gurnett, D. A. and L. A. Frank, VLF hiss and related plasma observations in the polar magnetosphere, J. Geophys. Res., 77, 172-190, 1972.

Hamilton, W. R., Mathematical Papers, Vol. I, Geometrical Optics, Cambridge, University Press, 1931.

Harang, L. and R. Larsen, VLF emissions observed near the auroral zone, Part I, Scientific Rep. No. 4, Norwegian Inst. of Cosmic Physics, Univ. of Oslo, 1964.

Harang, L. and R. Larsen, Radio wave emission in the VLF band observed near the auroral zone - I occurrence of emission during disturbances, J. Atmos. Terr. Phys., 27, 481-497, 1965.

Haselgrove, J., Ray theory and a new method for ray tracing, London Phycisal Society, Report of conference on Physics of the Ionosphere, 355-364, 1955.

Haselgrove, J., Oblique ray paths in the ionosphere, Proc. Roy. Soc. London, A, 70, (7), 653-662, 1957.

Helliwell, R. A., Whistlers and related ionospheric phenomena, Stanford University Press, Stanford, California, 1965.

Helliwell, R. A., VLF emissions, Plasma Waves in Space and Laboratory, Vol. I, American Elsevier Publishing Co., New York, 335-360, 1969.

Hines, C. O., Wave packets, the poynting vector and energy flow, Part IV- Poynting and McDonald velocities in dissipative anisotropic media (conclusion), J. Geophys. Res., 56, 535-544, 1951d.

Hines, C. O., Heavy ion effects in audio frequency radio propagation, J. Atmos. Terr. Phys. 11, (2), 36-42, 1957.

Holt, O. and G. M. Lerfeld, Results from a RF capacity probe experiment in the auroral ionosphere, Radio Science, 2, 1283-1294, 1967.

Iversen, I. B., O. H. Olesen and E. Ungstrup, Observations of VLF radio noise in the ionosphere during an auroral absorption event, Annales de Geophysique, E. 24, fasc. I, 1968.

Jørgensen, T. S. and E. Ungstrup, Ionosfaerelaboratoriet, Denmark Tekniske Høyskole, Rep. No. 13, Copenhagen, 1962.

Jørgensen, T. S., Interpretation of auroral hiss measured on OGO 2 and at Byrd station in terms of incoherent cerenkov radiation, J. Geophys. Res., 73, 1055-1069, 1968.

Kennel, C. F., Low frequency whistler model, Phys. of Fluids, 9, 2190-2202, 1966.

Kennel, C. F. and H. E. Petschek, Limit on stably trapped particle fluxes, J. Geophys. Res., 71, 1-29, 1966.

Kennel, C. F. and H. E. Petschek, Nonlinear effects in plasmas, Edited by Kalman and Feix, Gordon and Breach Science Publishers, 1969.

Kennel, C. F. and R. M. Thorne, Unstable growth of unducted whistlers propagating at an angel ot the geomagnetic field, J. Geophys. Res., 72, 871-878, 1967.

Kimura, I., Effects of ions on whistler mode ray tracing, Radio Science, 1, (3) (New Series), 269-283, 1966.

Kindel, J. M and C. F. Kennel, Topside current instabilities, J. Geophys. Res., 76, 3055-3078, 1971.

Lim, T. L. and Thomas Laaspere, An evaluation of the intensity of cerenkov radiation from auroral electrons with energies down to 100 eV (private communication), 1972.

Lyons, L. R. and R. M. Thorne, The magnetospheric reflection of whistlers, Planet. Space Sci. 18, 1753-1757, 1969.

Maeda, K. and I. Kimura, A theoretical investigation on the propagation path of the whistling atmospherics, Rept. Iono. Space Res. Japan, 10, 105-123, 1956.

Maeda, K. and I Kimura, Amplification of the VLF electromagnetic wave by a proton beam through the exosphere, J. Phys. Soc. Japan, 17, (Suppl. A-II), 92-95, 310 and 311, 1962.

Maeda, K. and I. Kimura, Origin and mechanism of VLF emissions, Space Science Research III, New York, Willey, 310 and 311, 1963.

McDiarmid, I. B. and E. E. Budzinski, Angular distribution and energy spectra of electrons associated with auroral events, Can. J. Phys., 42, (11), 2048-2062, 1964.

McEwen, D. J. and R. E. Barrington, Some characteristics of the lower hybrid resonance bands observed by the Alouette I satellite, Can. J. Phys., 45, 13-19, 1967.

Millington, G., The effect of earth's magnetic field on short communication by the ionosphere, Proc. Inst. Elec. Engrs., 98, (1), Part IV, 1-14, 1951.

Millington, G., Ray path characteristics in the ionosphere, Proc. Inst. Elec. Engrs., 101, (7), Part IV, 235-248, 1954.

Morozumi, H. M., A study of aurora australis in connection with association between VLF hiss and auroral arcs and bands observed at the south geographic pole, SUI 62-14, State University of Iowa, Iowa City, Iowa, 1962.

Morozumi, H. M., Examples of positive correlation between VLF chorus and CNA, Planet. Space Sci., 15, 207-208, 1967.

Morozumi, H. M. and R. A. Helliwell, A correlation study of the diurnal variation of upper atmospheric phenomena in the southern auroral zone, SU-SEL-66-124, Stanford University, Stanford, California, 1966.

Mullaly, R. F., Graphical construction for ray tracing in the ionosphere, London Phys. Soc., Report of conference on Physics of the ionosphere, 384-393, 1955.

Oliven, M. N. and D. A. Gurnett, Microbust phenomena 3. An association between microbust and VLF chorus, J. Geophys. Res., 73, 2355-2362, 1968.

Parthasarathy, R. and G. C. Reid., Magnetospheric activity and its consequences in the auroral zone, Planet. Space Sci., 15, 917-929, 1967.

Parthasarathy, R. and F. T. Berkey, Multiple frequency investigations of radio wave absorption during the down-breakup phase of auroras, Radio Science, 415-421, 1965.

Peoverlein, H., Strahlwege von Radiowellen in der ionosphere I, S. B. bayer Akad. Wiss., 175-201, 1948.

Poeverlein, H., Strahlwege von radiowellen in der ionosphere II, Z. angew. Phys., 1, (11), 517-525, 1949.

Poeverlein, H., Strahlwege von radiowellen in der ionosphere III, Z. Agnew. Phys., 2, (4), 152-160, 1950.

Reid, G. C. and R. Parthasarathy, Ionospheric effects of energetic electron bursts in the tail of the magnetosphere, J. Geophys. Res., 71, 3267-3272, 1966.

Russel, C. T., R. F. Holtzer and E. J. Smith, OGO 3 observations of VLF noise in the magnetosphere I. Spatial extent and frequency of occurrence, J. Geophys. Res., 74, 755-777, 1969.

Scarf, F. L., R. W. Fredricks and G. M. Crook, Detection of electromagnetic and electrostatic waves on OV3-3, J. Geophys. Res., 73, 1723-1745, 1968.

Shawhan, S. D., VLF ray tracing in a model ionosphere, University of Iowa Rep. 66-33, Iowa City, Iowa, August 1966.

Smith, R. L., The use of nose whistlers in the study of the outer ionosphere, Tech. Rept. No. 6, AFOSR-TN-60-681, Radio Science Lab., Stanford University, Stanford, California, July 1960.

Smith, R. L. and N. M. Brice, Propagation in multicomponent plasmas, J. Geophys. Res., 69, 5029-5039, 1964.

Srivastava, R. N. and D. W. Swift, VLF observations at Colliege, Alaska during the great magnetic substorm of March 8, 1970, WDCA Upper Atmospheric Geophysics Report, UAG-12, Pt II, April 1971.

Stix, T. H., The theory of plasma waves, McGraw Hill Book Co., 1962.

Swift, D. W., Private communication, 1972.

Swift, D. W., Very-low-frequency radio propagation in the ionosphere, Journal of Res., NBS-D., 66D, No. 6, 663-680, 1962.

Swift, D. W., A mechanism for energizing electrons in the magnetosphere, J. Geophys. Res., 70, 3061-3073, 1965.

Swift, D. W., A new interpretation of VLF chorus, J. Geophys. Res., 73, 7447-7456, 1968.

Taylor, W. W. L. and D. A. Gurnett, Morphology of VLF emissions observed with Injun 3 satellite, J. Geophys. Res., 73, 5612-5626, 1968.

Thorne, R. M., E. J. Smith, R. K. Burton and R. E. Holtzer, Plasmaspheric hiss, J. Geophys. Res., 78, 1581-1596, 1973.

Thorne, R. M. and C. F. Kennel, Quasi-trapped VLF propagation in the outer magnetosphere, J. Geophys. Res., 72, 857-870, 1967.

Ungstrup, E., Rocket observation of VLF hiss in aurora, Planet. Space Sci., 19, 1475-1495, 1971.

Walter, F., Nonducted VLF propagation in the magnetosphere, SU-SEL-69-061, Stanford University, Stanford, California, 1969.

Weinberg, S., Eikonal method in magnetohydrodynamics, Phys. Rev., 126, 1899-1909, 1962.

Whitten, R. C. and I. G. Poppoff, Physics of the lower ionosphere, Prentice Hall Inc., 134, 1965.

Yabroff, I., Computation of whistler ray paths, J. Res. NBS, 65D, (radio Propa) No. 5, 485-505, 1961.

APPENDIX A

Report on the great substorm of March 8, 1970 published in the World Data Center Report UAG-12, Part II, April 1971.

The purpose of this communication is to describe in detail the VLF emissions during the most intense magnetic substorm since the I.G.Y. The substorm was observed to start at 0417 150°WMT (1417 UT) at the College observatory (64.7° N) on March 8, 1970 with a negative bay reaching 4900γ at 0445 150° WMT, and was also recorded at a number of other polar and nonpolar stations at about the same time but with differing intensities. The substorm was unusual in that some of the most intense VLF emissions we have observed to date were recorded during it, especially in light of the fact that the VLF signals were observed during a time when there was heavy ionospheric absorption present and also during a part of the day when these emissions are seldom observed.

The VLF emissions were received on a triangular loop (I.G.Y. - type) antenna oriented with the normal to the plane of the antenna pointing geomagnetically east-west. Thus the system had greater sensitivity to signals propagating in the magnetic meridian plane than to signals propagating in an east-west direction. The receiver was essentially a wide-band amplifier. The output of the amplifier was passed through filters centered at 400, 800, 1500, 3500 and 8000 Hz. The filter outputs and the broadband signal were then passed through detectors and the DC outputs of the detectors were recorded on a 6-channel chart recorder at 1 mm/minute. The relative outputs of the various detectors provided an indication of the spectral content of the incoming VLF signals.

Figure A1 shows the amplitudes of VLF signals as detected on the 400, 800 and 1500 Hz channels. The ambient field strengths plotted against time are reduced to the same scale for comparison purposes. Note that most of the energy was concentrated near or below 400 Hz, and the spectral content is typical of the emission that is referred to as ELF hiss. Also it is likely that VLF chorus was present in the received data. We also recorded the signal amplitudes on the 3500 and 8000 Hz channels, but the signal level was considerably below the level measured on the other three channels.

Several other effects were observed simultaneously during this substorm. In particular, very intense radio wave absorption in the ionosphere and intense H-β emission from the aurora were observed at College. Figures A2, A3 and A4 show the ionospheric absorption as measured on the 30 MHz riometer, the H-component of the magnetic disturbance vector and the H-β photometer record, respectively, all recorded at College. These figures are shown so that the VLF data may be viewed in the context of the total substorm event. The riometer and the photometer data indicate the precipitation intensities of electrons and protons, respectively. It can be seen that the disturbance events shown in Figures A2-A4 begin almost simultaneously at 0417 150° WMT. Unfortunately, due to the remote location of the VLF receiver and chronic problems with power outages, we were not able to maintain a reliable time base for the VLF data. In fact, the original records indicated that the VLF event started at 0407 150° WMT. The onset of the VLF event was well defined and the onsets of the disturbances shown in Figures A2-A4 are also well defined and nearly coincident. This suggests that the most likely time base for the VLF data is that shown in Figure A1.

In other words, we have advanced the time base for the VLF data by 10 minutes over that indicated in the original chart record in order to make the VLF event coincident with the other substorm events.

It is useful to compare the riometer data and the VLF data since the ionospheric absorption of VLF signals can be related to absorption of 30 MHz radio waves. Assuming a model for the ionospheric electron density, it is possible to calculate the absorption at 30 MHz and at VLF frequencies. From the result it is possible to give a quantitative relationship between absorption at the two frequencies. Calculations carried out by D. Wallis (private communication, 1968) using the auroral model ionosphere of Holt and Lerfeld (1967) indicate that the ratio between absorption at 500 Hz and 30 MHz is 0.35. That is, an ionosphere which resulted in 10 db of absorption at 30 MHz could be expected to result in 3.5 db of absorption at 500 Hz. However, in interpreting these calculations, it should be kept in mind that the absorption ratio is sensitive to the model used. For example using the PCA model, calculations indicate that the magnitude of the absorption shown in Figure A2 should have an appreciable effect on the transmission of VLF energy through the ionosphere. The 30 MHz absorption observed at College at 0440 150° WMT was near 30 db or higher, indicating that the absorption at 500 Hz should have been at least 10 db. It should be pointed out here that the absolute magnitude of the ionospheric absorption higher than 15 db is not very meaningful although it has been reported here by making some finer calibration. Examination of other 30 MHz riometer data published by ESSA from other stations in Alaska indicated that the region of intense absorption extends south of Anchorage (61.2° N)

and northward to somewhere between Fort Yukon (66.34° N) and Barter Island (69.35° N). The actual magnitude of the absorption at the stations reported by ESSA is difficult to determine if the absorption was in excess of 9 db since the plots were folded back on themselves. However, the swath of 30 MHz absorption in excess of 9 db extended from Anchorage (61.2° N) to Fort Yukon (66.34° N).

Examination of Figure A1 indicates that there were measurable VLF signals during most of the substorm and that these signals were certainly present during the peak in absorption centered around 0440 150° WMT. Comparison of Figures A1 and A2 does not indicate a simple relationship between the intensity of VLF emissions and 30 MHz absorption but the period between 0520 and 0555 150° WMT does show a tendency towards positive correlation between the VLF amplitudes and the 30 MHz absorption.

In relating the intensity of the VLF emissions to 30 MHz absorption, it should be kept in mind that both events appear to be the consequence of the substorm and the two events may be related to the same source. That is, the agent responsible for the precipitation of electrons may also be responsible for the generation of VLF emission. A possible mechanism is pitch angle scattering of electrons by electromagnetic waves at VLF frequencies (Kennel and Petschek, 1966). In support of this idea Oliven and Gurnett (1968), with their instrumentation on the injun 3 satellite, report simultaneous occurrences of VLF chorus and electron microbursts. Moreover, Morozumi and Helliwell (1966) in their analysis of Antarctic VLF data indicate that VLF emissions are positively correlated with 30 MHz absorption, the intensities of VLF emissions appear to

be anticorrelated with 30 MHz absorption. Our data tend to support this conclusion.

As indicated earlier the substorm was unusual simply in that the VLF emissions were received during the predaylight morning hours. We think that the fact that VLF emissions were detected during the substorm cannot be entirely attributed to the intensity of the emitting source. Rather, it is likely that the propagation conditions in the upper ionosphere and magnetosphere were affected by the substorm in a manner to have allowed the signals to reach the ground rather than being reflected outward.

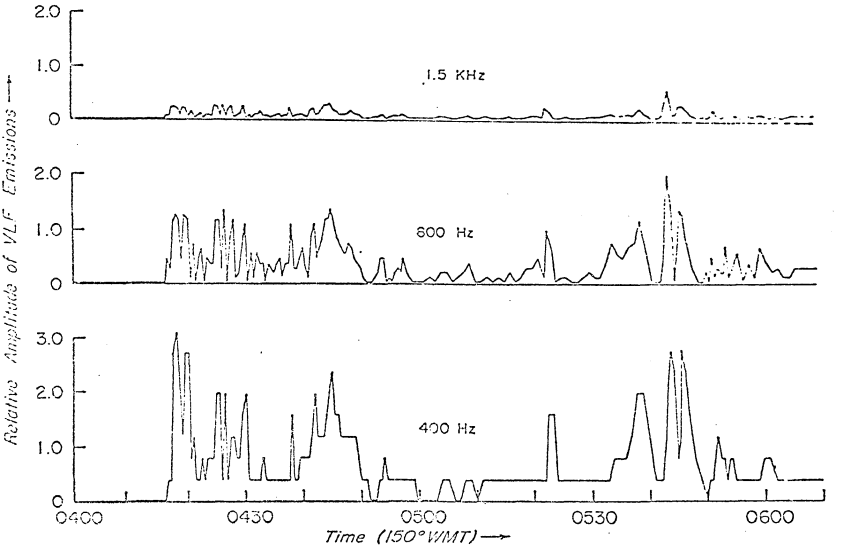

Figure A1 The VLF emissions recorded by the College Station at 400, 800 and 1500 Hz during the substorm on March 8, 1970. The emissions observed at 3500 and 8000 Hz were too small to be shown within the ordinate scale.

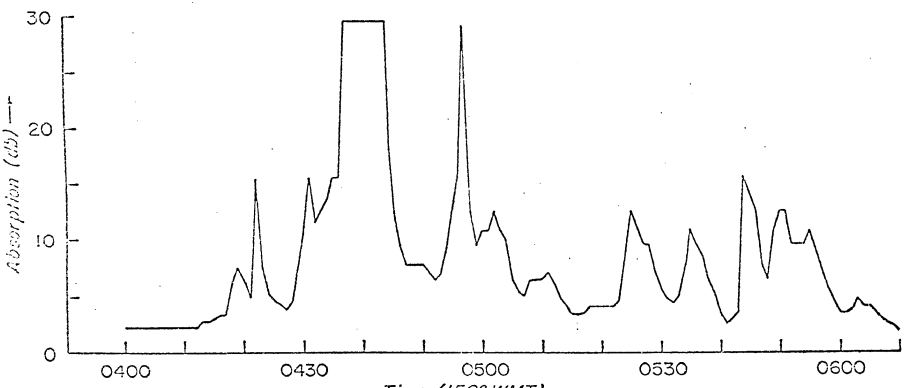

Figure A2 The 30 MHz riometer absorption data during the substorm at College on March 8, 1970

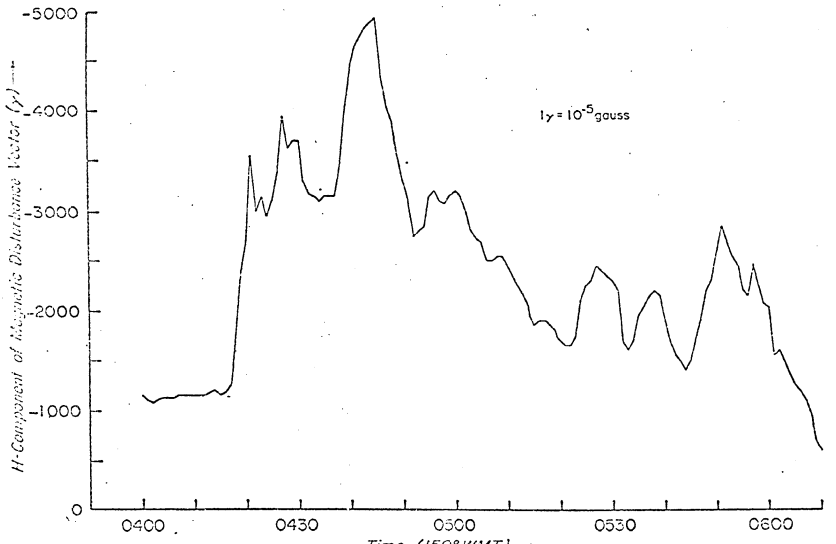

Figure A3 The H-component of the magnetic disturbance vector as recorded by the College observatory during the substorm on March 8, 1970

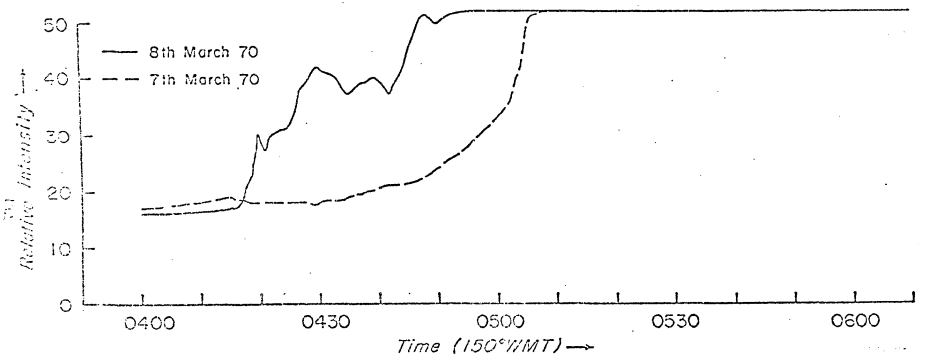

Figure A4 The H-β photometer record during the substorm on March 8, 1970. The dotted line represents the record for March 7, 1970. The two records merge into the twilight zone after 0508 (150° WMT). The strength of the emission could not be exactly determined due to the cloudy sky conditions but it was estimated to be of the order of 600 Rayleighs.